Journal of Sedimentary Research
November 2022, Volume 92 Issue 11 Pages 1022-1043
https://doi.org/10.2110/jsr.2022.033
https://archimer.ifremer.fr/doc/00807/91914/

The Zambezi deep-sea fan: mineralogical, REE, Zr/Hf, Nd-isotope, and zircon-age variability in feldspar-rich passive-margin turbidites

Garzanti Eduardo [1, *], Bayon Germain [2], Vermeesch Pieter [3], Barbarano Marta [1], Pastore Guido [1], Resentini Alberto [1], Dennielou Bernard [2], Jouet Gwenael [2]

[1] Laboratory for Provenance Studies, Department of Earth and Environmental Sciences, University of Milano–Bicocca, 20126 Milano, Italy
[2] University of Brest, CNRS, Ifremer, Geo-Ocean, F-29280 Plouzané, France
[3] London Geochronology Centre, Department of Earth Sciences, University College London, London WC1E 6BT, U.K.

* Corresponding author : Eduardo Garzanti, email address : eduardo.garzanti@unimib.it

Abstract :

We here present the first comprehensive provenance study of the Zambezi deep-sea fan, based on integrated petrographic, heavy-mineral, elemental-geochemistry, isotope-geochemistry, and detrital-zircon-geochronology analyses of middle Pleistocene to Holocene turbidites. The Zambezi Valley and Fan represent the submarine part of an ~ 5000-km-long sediment-routing system, extending from the heart of the South African Plateau to the abyssal depths of the Indian Ocean. Sediment is derived not only from the African side, but also from Madagascar Island mostly via the Tsiribihina Valley. Being shed by two dissected rifted margins, detritus supplied from opposite sides of the Mozambique Channel shares similar feldspar-rich feldspatho-quartzose composition, although with significant differences in heavy-mineral and geochemical signatures. The εNd values of Madagascar sand are markedly more negative and TNd model ages notably older. Zircon grains yield mostly Irumide (late Stenian) U-Pb ages in African-derived sand and mostly Pan-African (Ediacaran–Cryogenian) U-Pb ages in Madagascar-derived sand, which also yields a few grains as old as Paleoarchean and many discordant ages reflecting Pan-African reworking of Archean cratonic rocks. Lower Valley and Lower Fan deposits have intermediate fingerprints, indicating that sediment supply from Madagascar is not much less than from Africa despite a much smaller catchment area, which can be explained by deposition of a conspicuous part of Africa-derived sediment in the Intermediate Basin confined between the Zambezi Shelf, the Beira High, and the Îles Éparses.

By assuming that compositional differences between Quaternary submarine deposits and modern Zambezi River sands primarily resulted from sediment impoundment by large dams, we could evaluate the anthropogenic impact on natural sediment fluxes. Quaternary turbidites are somewhat higher in quartz and poorer in heavy minerals with higher relative amounts of durable ZTR species, and yield more Ediacaran, Neoarchean, and Carboniferous detrital-zircon ages than modern river sands. The Orosirian peak characterizing the Intermediate Basin sample points to prominent supply from the middle and upper parts of the Zambezi catchment in the middle Pleistocene. Rough calculations suggest that pre-dam Zambezi sediments were generated ≤ 10% in the upper catchment, ~ 60% in the middle catchment, and only ≥ 30% in the lower catchment that provides the totality of sediment reaching the Indian Ocean today.

"Roads were made for journeys, not destinations"
Kong Fu Zi (Confucius)

INTRODUCTION

Deep-sea fans are natural archives that faithfully preserve the long-term sedimentary record of tectonic and climatic change affecting the adjacent landmasses (Hessler and Fildani 2019). Compositional variability, however, is controlled by the interplay of multiple factors, the effect of which must be disentangled (Johnsson 1993; Weltje and von Eynatten 2004). The acquisition of high-resolution compositional data through a range of techniques is required to decrypt such a complex archive of information and to shed light on the functioning of sedimentary processes and on landscape changes across vast continental areas in the recent and less recent past (Dickinson 1988; Allen 2008; Caracciolo 2020). Understanding the work done by natural forces as well as the impact of anthropization is in turn a necessary prerequisite to produce quantitative models able to describe with reasonable approximation possible future scenarios, and thus devise sensible plans of environmental management apt to mitigate undesired effects such as accelerated soil loss, rapid siltation of reservoirs, severe coastal retreat, and enhanced concentration of pollutants (Sickmann et al. 2019).

The mineralogy of deep-sea fans has been long and widely investigated for arc - trench and orogenic systems (e.g., Ingersoll and Suczek 1979; Marsaglia and Ingersoll 1992; Zuffa et al. 2000; Garzanti et al. 2020; Pickering et al. 2020), but less so for passive margins (e.g., Thayer et al. 1986; Rimington et al. 2000). The present article, intended as a complement of previous studies on land, focuses on the Zambezi deep-sea fan deposited in the Mozambique Channel between the African landmass and Madagascar Island (Fig. 1), thus completing the source-to-sink study of the entire Zambezi sedimentary system (Garzanti et al. 2014a, 2014b, 2021a, 2022a, 2022b). Our primary aims are to illustrate and discuss the variability of petrographic, heavy-mineral, elemental-geochemistry, Nd-isotope, and U-Pb detrital-zircon geochronological signatures of Middle Pleistocene to Holocene turbidite deposits, highlight provenance changes in space and time, reconstruct sedimentary and geochemical budgets, and assess the relative amounts of detritus supplied from Africa *versus*

Madagascar as well as the changing contributions from different rivers of SW Madagascar. The effects of grain size and hydraulic sorting during transport and deposition, of glacial - interglacial cycles and associated major eustatic oscillations, and of artificial segmentation by the construction of large dams and of anthropization in general on detrital fluxes are also investigated.

THE ZAMBEZI SEDIMENT-ROUTING SYSTEM

The Zambezi sedimentary system extends for ~ 5000 km overall, half on land from the headwaters in the South African Plateau to the delta on the Mozambique coast, and half at sea from the continental shelf to the abysses of the Indian Ocean (Fig. 1).

The Zambezi River and Shelf

The complex drainage evolution of the Zambezi, the largest river in southern Africa (length 2575 km, basin area ~ 1.4 million km^2; Moore et al. 2007), was controlled directly or indirectly by the multiple rifting events that punctuated the ~ 280-Ma-long breakup history of Gondwana (Wellington 1955; Key et al. 2015). Sourced among low ridges of the Congo Craton near the triple boundary of Zambia, Congo, and Angola, the Zambezi River flows away from the domal uplift associated with the Early Cretaceous rifting of the South Atlantic in the west (Cox 1989), traverses unconsolidated eolian sands of the Kalahari Basin, plunges into the basaltic gorges downstream of Victoria Falls, and skirts around the Zimbabwe Craton along Karoo (Permian - Triassic) rift troughs superposed on the Pan-African suture zone (Goscombe et al. 2020). In Mozambican lowlands, the river follows the Lower Zambezi graben, originated as a failed arm of the Jurassic Mozambique Basin rift (Butt and Gould 2018), and eventually empties through a wave- and tide-dominated delta into the Indian Ocean (Beilfuss et al. 2000). The modern drainage developed in the late Cenozoic through diverse events of river capture and drainage reversal associated with uplift of the broad South African Plateau and southwestward propagation of the East African Rift (Moore and Larkin 2001; Kinabo et al. 2007; Ebinger and Scholz 2012). The drainage basin continued to expand in the Quaternary, with the capture of the Angolan

Cuando tributary and the presently incipient capture of the large endorheic Okavango River (Gumbricht et al. 2001).

In the last century, the course of the Zambezi was rigidly segmented by the construction of the large dams that created Lake Kariba (the world's largest artificial reservoir, completed in 1958) and Lake Cahora Bassa (Africa's fourth-largest reservoir, completed in 1974), which have disrupted the natural sediment transport by efficient trapping of detritus generated upstream (Bolton 1984; Ronco et al. 2010; Kunz et al. 2011). Other major dams were built on the Kafue River in Zambia and on the Shire River in southern Malawi. Segmentation of the Zambezi sediment-routing system is also induced by natural processes, much sediment being retained in large wetlands in the Kalahari Basin and along the Shire River (Fig. 1).

In pre-dam times, significant volumes of detritus were supplied to the Mozambican coast also by the Upper Zambezi and its Cuando tributary draining the Kalahari Basin in Zambia and Angola, and by major tributaries joining the Zambezi downstream, including the Kafue and Luangwa from Zambia and the Gwai from Zimbabwe (Fig. 1). At present, however, all sediment delivered to the Indian Ocean is generated in the Lower Zambezi catchment downstream of Lake Cahora Bassa, where major left (northern) tributaries are the Luia and the Morrunguze draining high-grade rocks of the Southern Irumide Province, and the Shire, the outlet of Lake Malawi, which drains largely garnet-free mafic granulites of the Blantyre domain (Goscombe et al. 2020). Among right (western) tributaries, the Mazowe and Luenha rivers sourced in the Archean Zimbabwe Craton and cutting across polymetamorphic gneisses remobilized during the Neoproterozoic Pan-African orogeny are estimated to provide between half and two-thirds of the sediment reaching the Zambezi Delta today (Garzanti et al. 2022a). Additional detritus is derived from Permian - Triassic Karoo clastic rocks (Fernandes et al. 2015).

Zambezi sediments have built through time the widest continental shelf along the Indian Ocean coast of Africa (Walford et al. 2005; Ponte et al. 2019), reaching more than 100 km in width and contributing to the highest tidal range in the western Indian Ocean (up to 5 m; Sete et al. 2002;

Hoguane et al. 2020). Large sediment volumes, however, are not deposited in front of the Zambezi mouth but are transported northeastward by longshore currents (Schulz et al. 2011; van der Lubbe et al. 2014), forming wide beaches as far as Quelimane and beyond (Fig. 1). The Mozambique Current, a western geostrophic boundary current flowing southward along the shelf break, forms subaqueous dune fields with up to 10-m-high dunes on the outer shelf, representing the current-modified early Holocene Zambezi paleodelta (Flemming and Kudrass 2018).

The Zambezi Valley and Fan

The Zambezi curvilinear valley and deep-sea fan constitutes one of the largest passive-margin turbidite systems on Earth, structurally confined among diverse tectono-magmatic elements, including the Davie and Madagascar ridges to the east, the Mozambique Ridge to the west, and the *Îles Éparses* in the middle (Fig. 2). The submarine valley is presently disconnected from the Mozambican shelf (Schulz et al. 2011). During the Last Glacial Maximum, instead, the Chinde - Zambezi paleovalley funnelled Zambezi sediment across the shelf toward gullies and channels on the continental slope (Beiersdorf et al. 1980; Wiles et al. 2017a, 2017b).

The 1500-km-long, deeply incised Upper Valley (average width 30 km, average relief 470 m) starts ~ 200 km to the NE of the Zambezi mouth and 175 km offshore of the shelf break at a depth of ~ 2500 m b.s.l. (Fierens et al. 2019). Oriented at first NW/SE transverse to the Mozambique margin, it deflects where it approaches the Davie Fracture Zone, and then continues southwards between the Madagascar margin to the east and volcanic seamounts topped by carbonate platforms in the west (*Îles Éparses*; Courgeon et al. 2016). Semi-confined between the *Îles Éparses* and the buried Beira High farther west lies the ponded intraslope Intermediate Basin (Fig. 2), a separate depocenter where fine-grained turbidites with thin sheet-like, coarse-grained interbeds are deposited at water depths of ~ 3000 m. Because no correspondence with climatic or eustatic changes was observed, gravitational failure from the continental slope is held to represent the main triggering process for turbidity currents (Fierens et al. 2020).

At ~ 22° S, the junction with the higher-sinuosity, narrower (2 - 3-km-wide), and steeper Tsiribihina Valley originating from the SW Madagascar margin is marked by a 17-m-high scarp. The Lower Zambezi Valley is deeply entrenched (up to 758 m) across an area affected by Late Miocene structural doming, and turbidite overflow is consequently limited (Fierens et al. 2019). Sediments on the valley floor include massive turbidites with average grain size up to 2 mm and containing rounded feldspar grains up to 1.5 cm in diameter, interbedded with hemipelagic sediments (Simpson et al. 1974 p. 184). Near the southern tip of Madagascar Island, the Lower Valley connects *via* a channel - levee system to the rather flat Lower Fan, lying at water depths between 4000 and 5000 m. Several distributary channels characterize the proximal Lower Fan, where largely sand deposition occurs as coarse-grained terminal lobes. Pelagic muds, fine-grained turbidites, and contourites characterize the distal Lower Fan (Kolla et al. 1980a).

Aggradational and erosional processes alternate in the Zambezi submarine system, where contouritic drift fed by turbiditic overflow has continued since the Oligocene (Fig. 2). The Mozambique Channel plays a major role in the exchange of surface-water masses between the Atlantic and Indian Oceans and forms a topographic barrier for deep-water circulation because of its northward-shallowing water depths. Topographically blocked to the north, Antarctic Bottom Water is deflected eastward forming 450-m-deep, 20-km-long and 3 - 7-km-wide erosional scours at the northeastern edge of the Mozambique Ridge, whereas steep sediment waves migrate upslope along the western flank of the fan beneath the southward flow of anticyclonic Mozambique Channel eddies (Kolla et al. 1980b; Breitzke et al. 2017). Bottom currents lasting up to one month reach peak velocities up to 40 - 50 cm/s and contribute to the erosion of valley flanks, thus explaining the scarcity of fine-grained overbank deposits (Miramontes et al. 2019).

Sediment Sources

After the multiple rifting phases leading to the separation of Madagascar from Africa and onset of seafloor spreading in the Mozambique Channel (Leinweber and Jokat 2012; Thompson et al. 2019), ~ 12 km of sediments accumulated on the Mozambique margin since the Early Cretaceous

(Ponte et al. 2019). The Zambezi deep-sea fan may have started as early as the Late Cretaceous - Eocene to the north of the Zambezi mouth (Castelino et al. 2017). In the Oligocene, multiple sediment sources were active from the African continent, including the Lurio River (length 600 km, catchment area ~ 61,000 km^2) *via* the N/S Serpa Pinto Valley parallel to the Davie Fracture Zone (Fig. 1; Droz and Mougenot 1987) and the Ligonha and Licungo rivers (lengths 290 and 340 km, catchment areas ~ 16,000 and ~ 28,000 km^2, respectively) *via* the Angoche submarine valley (Fierens et al. 2022). The shift to the present-day Upper Zambezi Valley occurred in the mid-Miocene, after abandonment of the Serpa Pinto Valley and consequent to development of the East African Rift (Droz and Mougenot 1987). Since then, the major sediment source has remained the Zambezi River, with increasing sediment load through the Neogene owing to progressive catchment expansion (Moore and Larkin 2001; Walford et al. 2005). Major supply from the Zambezi River is testified by the high sedimentation rates recorded on the upper slope (~ 1 m/kyr in the last 120 kyr, Hall et al. 2016; up to 2 - 4 m/kyr during the Last Glacial Maximum, Zindorf et al. 2021).

Since the middle Miocene, the Zambezi Fan has been fed also from the Madagascar side with sediment funnelled along the Tsiribihina Valley. Major contributions are held to be derived from two main rivers, the Tsiribihina (length 460 km, catchment area ~ 45,000 km^2) and the Mangoky, the longest in the entire Madagascar Island (length 564 km, catchment area ~ 59,000 km^2). The Finerenana and Onilahy rivers to the south (lengths 290 km and 340 km, catchment areas ~ 16,000 km^2 and ~ 28,000 km^2, respectively) directly feed the deep Mozambique Basin (Figs. 1 and 2).

SAMPLING AND ANALYTICAL METHODS

Nineteen Middle Pleistocene to Holocene sediment samples ranging from very coarse silt to medium sand were collected in 2014 and 2015 during oceanographic cruises PAMELA MOZ01, MOZ02, and MOZ04 to the Mozambique Channel, at water depths between -2500 and -4400 m below sea level. Five depositional areas were considered along the Zambezi submarine sediment-dispersal system: Upper Channel (six uppermost Middle Pleistocene - Holocene samples from four turbidite beds, < 190 ka, Marine Isotope Stages 6 to 1), Intermediate Basin (five Middle Pleistocene to Holocene samples, < 480 ka, MIS 12 to 1), Tsiribihina Valley (four upper Middle to lower Upper Pleistocene samples, 70-280 ka, MIS 8/9 to 5a), Lower Valley (two uppermost Middle Pleistocene - Holocene? samples, < 190 ka, MIS 6 to 1-2?), and Lower Fan (two lower Middle Pleistocene samples, > 500 ka?) (Table 1).

During the PAMELA MOZ04 survey (Jouet and Deville 2015), another five samples ranging from fine to medium silt were collected on the Mozambique outer shelf to uppermost slope (core MOZ4-CS14 offshore of Quelimane, water depth -181 m; core MOZ4-CS17 offshore of the Zambezi delta, water depth -550 m). These sediments were deposited during the last glacial lowstand (MOZ4-CS17-2402-2407cm, 24.1 ka), the postglacial warming and sea-level rise (MOZ4-CS14-1602-1607cm, 15.9 ka; MOZ4-CS17-702-707cm, 14.6 ka), and the Holocene highstand (MOZ4-CS14-21-26cm, 4.3 ka; MOZ4-CS17-52-57cm, 4.0 ka). Sediments were dated using accelerator mass spectrometer standard radiocarbon methods on marine mollusc shells and bulk assemblages of planktonic foraminifera by applying a local marine reservoir correction of mean ΔR 158 ± 42 years (analyses, calibrated dates, and interpolated age models from Zindorf et al. 2021). Another very fine silt of Holocene age was collected just below the sea floor by advanced piston corer from Hole 1477B during IODP Expedition 361 (Hall et al. 2017).

To characterize sediment sources in Madagascar Island, five sand samples from four major rivers in SW Madagascar (Manambolo, Tsiribihina, Mangoky, and Finerenana) and from the Morondava beach were analyzed. Full information on all sampling sites is provided in Appendix Table A1 *Sample information* and in Google Earth™ file *Zambezi Fan.kmz*. Grain-size data obtained by wet sieving on the 19 samples from the Zambezi turbidite system are provided in Appendix Table A2 *Grain size*.

Petrography and Heavy Minerals

Petrographic analysis was carried out by counting 400 points in thin section under the microscope following the Gazzi-Dickinson method (Ingersoll et al. 1984). Sand classification was based on the relative abundance of the three main framework components quartz (Q), feldspars (F), and lithic fragments (L), which include carbonate and chert (Zuffa 1985). Subtle distinctions are essential to discriminate among lithic-poor suites (L < 10%QFL) deposited along passive continental margins in various tectonic and climatic settings (Garzanti et al. 2018a). Quartzo-feldspathic (Q/F < 1), feldspar-rich feldspatho-quartzose (1 < Q/F < 2), feldspatho-quartzose (2 < Q/F < 4), quartz-rich feldspatho-quartzose (4 < Q/F < 9), quartzose (90% < Q/QFL < 95%), and pure quartzose compositions (Q/QFL > 95%) are thus distinguished (classification scheme after Garzanti 2019). Petrographic parameters used in this article include the Q/F, P/F, and Mic*/F ratios (P, plagioclase, Mic*, microcline with cross-hatched twinning). Median grain size was determined in thin section by ranking and visual comparison with standards of phi/4 classes prepared by sieving in our laboratory.

From a split aliquot of the 5 phi-wide 15 - 500 μm size window obtained by wet sieving (> 5 μm for the IODP very fine silt sample), heavy minerals were separated by centrifuging in Na-polytungstate (2.90 g/cm^3) and recovered by partial freezing with liquid nitrogen (procedure described in Andò 2020). For each sample, at least 200 transparent heavy minerals were point-counted at appropriate regular spacing to minimize overestimation of smaller grains (Garzanti and Andò 2019). Transparent heavy-mineral assemblages, called for brevity "tHM suites" throughout the text, do not include phyllosilicates and carbonates. According to the transparent-heavy-mineral concentration in the sample (tHMC, expressed as % of total extrabasinal detritus), tHM suites are defined as poor (tHMC < 1), moderately poor (1 ≤ tHMC < 2), moderately rich (2 ≤ tHMC < 5), or rich (tHMC ≥ 5). The ZTR index (sum of zircon, tourmaline, and rutile relative to total transparent heavy minerals; Hubert 1962) evaluates the durability of the tHM suite through multiple sedimentary cycles (Garzanti 2017). Significant detrital components are listed in order of abundance (high to low) throughout the text. Petrographic and heavy-mineral data are summarized in Table 2 and provided in full in Appendix Tables A3 *Sand petrography* and A4 *Heavy minerals*.

Manual and Semi-Automated Raman Counting

Manual Raman counting (carried out by coupling optical-microscope and Raman-spectroscope identification on each detrital grain; Andò et al. 2011) and semi-automated Raman counting (Lünsdorf et al. 2019) are suitable techniques to determine the mineralogy of silt and sand containing few rock fragments, as in Zambezi deep-sea sediments.

Manual Raman grain counting was performed on six phi classes separated by wet sieving – from very coarse silt (32 - 63 μm) to very coarse sand (1000 - 2000 μm) – of the low-density (< 2.90 g/cm^3) fraction of Lower Fan sample 5976, with the specific aim to assess the grain-size-dependent intrasample variability of relative tectosilicate abundances. Detrital tectosilicates have distinct Raman spectral features. Quartz is most readily identified by intense Raman scattering and main peak at 464 cm^{-1}. Instead, the main peak is observed at 513 cm^{-1} for K-feldspar, at 506 - 507 cm^{-1} for albite, and at 509 - 511 cm^{-1} for oligoclase to labradorite (Freeman et al. 2008). Among K-feldspars, which display another distinctive peak at ~ 748 cm^{-1}, the width of all peaks increases, and the total number of vibrational modes decreases, with increasing disorder in the crystalline structure. Well-ordered triclinic microcline is thus identified by three sharp peaks between 155 cm^{-1} and 286 cm^{-1}, whereas orthoclase displays only two broader peaks in this frequency region. Data are provided in Appendix Table A5 *Intrasample tectosilicate variability*.

Semi-automated Raman grain counting was carried out separately on quartered aliquots of both dense (> 2.90 g/cm^3) and low-density (< 2.90 g/cm^3) fractions of the 15 - 500 μm size window of eleven selected samples, impregnated with Araldite and polished to expose grain surfaces. Because semi-automated analysis can handle a larger number of grains, this technique resulted particularly useful to increase analytical precision on the content of important accessory minerals such as zircon and monazite, and thus more firmly constrain provenance and REE budgets. Photomosaics of grain mounts were referenced in *Qgis* (http://www.qgis.org) to match the Raman coordinate system. Grain outlines were obtained by using standard thresholding techniques and visually checked to avoid over-segmentation. For each grain, particle features such as perimeter, area, and long and short axes were extracted in *Qgis*. Grain size was determined as the equivalent diameter. Textural information thus obtained allowed us to verify the consistency of grain-size-dependent intrasample variability of relative tectosilicate abundances throughout the Zambezi deep-sea sedimentary system and to evaluate the relative average volume of REE-bearing minerals in each sample.

Coordinates of grain centroids determined by image analysis were passed over to a confocal Renishaw Qontor Raman spectrometer equipped with a Leica microscope, 532 nm solid state laser (~ 100 mW power), motorized stage, and autofocus. Raman spectra were obtained using 50x LWD magnification applying 10% laser power for 0.4 s (repeated for 35 cycles) on each grain. Baseline correction and spectra normalization were performed using Renishaw Wire software. Grains were identified using a Matlab routine that matches the obtained spectra with an in-house-built reference database of known mineral spectra (Andò and Garzanti 2014). Goodness of fit was assessed by the correlation coefficient *r* (0 = no match; 1 = perfect match), accepting only values ≥ 0.7. Feldspars were identified as albite *vs.* Ca-plagioclase and orthoclase *vs.* microcline by applying a peak-fitting routine (Lunsdorf and Lunsdorf 2016) to retrieve the position and width of the main Raman bands. The > 10,000 analyzed feldspar grains were classified according to a decision tree based on Raman peak features and created by manual classification performed on a training set of 1000 grains according to data reported in Freeman et al. (2008). Raman-counting data are provided in Appendix Tables A6 *Mineralogy of the low-density fraction* and A7 *Mineralogy of the dense fraction*.

Geochemistry

Samples were treated using a sequential leaching procedure for quantitative removal of carbonates, Fe-oxide phases, and organic matter (Bayon et al. 2002). The remaining residue was cleaned from any clay-size material by low-speed centrifugation. Before analysis, ~ 80 mg of powdered samples were digested by alkaline fusion. The concentration of selected major and trace elements (including light and heavy rare earth elements; LREE, HREE) were determined at the Pôle Spectrométrie Océan with a Thermo Scientific Element XR sector field ICP-MS, using the Tm addition method (Barrat et al. 1996). REE patterns were normalized to CI carbonaceous chondrites

(Barrat et al. 2012). Both the accuracy and precision of measured concentrations were assessed by analyzing three certified reference materials (AN-G, AGV-1, BCR-1).

Neodymium isotopes were measured at the Pôle Spectrométrie Océan using a Thermo Scientific Neptune multi-collector ICP-MS, after Nd purification by conventional ion chromatography. Repeated analyses of a Jndi-1 standard solution gave $^{143}Nd/^{144}Nd$ of 0.512113 ± 0.000006 (2σ, n = 10), in agreement with the recommended value of 0.512115 (Tanaka et al. 2000) and corresponding to an external reproducibility of ± 0.11 ε (2σ). Epsilon Nd values were calculated using the present-day chondritic (CHUR) value of $^{143}Nd/^{144}Nd = 0.512630$ (Bouvier et al. 2008). Neodymium depleted mantle model ages ($T_{Nd,DM}$) were calculated following De Paolo (1981) and using measured Sm and Nd concentrations ($^{147}Sm/^{144}Nd = Sm/Nd \times 0.6049$) and present-day depleted-mantle values of $^{143}Nd/^{144}Nd = 0.513073$ and $^{147}Sm/^{144}Nd = 0.21083$ (Garçon 2021). Elemental geochemistry and Nd-isotope data are summarized in Table 3. The complete geochemical dataset is provided in Appendix Table A8 *Elemental and isotope geochemistry*.

Detrital-Zircon Geochronology

Detrital zircons were identified by automated phase mapping (Vermeesch et al. 2017) with a Renishaw inVia^{TM} Raman microscope on the heavy-mineral separates of 13 samples (two from the Upper Channel, one from the Intermediate Basin, two from the Lower Valley, one from the Lower Fan, two from the Tsiribihina Valley, and five from Madagascar rivers and beach), concentrated with standard magnetic techniques and directly mounted in epoxy resin without any operator selection by hand picking. U-Pb zircon ages were determined at the London Geochronology Centre using an Agilent 7700x LA-ICP-MS system, employing a NewWave NWR193 Excimer Laser operated at 10 Hz with a 25 μm spot size and ~ 2.5 J/cm^2 fluence. No cathodo-luminescence imaging was done, and the laser spot was always placed blindly in the middle of zircon grains to treat all samples equally and avoid bias in intersample comparison ("blind-dating strategy" as discussed in Garzanti et al. 2018b). Because of limited polishing of the epoxy pucks, many laser spots sampled rims rather than cores. The mass spectrometer data were converted to isotopic ratios using GLITTER 4.4.2 software

(Griffin et al. 2008), employing Plešovice zircon (Sláma et al. 2008) as a primary age standard and GJ-1 (Jackson et al. 2004) as a secondary age standard. A NIST SRM612 glass was used as a compositional standard for U and Th concentrations. GLITTER files were post-processed using IsoplotR (Vermeesch 2018). Concordia ages were calculated as the maximum likelihood intersection between the concordia line and the error ellipse of $^{207}Pb/^{235}U$ and $^{206}Pb/^{238}U$ (Ludwig 1998). The discordance cutoff was set at -5/+15 of the concordia distance (Vermeesch 2021). The complete geochronological dataset of 3128 ages, only 1677 (50.2%) of which considered concordant, is provided in Appendix B *Detrital-zircon geochronology*.

Forward Mixing Models

Terrigenous sediments are complex mixtures of single detrital minerals and rock fragments supplied in various proportions by numerous different end-member sources (e.g., rivers or source-rock domains). If the compositional signatures of detritus in each end-member source are known accurately, then the relative contribution of each source to the total sediment flux (provenance budget) can be quantified mathematically with forward mixing models (Garzanti et al. 2012; Resentini et al. 2017). The forward mixing model calculates a row vector of compositional data (with columns representing variables) as a non-negative linear combination between a matrix of fixed end-member compositions (with rows representing observations and columns representing variables) and a row vector of coefficients representing the proportional contribution of each end member to the observation (Weltje 1997). The robustness of the calculations is guaranteed only if the end-member signatures of each potential source are well distinct and precisely assessed with little variability dependent on grain size, weathering, or hydraulic sorting. Because sediment composition is controlled by multiple physical and chemical processes, their effects must be carefully evaluated before provenance and environmental information could be correctly disentangled and understood. A mathematical description of the method together with additional explanations on its founding assumptions and limitations are provided in Appendix A *Forward mixing calculations*.

COMPOSITIONAL SIGNATURES

The aim of this section is to describe the petrographic (Fig. 3), mineralogical (Fig. 4), major-element and trace-element (Fig. 5), Nd-isotope (Fig. 6), and detrital-zircon U-Pb age signatures (Fig. 7) of the Zambezi sedimentary system from coastal Mozambique to the deep-sea fan, including detritus generated in SW Madagascar. The composition of sediment carried by the Zambezi River and its tributaries, together with the geological and geomorphological characteristics of the vast Zambezi catchment, are illustrated and discussed in full detail in two companion papers (Garzanti et al. 2021a and 2022a).

Zambezi River and Shelf

Very fine to fine-grained sand carried today by the Zambezi River to the sea is quartzo-feldspathic to feldspar-rich feldspatho-quartzose, with K-feldspar ≥ plagioclase, common biotite, and a rich tHM suite including mostly amphibole (blue/green to green/brown hornblende and actinolite), subordinate epidote, and minor titanite, clinopyroxene, garnet, hypersthene, zircon, staurolite, and kyanite (ZTR 3 ± 2) (Fig. 4). In modern Lower Zambezi River sand, SiO_2 is 78 - 80 wt%, and chemical elements — excepting Ba, Ti, Eu, Zr, and Hf — are only moderately depleted relative to the Upper Continental Crust standard (UCC; Taylor and McLennan 1995; Rudnick and Gao 2003). In the cohesive mud fraction (< 32 µm), where SiO_2 is only ~ 48 wt%, many elements are enriched relative to the UCC by factors of ~ 2 (Fe, Sc, Y, REE, Ti) or even 2.5 - 3 (Th, Zr), whereas Mg and Ba are moderately depleted, and Ca and Sr strongly depleted (Table 3). REE patterns display classical shapes with higher LREE than HREE fractionation. They are steeper for cohesive mud, where the Eu anomaly (Eu/Eu*) is negative, than for sand, where Eu/Eu* ranges from slightly negative to slightly positive (Fig. 5F). The ε_{Nd} value is -14.6 ± 0.2 in sand and -15.2 ± 1.2 in cohesive mud (Fig. 6). Nd model ages calculated relative to CHUR are Calymmian for mud ($T_{Nd,CHUR}$ 1470 ± 34 Ma) and Statherian for sand ($T_{Nd,CHUR}$ 1664 ± 30 Ma), whereas depleted mantle model ages are Orosirian for mud ($T_{Nd,DM}$ 1947 ± 6 Ma) and Rhyacian for sand ($T_{Nd,DM}$ 2173 ± 39 Ma). The U-Pb zircon-age distribution displays a dominant late Stenian (Irumide) peak, with common lower Ordovician to Tonian ages, some Orosirian ages, and a few Neoarchean, Permian, and mid-Cretaceous ages (Fig. 7).

Very fine estuary and beach sand near Quelimane, 100 - 130 km north of the Zambezi mouth, is feldspatho-quartzose (i.e., more quartzose than Zambezi River sand; Table 2), with plagioclase ≥ K-feldspar and a rich tHM suite including mostly blue/green amphibole, subordinate epidote, clinopyroxene, and minor titanite, garnet, hypersthene, mostly prismatic sillimanite, zircon, and apatite (ZTR 5 ± 3). Sand in the Quelimane (Bons Sinais) estuary has a similar geochemical signature as Lower Zambezi River sand, whereas beach sand, being enriched in quartz, is notably depleted in most elements other than Ba (Table 3). The ε_{Nd} value of bulk sand ranges between -12.7 (beach) and -18.3 (estuary; Fig. 6). The Eu anomaly is negative in estuary sand and positive in beach sand (Fig. 5E). $T_{Nd,CHUR}$ model ages range from Ectasian (1380 Ga) to Orosirian (1855 Ga) and $T_{Nd,DM}$ model ages from Orosirian (1917 Ga) to Rhyacian 2285 Ga) (Table 3). The U-Pb zircon-age distribution displays a dominant late Stenian (Irumide) peak with common Neoproterozoic, some Orosirian, and a few Neoarchean and Permian ages (Fig. 7).

Very coarse silt to very fine sand deposited on the uppermost continental slope ~ 85 km offshore of the Zambezi delta is feldspar-rich feldspatho-quartzose (i.e., more similar as Zambezi River sand; Table 2) with K-feldspar ≈ plagioclase and a moderately rich tHM suite including mostly blue/green amphibole, epidote, clinopyroxene, and minor prismatic sillimanite, titanite, tourmaline, apatite, hypersthene, and garnet (ZTR 4 ± 2). Benthic foraminifera are abundant. The very fine silt collected during IODP Expedition 361 yielded a moderately poor tHM suite including mostly amphibole, epidote, and minor sillimanite, zircon, titanite and clinopyroxene.

Southwestern Madagascar Rivers and Beach

The studied fine and medium sands (2.1 to 1.6 phi) range in composition from feldspar-rich feldspatho-quartzose for the major Tsiribihina and Mangoky rivers (P/F 33 - 38) to feldspatho-quartzose for the Morondava beach and Manambolo and Finerenana rivers (P/F 22 - 30). The few rock fragments include granitoid/gneiss, greenschist-facies metabasite, mafic volcanic and subvolcanic (Finerenana), and shale/schist/metasandstone (Manambolo and Mangoky) types. Mica is common (biotite > muscovite). In sand of northern rivers, tHM suites are moderately rich and dominated by blue/green and subordinately green/brown amphibole with significant (Manambolo) or minor (Tsiribihina) clinopyroxene (Table 2). In sand of the Morondava beach and southern rivers, tHM suites range from poor to moderately rich with much more abundant garnet associated with brown augitic clinopyroxene (most common in Finerenana sand) and minor epidote-group and durable minerals (ZTR 7 - 10 *vs*. 1 - 4 in northern rivers). Blue/green and green/brown amphibole is common and prismatic sillimanite occurs in Mangoky sand. Zircon, rutile, and apatite are most frequent in the Morondava beach sand (ZTR 23).

Among the analyzed chemical elements, Mg, Sc, and Ca are strongly depleted relative to the UCC standard, whereas Zr, Hf, and Ba are moderately enriched (Table 3). Manambolo sand displays a sharply rising HREE pattern, which indicates prominent zircon contribution as supported by high Zr (522 ppm) (Fig. 5C). Zr concentration is high also in Mangoky and Morondava sands (408 and 394 ppm, respectively), which show slightly rising HREE patterns. The Eu anomaly is positive in Manambolo and Tsiribihina sands, slightly positive in Finerenana sand, and negative in Mangoky and Morondava sands (Fig. 5E). Tsiribihina sand displays a positive Ce anomaly.

The ε_{Nd} value is less negative in Manambolo and Tsiribihina sands to the north (-16.8 and -18.3) than in Mangoky and Finerenana sands to the south (-23.9 and -22.0, respectively) (Fig. 6). Nd model ages are latest Statherian and latest Rhyacian in Manambolo and Tsiribihina sands to the north ($T_{Nd,CHUR}$ 1613 and 1631 Ma, and $T_{Nd,DM}$ 2051 and 2063 Ma, respectively) and early Orosirian and late Siderian in Mangoky and Finerenana sands to the south ($T_{Nd,CHUR}$ 2037 and 1948 Ma, and $T_{Nd,DM}$ 2383 and 2318 Ma, respectively). Morondava beach sand displays intermediate values (ε_{Nd} -21.2, $T_{Nd,CHUR}$ 1720, $T_{Nd,DM}$ 2095) (Table 3).

U-Pb age spectra of detrital zircons are dominated by Neoproterozoic (Pan-African) ages, becoming younger from north to south (Fig. 7). Ages are mainly Cryogenian in Manambolo and Tsiribihina sands, both Ediacaran and Cryogenian in the Morondava beach, mainly Ediacaran in Mangoky sand, and both Ediacaran and Cambrian in Firenenana sand. Younger ages include two Permian-Triassic zircons in Manambolo sand. Older ages are mainly Paleoproterozoic, largely Siderian in Manambolo sand, Orosirian to Siderian in Tsiribihina sand, Siderian to Neoarchean in the Morondava beach, Orosirian - Rhyacian in Mangoky sand, and Statherian to Siderian in Finerenana sand. Noteworthy is the occurrence of a few grains as old as the late Paleoarchean in Morondava, Mangoky, and Finerenana sands, which are distinctive of Madagascar provenance, and of many discordant ages reflecting Pan-African reworking of Archean cratonic rocks (Collins et al. 2003).

Upper Channel and Intermediate Basin

In the Upper Channel, sample pairs collected within two graded turbidite beds fine upward from 1.9 to 3.0 phi and from 3.4 to 4.0 phi. Most Upper Channel and all Intermediate Basin samples have homogeneous coarsest silt to finest sand size (4.2 - 3.9 phi) and feldspar-rich feldspatho-quartzose composition (Fig. 4). The base of the coarsest turbidite bed is feldspatho-quartzose (Fig. 3A), and one very coarse silt is quartzo-feldspathic. The few rock fragments include mostly low- to high-rank metasedimentary, some granitoid, and a few sedimentary types. Mica (mostly biotite) is abundant in very coarse silt. The mostly moderately rich tHM suite includes abundant blue/green and subordinately green/brown amphibole, epidote, and minor clinopyroxene, titanite, garnet, zircon, mostly prismatic sillimanite, hypersthene, tourmaline, and apatite (ZTR 5 ± 2). The coarsest sample is enriched in garnet (Table 2). Allochems make up 31 ± 19% of framework grains. In Upper Channel samples, planktonic and benthic foraminifera are associated with encrusting forams, red and green algae, echinoid plates and spines, mollusks, and peloids. In Intermediate Basin samples, planktonic foraminifera become dominant and benthic forams and red or green algae rare (Fig. 3B). Glaucony is minor (≤ 2%; Fig. 3A).

Among the analyzed chemical elements, most depleted relative to the UCC standard are Mg, Co, Ca, Fe, Sc, and to a lesser extent Sr (Table 3). Enriched are Zr, Hf, and to a lesser extent Ti and Ba, as in Zambezi River sand. The REE patterns are similar as in Zambezi River sediments, with moderately to strongly negative Eu anomaly (Eu/Eu* 0.71 ± 0.14) (Fig. 5E). The ε_{Nd} values and model ages display limited variability (ε_{Nd} -15.4 ± 1.0, $T_{Nd,CHUR}$ 1520 ± 87, $T_{Nd,DM}$ 1994 ± 75) (Fig. 6). The U-Pb zircon-age spectra of Upper Channel samples display a main Irumide (late Stenian) peak, with common Pan-African (Neoproterozoic) ages, minor Carboniferous and Orosirian ages, and rare Neoarchean ages. The Intermediate Basin sample shows a distinct Orosirian peak (Fig. 7).

Tsiribihina Valley

The four studied very coarse silts to very fine sands (4.1 to 3.4 phi) are feldspar-rich feldspatho-quartzose and display progressively increasing quartz/plagioclase ratio with increasing grain size (from F 43%QFL and P/F 57% to F 36%QFL and P/F 39%) (Fig. 3C). Rock fragments are negligible, but mica is common (biotite ≥ muscovite). The moderately rich tHM suite is dominated by mostly blue/green and subordinately green/brown amphibole with minor garnet, zircon, prismatic sillimanite, epidote, clinopyroxene, apatite, tourmaline, titanite, and rare anatase, rutile, kyanite, monazite, staurolite and hypersthene (ZTR 6 - 10). Allochems (mostly planktonic foraminifera) make up 15 ± 4% of framework grains.

Tsiribihina Valley sediments are richer in Sr, Ba, LREE, Th, Zr, and Hf than other turbidite samples (Table 3). REE patterns are steeper, with negative to strongly negative Eu anomaly (Eu/Eu* 0.59 ± 0.12) (Fig. 5E). The ε_{Nd} values are more negative (ε_{Nd} -20.6 ± 1.9), and model ages older ($T_{Nd,CHUR}$ 1772 ± 36, $T_{Nd,DM}$ 2160 ± 15) (Fig. 6). All isotope values are intermediate between Madagascar river sands in the north and in the south, and closer to Morondava beach sand in the central part of the region. U-Pb ages of detrital zircons are mostly Neoproterozoic (mainly Ediacaran and subordinately Cryogenian) and subordinately Paleoproterozoic (mainly Orosirian) (Fig. 7). A few Paleoarchean zircons also occur.

Lower Valley and Lower Fan

Both Lower Valley samples are very fine sands (3.8 phi), whereas the studied Lower Fan turbidites include a very fine sand (3.7 phi) and a medium sand (1.7 phi) containing 12% very coarse sand (maximum diameter observed in thin section 1.6 mm; Fig. 3D). Composition is invariably feldspar-rich feldspatho-quartzose (Table 2). Rare granitoid rock fragments occur, and mica is common (biotite ≥ muscovite). Moderately rich tHM suites are dominated by blue/green and subordinately green/brown amphibole with epidote and minor garnet, zircon, clinopyroxene, titanite, mainly prismatic sillimanite, apatite, tourmaline, and rare hypersthene, rutile, kyanite, staurolite, and monazite. Allochems (mostly planktonic foraminifera) make up 14 ± 3% of framework grains in very fine sand.

Lower Zambezi Valley and Fan sediments are enriched in Ba and Sr relative to Upper Channel and Intermediate Basin sediments and depleted in all other analyzed elements (Table 3). The steepness of REE patterns is intermediate between Upper Channel and Tsiribihina Valley turbidites, with moderately negative Eu anomaly (Eu/Eu* 0.78 ± 0.06) (Fig. 5E). The ε_{Nd} value (-19.2 ± 2.2) and Nd model ages ($T_{Nd,CHUR}$ 1725 ± 132, $T_{Nd,DM}$ 2136 ± 101) are more negative and older than for sediments in the upper part of the Zambezi submarine system, and closer to Madagascar river and beach sands (Fig. 6).

U-Pb ages of detrital zircons are mostly Cambrian to Stenian. Cryogenian and subordinately Ediacaran (Pan-African) ages prevail in Lower Valley samples and late Stenian (Irumide) ages prevail in the Lower Fan sample (Fig. 7). Siderian and Statherian ages occur in Lower Valley samples, whereas the Lower Fan sample yielded sparse Mesoproterozoic to Neoarchean ages and a few Carboniferous-age grains.

COMPOSITIONAL VARIABILITY

This section focuses on the mineralogical and geochemical variability observed in the Zambezi deep-sea sedimentary system among different turbidite beds, within the same bed, and among different grain-size classes within the same sample. The potential controlling factors (grain size, settling equivalence, selective entrainment, transport mechanism, transport distance, mechanical breakdown, chemical weathering, eustasy, and age) are discussed. The eleven Upper Channel to Intermediate Basin samples were considered as a first approximation of unvaried provenance.

Intersample Mineralogical and Geochemical Variability

Upper Channel to Intermediate Basin samples display a significant grain-size-dependent intersample compositional variability (Table 2). Quartz increases with grain size, whereas K-feldspar remains roughly constant, and plagioclase decreases (P/F 53 ± 5% in silt and 37 ± 8% in medium sand; correlation coefficients *r* mostly ~ 0.70, significant at the 0.1% level). Mica is most abundant in very coarse silt (< 60 µm; 11 - 26%), decreases in very fine sand (60 - 100 µm; 2 - 9%), and becomes minor in fine to medium sand (1 - 2%). No clear correlation is observed between heavy-mineral concentration and grain size. Coarser samples tend to have more garnet, staurolite, sillimanite, rutile, and zircon, and less epidote and pyroxene ($r \geq 0.68$, significant at the 2% to 1% level). Negative correlation with grain size is observed for Mg, Ca, Sr, Sc, Co, Eu ($r < -0.85$, sign. lev. 1‰) and to a lesser extent Fe and Ba. The Eu anomaly, moderately negative in very coarse silt to very fine sand (Eu/Eu* 0.78 ± 0.04), becomes more strongly negative in fine (Eu/Eu* 0.46) and medium sand (Eu/Eu* 0.42). No significant correlation is observed between ε_{Nd} and T_{Nd} model ages with grain size.

Intrabed Mineralogical and Geochemical Variability

To investigate compositional change during deposition by a turbidity current, sample pairs were collected in the lower and upper parts of two graded Upper Channel turbidite beds. In the coarser bed, quartz decreases, plagioclase doubles, and untwinned K-feldspar increases faster than cross-hatched microcline from medium sand at the base of the bed (5959; median grain size 266 µm) to lower fine sand above (5958; median grain size 127 µm). Biotite also increases upward. Especially opaque Fe-Ti-Cr oxides, as well as garnet, staurolite, kyanite, sillimanite, zircon, and monazite are more common in sample 5959, whereas pyroxene, epidote, amphibole, titanite, and andalusite are more common in sample 5958, suggesting that lower-density minerals tend to increase upward at the expense of higher-density minerals. All analyzed chemical elements increase in sample 5958, largely as an effect of decreasing quartz content. The ε_{Nd} value is more negative and model ages slightly older in the finer upper sample 5958 (Fig. 6).

Changes in grain size and composition are minor in the finer turbidite bed. Biotite and heavy minerals increase in the upper sample (5961; median grain size 60 μm) but with no significant relative variations among species. Most elements tend to increase in sample 5961, but Fe and Ba decrease, and Sr, Th, and Co remain constant. The ε_{Nd} value is more negative and model ages older in the coarser lower sample (5962; median grain size 93 μm) (Fig. 6).

Intrasample Mineralogical Variability

Manual Raman counting of six phi classes (from 32 - 63 μm to 1000 - 2000 μm) of the low-density fraction of Lower Fan sample 5976 (median grain size 307 μm) allowed us to document a steady mineralogical trend, with marked concentration of plagioclase in the fine tail of the size distribution and of quartz in the coarse tail (Fig. 8; full dataset provided in Appendix Table A5 *Intrasample tectosilicate variability*). Plagioclase decreases more rapidly than orthoclase in coarser classes, orthoclase more rapidly than microcline, and microcline more rapidly than quartz. The systematic decrease of plagioclase and the tendency of microcline and quartz to concentrate in coarser classes (Fig. 8) are confirmed by combined mineralogical and grain-size information obtained by semi-automated Raman analysis ($r \geq 0.96$, considering only samples in which enough grains were identified in four phi classes at least). The tendency of the Q/F ratio to increase with grain size, long reported from continental to shallow-marine sandstone suites (Graham 1930; Odom et al. 1976), is thus firmly documented to occur in deep-sea turbidites as well (Marsaglia et al. 1996; Garzanti et al. 2021b).

Phyllosilicates are common in the very coarse silt class, minor in the very fine sand class, and rare in the fine sand class. The same trend is displayed by carbonates that occur in the very coarse silt class, where calcite predominates over dolomite, but only sporadically in the very fine and fine sand classes. Among heavy minerals, less dense amphibole is systematically concentrated in coarser classes relative to epidote (r mostly ≥ 0.98). Low-density sillimanite and tourmaline are also preferentially concentrated in coarser classes, and high-density monazite, zircon, and rutile in finer classes, which is explained by the settling-equivalence principle (Rubey 1933; Garzanti et al. 2008).

Because differences in density are minor among tectosilicates (microcline and orthoclase 2.56 g/cm^3, albite 2.62 g/cm^3, quartz 2.65 g/cm^3, andesine 2.67 g/cm^3), the observed systematic size relationships (quartz > microcline > orthoclase > plagioclase) can hardly be accounted for by settling equivalence. They rather reflect the different ability of detrital tectosilicates to survive weathering and recycling, quartz being most durable and well-ordered triclinic microcline more resistant than monoclinic orthoclase, whereas Ca-rich plagioclase is widely considered as least resistant in most chemical environments (e.g., Blatt 1967; Todd 1968; Nesbitt et al. 1997). The clear grain-size-dependent intrasample variability of relative tectosilicate abundances is thus mainly ascribed to chemical reduction in size by weathering favored by the good cleavability especially of plagioclase grains (Basu 1976; Garzanti 1986). Lower density and larger size in source rocks of K-feldspar relative to plagioclase are possible additional factors.

Mineralogical and Geochemical Variability in Space

The concentration of many chemical elements (e.g., Sc, Mg, Co, Fe, Eu, Co, Ti, and Sr) tends to be higher in Intermediate Basin samples than in Upper Channel samples largely as an effect of finer grain size and lower quartz content. Higher heavy-mineral concentration in Intermediate Basin samples, independently indicated by their slightly higher Zr and REE contents (Fig. 5B), points to winnowing and selective entrainment of lower-density grains by contour currents. The more marked mineralogical and geochemical changes observed in the Lower Valley and Lower Fan samples are chiefly provenance-related and caused by mixing of Africa-derived and Madagascar-derived sediment in similar proportions (as discussed below). The coarsest studied sample from the Zambezi submarine system is from the Lower Fan, and downcurrent fining and sorting with transport distance was not observed.

Sediment mixing and homogenization on submarine valley floors occur through repeated episodes of erosion and reworking by turbidity currents and contour currents, as suggested by a variety of bedforms indicative of seabed transport (e.g., sand waves, ripples, scours, knickpoints; Mitchell 2006; Rodrigues et al. 2022). Very coarse sand contains small pebbles in the Lower Valley (Simpson et al. 1974) and is transported to as far as the Lower Fan, indicating that coarse sediment travels as bedload in the dense basal part of the current. This implies that sand is not necessarily carried all the way to the fan in one shot, but it is mainly dragged stepwise along the thalweg by recurrent deposition and reworking, leading to progressive compositional homogenization. This mechanism explains why sand below the junction of the Zambezi and Tsiribihina valleys can be considered as a mixture of detritus supplied from both Africa and Madagascar homogenized through time to various degrees. Mixing does not take place equally effectively in the steeper Tsiribihina Valley, where different turbidite beds maintain a distinct composition.

Mineralogical and Geochemical Variability in Time

Inspection of the compositional signatures of six Upper Channel, five Intermediate Basin, and six outer-shelf to uppermost-slope samples fails to display a clear time-dependent trend. Middle Pleistocene turbidites tend to be richer in Fe, Mg, Sc, and Co, which can be accounted for by their finer grain size. The sample pair collected in the MIS5 turbidite bed shows an intrabed compositional variability of the same order of, or greater than, differences with older and younger samples.

Because the studied turbidites were mostly deposited during glacial (lowstand) stages, compositional differences between lowstand and highstand deposits could be investigated only for outer-shelf to uppermost-slope samples. No systematic mineralogical difference, however, could be observed among sediments deposited during the last glacial lowstand, the postglacial warming and sea-level rise, and the Holocene highstand, possibly because of sediment reworking and homogenization in coastal areas and across wide continental shelves (Sharman et al. 2021; Malkovski et al. 2022).

GEOCHEMICAL BUDGETS

Geochemical data integrated with precise information obtained by semi-automated Raman analysis on the relative abundances of REE-bearing accessory minerals (e.g., monazite, titanite, apatite, zircon, allanite) and on their distribution in different grain-size classes provide firmer constraints on the REE budget while shedding additional light on grain-size-dependent mineralogical variability. The abundances given in this section are corrected for volumetric effects but do not consider inclusions (e.g., zircon in biotite) and should thus be taken as minimum values. The contributions of zircon to the Zr budget and of monazite and other REE-bearing minerals to the Nd budget of each turbidite sample are calculated assuming Zr 465,000 ppm in zircon, Nd 94,000 ppm in monazite, Nd 140 ppm in epidote, Nd 60 ppm in amphibole, Nd 18 ppm in mica, Nd 5 ppm in feldspar, and Nd 0.7 ppm in quartz (values after Garzanti et al. 2010, 2011). No allanite grain was detected during either point counting or semi-automated Raman counting. More careful manual and semi-automated Raman reanalysis confirmed that single allanite grains are indeed exceedingly rare but may be present at the core of some epidote grains (Fig. 9). In the impossibility to precisely assess the very low allanite content, we did not consider allanite as separate from epidote in the following calculations, which may result in a slight overestimation of the monazite contribution to the REE budget.

Zircon, the Zr/Hf Ratio, and the Zr Budget

Geochemical data indicate that all studied turbidite samples have higher to much higher (3.3 ± 1.6 times) Zr concentration than the UCC standard (i.e., Zr 192 ppm), with maximum values obtained for Tsiribihina Valley samples (Zr 953 ± 344 ppm). Integration of point-counting and semi-automated Raman-counting data indicate that the average zircon content is lower (0.07 ± 0.03 wt%) in Upper

Channel and Intermediate Basin turbidites, higher (0.14 ± 0.06 wt%) in very fine Tsiribihina Valley sand, and intermediate (0.10 ± 0.03 wt%) in the Lower Valley and Lower Fan.

The systematic increase of the Zr/Hf ratio from mud samples, where Zr/Hf is close to chondritic values (i.e., 34 - 37; McDonough and Sun 1995; Weyer et al. 2002), to sand samples, where Zr/Hf is close to the expected average ratio in zircon (i.e, ~ 47; Bea et al. 2006), indicates that the zircon contribution to the Zr budget is strongly dependent on grain size. On the African side, Zr/Hf decreases steadily from 45.8 in fine sand to 44.0 in very fine sand of the Zambezi River, and from 48.2 in medium sand to 40.3 in fine sand and to 38.6 ± 0.8 in very fine sand of Upper Channel and Intermediate Basin turbidites (Table 3). It does not change significantly, instead, from the very coarse silt fraction to the cohesive silt fraction of Zambezi River sediments (32 - 63 µm class: Zr/Hf 35.7 ± 0.5; < 32 µm fraction: Zr/Hf 35.2 ± 1.1). On the Madagascar side, the Zr/Hf ratio varies from 41.9 ± 0.8 in upper fine to lower medium river sands to 39.5 ± 0.7 in very fine turbidite sand of the Tsiribihina Valley. In the Lower Valley and Lower Fan, Zr/Hf is 41.2 in medium sand and 39.6 ± 1.9 in very fine sand (Table 3). This implies that, although most Zr is contained in zircon (up to 96% in coarser sand samples), a significant fraction of Zr is contained in other minerals that are concentrated in finer-grained sediment and have lower Zr/Hf ratio (e.g., phyllosilicates and feldspars; Bea et al. 2006). The alternative explanation that finer-grained zircon grains (e.g., inclusions in biotite) have a significantly lower Zr/Hf ratio is considered unlikely. Our data also indicate that zircon grains in upper fine to lower medium Lower Zambezi River sand have a higher average Zr/Hf ratio than in Madagascar sands of the same grain size (Table 3). Because the Zr/Hf ratio in magmatic rocks decreases regularly with progressive differentiation (Wang et al. 2010; Wu et al. 2017), this reflects a greater abundance of heavily fractionated leucocratic granitic source rocks in Madagascar than in Mozambique.

Monazite and the Nd Budget

As for zircon, monazite content is estimated to be lower in Upper Channel and Intermediate Basin turbidites – where it increases from 0.002 ± 0.001 wt% in very coarse silt and extremely fine sand to 0.008 ± 0.002 wt% in fine sand −, notably higher (0.040 ± 0.009 wt%) in very fine sand of the Tsiribihina Valley, and intermediate although highly variable (0.021 ± 0.019 wt%) in very fine to lower medium sand of the Lower Valley and Lower Fan. The monazite contribution to the Nd budget is calculated to increase steadily with median grain size in Upper Channel to Intermediate Basin turbidites – from 9 ± 3% (~60 μm) to 25 ± 7% (~125 μm) and up to 44 ± 3% (~250 μm) –, and to be markedly higher (67 ± 13%) in very fine sand of the Tsiribihina Valley and intermediate but poorly constrained in the Lower Valley and Lower Fan. Other major contributors to the Nd budget are epidote-group minerals and titanite, which are estimated to account for ~ 25% Nd (somewhat more if allanite was underestimated) and ~ 15% Nd on average. Apatite and amphibole account for no more than 5% Nd each. The remaining Nd is contributed mostly by tectosilicates (10 ± 5%) and phyllosilicates (up to 10% in very coarse silt).

Controls on the Variability of ε_{Nd} Values

Epsilon Nd values are less negative in Africa-derived sand (ε_{Nd} -15.1 ± 1.9 for the Lower Zambezi River and Quelimane estuary and beach; ε_{Nd} -15.4 ± 1.0 in the Upper Channel and Intermediate Basin) than in Madagascar-derived sand (ε_{Nd} -20.4 ± 2.9 in SW Madagascar rivers and beach; ε_{Nd} -20.6 ± 1.9 in the Tsiribihina Valley). Markedly negative values (ε_{Nd} -19.2 ± 2.2) also characterize the Lower Valley and Lower Fan. In Upper Channel and Intermediate Basin turbidites, ε_{Nd} tends to become more negative with increasing monazite contribution (e.g., in sample 5958 from the upper part of the coarsest Upper Channel turbidite, where enrichment in monazite is indicated by higher LREE, Th, and Nd/Sm ratio) (Figs. 5B and 6). The good correlation between ε_{Nd} and Nd/Sm in all 19 turbidite samples (*r* -0.93, sign. lev. << 1‰) further suggests that monazite carries a more negative ε_{Nd} signal than other Nd-bearing detrital components.

TRACING SEDIMENT COMPOSITION IN TIME AND SPACE

This study of the Zambezi deep-sea channel and fan, jointly with complementary information acquired on sedimentary processes in the entire Zambezi drainage basin and SW Madagascar, sheds new light on the Middle Pleistocene to recent evolution of this complex sedimentary system. Inferences about the anthropogenic impact on natural Zambezi sediment transport are made by assuming that the compositional differences between modern river sand and Quaternary submarine deposits principally resulted from sediment impoundment by large dams constructed since the second half of the 20th century. Provenance and relative detrital supply from the two sides of the Mozambique Channel are next evaluated based on the compositional variability of deep-water deposits.

Zambezi Sediment Transport in Pre-Dam **vs.** *Post-Dam Times*

The Zambezi catchment is ~ 1.38 million km^3, subdivided among the upper catchment upstream of Kariba Dam (663,800 km^3; 48%), the middle catchment between Kariba and Cahora Bassa dams (386,200 km^3; 28%), and the lower catchment from Cahora Bassa to the Delta (328,000 km^3; 24%). Water discharge is subdivided in similar proportions among the upper (annual average 1276 m^3/s; 37%), middle (1166 m^3/s; 34%), and lower catchments (982 m^3/s; 29%) (Beilfuss and Dos Santos 2001). The sediment mass reaching the Indian Ocean today is much lower than it was before the construction of the Kariba and Cahora Bassa Dams (Ronco et al. 2010; Mikhailov et al. 2015). Because different geological units are exposed and eroded in different parts of the Zambezi catchment, the effect of such a profound artificial river segmentation by dams is reflected in the composition of modern Lower Zambezi sediments, which are derived today only from the erosion of medium- to high-grade basement rocks of Irumide and Pan-African orogens exposed downstream of Cahora Bassa Dam.

In many segmented river systems where all detritus generated upstream is impounded in large dams, the mineralogical signal can be nevertheless transmitted downstream by reworking of previously deposited channel, floodplain, and terrace deposits, thus damping the dam effect (e.g., Garzanti et al. 2000, 2015; Vezzoli et al. 2016; Malkovski et al. 2019; Thomson et al. 2022). This may well occur where the dominant erosional *foci* are located upstream of the dams and the river flows across open lowland landscape downstream, which is hardly the case for the Zambezi River, where all compositional signatures change radically and irreversibly downstream of Lake Kariba first, and of Lake Cahora Bassa next (Garzanti et al. 2021a, 2022a). The narrow and steep river valley lacks floodplains downstream of the dams, where the youthful river course is largely carved in bedrock, forming particularly impressive rapids along the Cahora Bassa Gorge (Davies et al. 2000).

Any accurate estimate of sediment yields and erosion rates in the Zambezi catchment is prevented by the virtually complete absence of gauged sediment fluxes and uncertain assessment of sediment volumes accumulating in the reservoirs. Estimates on annual solid transport range widely between 20 and 100 million tons (Hay 1998), with a median value around 50 million tons (ESIA 2011; Milliman and Farnsworth 2011), corresponding to average annual sediment yields between 15 and 70 t/km^2. Total sediment production can be tentatively apportioned among the upper, middle, and lower catchments based on the available estimates of sediment yields. Cosmogenic nuclides in the uppermost Zambezi catchment (Wittmann et al. 2020), sediment concentration in the middle catchment (Bolton 1984), and numerical models in the middle and lower catchment (Ronco et al. 2010) suggest that annual sediment yields vary from as low as 2 ± 2 t/km^2 for the low-relief Kalahari Basin to 200 t/km^2 for Middle and Lower Zambezi tributaries flowing steeply across basement rocks exposed in the Archean Zimbabwe Craton or in the Proterozoic lrumide, Umkondo, and Zambezi Belts in southern Zambia, northern Zimbabwe, and western Mozambique. By integrating all available constraints (see Garzanti et al. 2022a), our best guess is that 5 - 10 million tons (≤ 10%) are generated in the upper catchment and trapped in the Kariba reservoir, 50 - 60 million tons (60 - 65%) in the middle catchment and trapped in the Cahora Bassa reservoir, and 20 - 25 million tons (25 - 30%) in the lower catchment and carried to the Zambezi Delta annually. These estimates imply that less than a third of the original sediment flux is making its way to the ocean today. Such a strong change can be tested by comparing the compositional signatures of modern Lower Zambezi fluvial sediments and pre-dam turbidites accumulated in the deep sea.

Zambezi Provenance Signatures: The Anthropogenic Effect

The petrographic, mineralogical, geochemical, and geochronological study of the Zambezi sedimentary system through space and time allows us to determine the compositional variability of sediments generated in the Zambezi catchment and supplied to the Mozambique passive margin before and after the construction of the big dams, and thus to tentatively assess the effect of anthropogenic modifications on natural sediment transport.

Because of significant grain-size-dependent intersample compositional variability, and because of other potential superposed factors, a sharp difference between pre-dam and post-dam Zambezi sediments does not emerge immediately from a cursory inspection of our integrated petrographic - mineralogical database, which includes mostly feldspar-rich feldspatho-quartzose very coarse silts and sands (Table 2). Once samples of different grain size are separately examined, however, a systematic difference between modern fluvial sediments and Quaternary submarine deposits clearly appears. Quaternary Upper Channel and Intermediate Basin turbidites are invariably richer in quartz, poorer in feldspars (with higher Mic*/F), and somewhat poorer in heavy minerals with higher relative amounts of durable ZTR species, thus revealing a significant supply of detritus generated in the middle catchment plus lesser amounts of recycled quartz-rich eolian sediment from the Kalahari Basin (Fig. 3A).

The relative contributions from the upper, middle, and lower catchments can be tentatively quantified by forward mixing calculations based on integrated petrographic and heavy-mineral data and performed separately for groups of samples with different grain size (i.e., ~ 4 phi, *vs.* ~ 3 phi, *vs.* ~ 2 phi). The results suggest that Quaternary Zambezi River sediments were generated ≤ 10% in the upper catchment, ~ 60% in the middle catchment, and ≥ 30% in the lower catchment. These approximate figures are consistent with estimates of sediment generation based on sediment yields and represent our best estimate given the available information.

Geochemical data confirm more quartz dilution for pre-dam turbidites, with lower concentration especially of Fe, Mg, Sc, and Co (Table 3), and more negative Eu anomaly (Fig. 5), indicating a lower percentage contribution from mafic rocks of the Irumide orogen exposed in the Lower Zambezi catchment (e.g., Tete gabbro-anorthosite and Blantyre mafic granulites). Epsilon Nd values, however, do not differ significantly in modern Zambezi River (-14.9 ± 0.8) and Quaternary Upper Channel to Intermediate Basin sediments (-15.4 ± 1.0).

Further consistent information is provided by U-Pb age spectra of detrital zircons. Upper Channel samples yielded more Ediacaran and Carboniferous zircon ages than modern Lower Zambezi sand, and locally a few more Neoarchean ages. Most significant is the Orosirian age peak displayed by the Intermediate Basin sample, which points to a conspicuous sediment supply from the Zambezi catchment upstream of Cahora Bassa in the Middle Pleistocene (Fig. 7). Multidimensional scaling analysis highlights the affinity of zircon-age spectra in sand generated today in the Lower and Middle Zambezi catchments with that of Upper Channel and Intermediate Basin samples, respectively (Fig. 10). In this regard it must be noted that zircon contribution from the Upper Zambezi is expected to be barely observable, because zircon concentration is one order of magnitude less in Upper Zambezi sand (~ 0.01%) than in Middle and Lower Zambezi sands (~ 0.2%).

Provenance from Madagascar

The four Tsiribihina Valley samples are compositionally heterogeneous, indicating mixed supply in various proportions not only from the Tsiribihina River and subordinately Manambolo River to the north of the canyon, but largely from the Mangoky River in the south. This is explained by the mainly northward littoral sand drift along the shores of SW Madagascar, as indicated by numerous deltaic spits in the region, although counter-transport locally prevails with smaller spits oriented southward in response to wave diffraction (see Figure 17 in Anthony 2015).

Samples 5969 and 5971 contain less amphibole and more garnet, and have notably steeper REE patterns (Fig. 5E, 5F) and much more negative ε_{Nd} (Fig. 6) than samples 5970 and 5972. The elemental geochemistry of Tsiribihina Valley samples is closer to Tsiribihina sand than to Mangoky sand. Independent calculations based on the integrated petrographic and heavy-mineral suites and on Nd-isotope data consistently indicate predominant supply from the Mangoky River for sample 5971

(MIS8, ~ 250 ka) and to a lesser extent for sample 5969 (MIS5a, ~ 80 ka), and from the Tsiribihina River for samples 5970 (MIS6, ~ 160 ka) and 5972 (MIS 8/9, ~ 280 ka). Calculations based on zircon ages indicate that 80 - 85% of zircon grains in samples 5969 and 5971 combined are supplied by the Mangoky River, an affinity highlighted by the MDS plot (Fig. 10). All data considered, sample 5971 is held to contain 75 - 80% Mangoky sand and ~ 20% Tsiribihina sand, sample 5969 55 - 60% Mangoky sand and 35% Tsiribihina sand, and samples 5970 and 5972 50 - 60% Tsiribihina sand and ≤ 30% Mangoky sand, the rest being supplied by the Manambolo and other smaller rivers.

Provenance Budget: Africa* vs. *Madagascar

The Zambezi Fan is fed chiefly by the Zambezi River from the African side but partly also from the Madagascar side, mostly *via* the Tsiribihina Valley. Being produced by the erosion of two largely dissected rifted margins, sediment generated in Africa and Madagascar shares similar quartzo-feldspathic to feldspatho-quartzose composition (Garzanti et al. 2001). Madagascar supplies somewhat more quartz and K-feldspar and less mica and heavy minerals, notably less epidote, less pyroxene and titanite, and relatively more ZTR minerals, amphibole, and garnet (Table 2). Madagascar-derived sediment contains less Fe, Ca, Sc, and Co, more Sr, and much more Ba, reflecting more felsic crustal sources overall (Table 3). Y, REE, Th, Zr, and Hf are also higher, and LREE patterns steeper (Fig. 5E), indicating greater amounts of monazite and zircon. Zircon grains yield mostly Irumide (late Stenian) U-Pb ages in African-derived sediment and mostly Pan-African (Ediacaran and Cryogenian) U-Pb ages in Madagascar-derived sediment, which also contains a few grains as old as the Paleoarchean. The ε_{Nd} values are more negative and T_{Nd} model ages older in Madagascar sands, which can be explained by extensive remelting of Archean and Paleoproterozoic crustal protoliths (Kröner et al. 2000; Collins 2006).

Mineralogical (Fig. 4), geochemical (Fig. 6), and geochronological (Figs. 7, 10, and 11) parameters are all intermediate and variable in Lower Valley and Lower Fan deposits, indicating prominent sediment contribution from SW Madagascar despite a much smaller catchment area (Fig. 12).

Forward mixing calculations based on integrated petrographic and heavy-mineral suites indicate that sediment supply from Africa and Madagascar are of the same order of magnitude but lack precision, because of broadly similar signatures and superposed grain-size and hydraulic-sorting effects. Calculations based on elemental geochemistry confirm the importance of Madagascar supply, and calculations based on Nd isotopic signatures even suggest a predominance of Madagascar detrital sources. Calculations based on geochronological data suggest that zircon grains are mostly (up to 85%) derived from Madagascar in Lower Valley samples and largely (55 - 60%) from Africa in the Lower Fan sample, consistently with multidimensional scaling analysis (Fig. 10). Most robust are calculations based on integrated petrographic, heavy-mineral, elemental-geochemistry, and Nd-isotope datasets, which indicate that sediment in the Lower Valley and Lower Fan is largely fed from the Zambezi River but with no less than a third of the total volume supplied from SW Madagascar (Fig. 12). This can be explained if a conspicuous fraction of Africa-derived sediment is trapped in the Intermediate Basin and thus only partly reaches as far as the deep-sea fan.

CONCLUSIONS

The Zambezi submarine valley and deep-sea fan, located in the Mozambique Channel between the African landmass and Madagascar Island, represent the final part of the Zambezi sediment-routing system, extending over ~ 5000 km from the South African Plateau to Indian Ocean floors. Sediment derived from Africa and Madagascar shares similar feldspar-rich feldspatho-quartzose composition with moderately rich transparent heavy-mineral suites including amphibole, subordinate epidote, and minor clinopyroxene and garnet. Madagascar-derived sediment has somewhat more quartz and K-feldspar, notably less epidote, less pyroxene and titanite, and relatively more ZTR minerals, amphibole, and garnet. It contains less Fe, Ca, Sc, and Co, more Sr, and much more Ba, testifying to more felsic crustal sources overall. REE and Zr concentrations are also higher, and LREE patterns steeper with more pronounced negative Eu anomaly, reflecting greater amounts of ultradense monazite and zircon. Moreover, ε_{Nd} values are markedly more negative and T_{Nd} model ages notably older, reflecting extensive remelting of Archean and Paleoproterozoic crustal protoliths.

U-Pb age spectra of detrital zircons clearly differentiate between Zambezi River sand, dominated by Irumide (late Stenian) grains, and Madagascar-derived sand, dominated by Pan-African (Ediacaran - Cryogenian) grains. SW Madagascar river sands and Tsiribihina Valley turbidites yield a few zircon grains as old as Paleoarchean and many discordant ages, reflecting Pan-African reworking of Archean cratonic rocks. Age spectra of Mangoky River and Tsiribihina Valley zircons are quite similar, which suggests that the Mangoky River is a major sediment contributor from the Madagascar side, as consistently indicated by petrographic, heavy-mineral, and geochemical signatures. Lower Valley and Lower Fan samples display both Irumide and Pan-African peaks, confirming subequal zircon contribution from Africa and Madagascar. Major sediment supply from SW Madagascar to the Lower Valley and Fan despite a much smaller catchment area can be explained by deposition of a conspicuous part of Africa-derived detritus in the Intermediate Basin.

Although compositional variability is chiefly provenance-related and caused by mixing of Africa-derived and Madagascar-derived sediment in Lower Valley and Lower Fan turbidites, other controls are also relevant. With increasing grain size, both among and within samples, quartz progressively increases relative to microcline, microcline relative to orthoclase, and orthoclase relative to plagioclase, as documented by manual and semi-automated Raman counting. Higher heavy-mineral concentration in Intermediate Basin samples is ascribed to winnowing and selective entrainment of lower-density grains by contour currents. No systematic downcurrent-fining trend is apparent, the coarsest studied sample being a medium sand from the Lower Fan containing 12% very coarse sand fraction.

This provenance study of Quaternary turbidites of the Zambezi submarine valley and fan allowed us to investigate the impact caused by anthropogenic modifications of the natural Zambezi sediment-routing system. Quaternary deep-sea deposits of the Upper Channel are richer in quartz than sand in the modern Lower Zambezi River, poorer in feldspars (with a higher microcline proportion), and somewhat poorer in heavy minerals with higher relative amount of durable ZTR species. Upper Channel turbidites yielded more zircon grains with Ediacaran, Carboniferous, and Neoarchean ages than modern Lower Zambezi sand, and the Intermediate Basin sample displays a prominent Orosirian age peak lacking in modern Lower Zambezi sand. All these differences are explained by prominent detritus from the Middle Zambezi catchment reaching the ocean before construction of the Kariba and Cahora Bassa dams, together with minor amounts of rounded quartz recycled from the Kalahari Basin.

ACKNOWLEDGMENTS

We are very grateful to captains, crew, and scientists of the oceanographic cruises PAMELA MOZ01, MOZ02, and MOZ04 onboard the research vessels *L'Atalante* and *Pourquoi pas*, who allowed us to collect offshore and deep-sea samples. The PAMELA (Passive Margin Exploration Laboratories) scientific project is led by IFREMER and TOTAL in collaboration with the Université de Bretagne Occidentale, Université Rennes 1, Université Pierre et Marie Curie, CNRS, and IFPEN. The IODP sample from Site U1477 and sand samples from the Quelimane area were kindly provided by Hucai Zhang and Junsheng Nie (Lanzhou University) and by Celso de Carvalho Matsinhe (Tongji Univeristy, Shanghai). Marta Padoan collected samples in Madagascar and Sergio Andò provided precious advice during Raman analysis of tectosilicates and heavy minerals. The article, an outcome of Project MIUR – Dipartimenti di Eccellenza 2018-2022, Department of Earth and Environmental Sciences, University of Milano - Bicocca, benefited from careful handling by JSR Editor Kathleen Marsaglia, Associate Editor Shane Tyrrell, and excellent critical reviews and advice by Tim Lawton and a second anonymous reviewer.

SUPPLEMENTARY MATERIALS

Supplementary data associated with this article include detailed information on sampling sites (Table A1) along with grain-size (Table A2), petrographic (Table A3), heavy-mineral (Table A4), manual

Raman counting (Table A5), semi-automated Raman counting (Tables A6 and A7), and elemental geochemistry and Nd-isotope datasets (Table A8). Appendix A contains the appendix table captions as well as detailed information on the rationale and method of forward compositional modelling. Appendix B contains the complete dataset of U-Pb detrital-zircon ages. The Google-Earth^{TM} map of sampling sites *Zambezi Fan.kmz* is also provided. Supplementary data can be found online at https://doi.org/_______ or provided by the corresponding author upon request.

DATA AVAILABILITY

Sediment cores collected in the Zambezi deep-sea sedimentary system are curated at IFREMER (*Institut Français de Recherche pour l'Exploitation de la Mer*) core repository in Plouzané, France. Core data related to this article can be requested at http://igsn.org/BFBGX-127456/461/680/682 and http://igsn.org/BFBGX-128005/007/010.

FIGURE CAPTIONS

Figure 1. The Zambezi sediment routing system from source to sink, with location map and sampling sites (base map from Google Earth™). Topographically and tectonically confined southward sediment dispersal in the Mozambique Channel according to Fierens et al. (2019, 2022); VF = Victoria Falls; pv = paleovalley.

Figure 2. The mixed turbiditic - contouritic Zambezi submarine system (redrawn after Fierens et al. 2022). Depositional areas include the ponded intraslope Intermediate Basin, semi-confined between the buried Beira High and the *Îles Éparses*, and the coarser-grained channelized Lower Fan, flanked along the western side by sediment waves testifying to extensive reworking by bottom currents.

Figure 3. Petrographic photomicrographs of turbidites in the Zambezi deep-sea channel and fan (sample number, median grain size in microns, and quartz/feldspar ratio are indicated; all photos with crossed polars, blue bar for scale = 100 μm). Composition is feldspatho-quartzose to feldspar-rich feldspatho-quartzose with common cross-hatched microcline (K). **A**) Rounded quartz (rQ), plausibly recycled from Kalahari eolian sands, and green glaucony (g); **B**, **C**) mica (m) and planktonic foraminifera (*f*) increase with decreasing grain size; **D**) abraded overgrowths on quartz grain (Q; arrows) indicate recycling.

Figure 4. Sand petrography and heavy minerals. Grain-size-dependent intersample and intrabed compositional variabilities are indicated by symbol size (increasing with sample grain size) and orange arrows (connecting bottom to top of same turbidite bed). **A)** QFL plot. Quartz is enriched in coarser samples. **B)** QPK plot. Plagioclase is enriched in finer samples. **C)** Biplots based on heavy mineral data (tHMC, transparent heavy-mineral concentration; ZTR, zircon + tourmaline + rutile); **D**) Biplot based on integrated mineralogical data (GSZ, grain size; Q, quartz; K, K-feldspar; P, plagioclase). Biplots (Gabriel 1971) allow discrimination among multivariate observations (points), while highlighting relationships among multiple variables (rays); length of rays is proportional to the

variance of corresponding variables, which are correlated if the angle between rays is 0° (anticorrelated if it is 180°).

Figure 5. Chondrite-normalized REE patterns (arrows indicate the effect of increasing quartz, monazite, or zircon percentages). **A**, **B**) Zambezi-derived sediments display similar patterns, but REE decrease with increasing quartz dilution in coarser samples; the coarser Upper Channel turbidite bed (samples 5959 -> 5958) is distinguished by a strong Eu anomaly. **C, D, E, F**) Sand generated in Madagascar shows higher LREE fractionation (samples 5969 and 5971), indicating enrichment in monazite. Manambolo sand shows convex-upward HREE pattern reflecting contribution of heaviest-HREE-rich zircon and rarity of monazite, as testified by the highest Zr/Th ratio. Lower Valley (5973, 5974) and Lower Fan (5975, 5976) turbidites display intermediate features, indicating mixing of Africa-derived and Madagascar-derived detritus.

Figure 6. Multiple controls on Nd isotopes. Madagascar-derived sand has more negative ε_{Nd} values and older T_{DM} ages than Africa-derived sediments. Zambezi sediments have lower Nd/Sm ratio than the UCC standard and thus plot above the theoretical relationship between ε_{Nd} and T_{DM} age (thicker line), whereas those Madagascar-derived sediments displaying highest LREE fractionation plot below it. Tsiribihina Valley samples yield heterogeneous ε_{Nd} values, indicating main supply either from Tsiribihina (5970, 5972) or Mangoky (5969, 5971) rivers. Signatures of Lower Valley and Lower Fan samples suggest important contribution from Madagascar (5974, 5976). Both intersample and intrabed variability is unrelated to grain size (orange arrows point toward finer-grained upper sample in same Upper Channel turbidite bed).

Figure 7. U-Pb age spectra of detrital zircons (plotted as kernel density estimates with the *provenance* package of Vermeesch et al. 2016; full dataset provided in Appendix B). Zambezi sand is dominated by late Stenian (~ 1.05 Ga; Irumide) ages, whereas ages in Madagascar river sands are mostly Neoproterozoic (Pan-African), the main peak becoming younger from north to south. In the submarine system, Upper Channel samples display more Pan-African ages than Zambezi River

samples, and the Intermediate Basin sample yielded many more Orosirian (Eburnean) ages. Tsiribihina Valley zircons show very similar spectra to Mangoky and Morondava sands. Lower Valley zircon ages are mostly Neoproterozoic, indicating clear Madagascar affinity, whereas the Lower Fan sample displays both Irumide and Neoproterozoic peaks indicating similar zircon contribution from Africa and Madagascar. Data for Upper Channel, Lower Valley, and Tsiribihina Valley are combined from sample pairs. Lower and Middle Zambezi spectra are also composite, the latter including ages from the Gwai, Kafue, and Luangwa rivers.

Figure 8. Strong grain-size-dependent intrasample variability of relative tectosilicate abundances assessed by manual Raman grain counting of six phi classes of Lower Zambezi Fan sample 5976 (median grain size 307 μm; Fig. 3A). Plagioclase concentrates in the fine tail of the size distribution relative to orthoclase, orthoclase relative to microcline, and microcline relative to quartz. Q, quartz; K, K-feldspar; P, plagioclase.

Figure 9. Occurrence of allanite concealed at the core of an epidote grain (**A**; sample 5971 Tsiribihina Valley). **B**) Raman map based on point analysis at 2.5 µm distance (brown: allanite; green: epidote; white: low signal). Diagnostic peak positions of epidote (**C**) and allanite (**D**) after Andò and Garzanti (2014).

Figure 10. Multidimensional scaling (MDS) map based on U-Pb zircon-age spectra shown in Fig. 7. Zambezi River zircons yielded mostly late Stenian (Irumide) ages, zircons in Madagascar sands mostly Pan-African ages. MDS analysis produces a map of points in which the distance among samples is approximately proportional to the Kolmogorov-Smirnov dissimilarity of their chronological signatures. Closest and second-closest neighbors are linked by solid and dashed lines, respectively. The goodness of fit is evaluated by the "stress" value of the configuration (20, poor; 10, fair; 5, good; Vermeesch 2013, 2018).

Figure 11. The three-way MDS plot combines five independent datasets (petrography, heavy minerals, elemental geochemistry, Nd isotopes, and zircon ages) to reveal significant detrital supply

from SW Madagascar rivers to Lower Zambezi Valley and Fan deposits. The graphical output of three-way MDS results from stretching or shrinking of dissimilarity matrices of heterogeneous datasets in *x* and *y* dimensions to a degree measured by the "source weights" (plotted in inset; Kruskal and Wish 1978; Vermeesch and Garzanti 2015). All samples are plotted individually.

Figure 12. The segmented Zambezi sedimentary system from source to sink. Pie diagrams illustrate average QFL and transparent-heavy-mineral (tHM) proportions in diverse parts of the system (diameter of QFL and tHM pies proportional to sediment flux and tHM concentration, respectively). Average ε_{Nd} values are shown. No less than a third of detritus in the Lower Valley and Fan is derived from SW Madagascar (mostly from Mangoky and Tsiribihina rivers) even though the Zambezi River catchment is ~ 10 times larger. Q, quartz; F, feldspar; L, lithics; ZTR, zircon + tourmaline + rutile; GSK, garnet + staurolite + kyanite + sillimanite; Ep, epidote; Amp, amphibole; Px, pyroxene; &tHM, others (mostly titanite and apatite).

Table 1. Information on the 19 studied deep-sea sediment samples from the Zambezi submarine system. Cores MOZ1-KS26 and MOZ4-CS22 are only 35 m apart. CS, Calypso coring system; KS, Kullenberg system. IGSN, International Geo Sample Number with hyperlink for core data request. Ages of Marine Isotope Stages (MIS) from Railsback et al. (2015).

Table 2. Key petrographic and heavy-mineral parameters. GSZ (median grain size in phi units); Q, quartz; F, feldspars (P, plagioclase); L, lithic grains; tHMC, transparent heavy-mineral concentration; ZTR, zircon + tourmaline + rutile; Ep, epidote; Grt, garnet; SKA, staurolite + kyanite + andalusite + sillimanite; Amp, amphibole; Px, pyroxene; &tHM, other transparent heavy minerals (titanite, apatite, minor anatase and monazite); n°, number of samples.

Table 3. Key geochemical parameters. GSZ (grain size in phi units); n°, number of samples; n.d., not determined.

REFERENCES

Allen, P.A., 2008, From landscapes into geological history: Nature, v. 451(7176), p. 274-276.

Andò, S., 2020, Gravimetric separation of heavy minerals in sediments: Minerals, v. 10(3), n° 273, doi:10.3390/min10030273.

Andò, S., and Garzanti, E., 2014, Raman spectroscopy in heavy-mineral studies, in Scott, R.A., Smyth. H.R., Morton, A.C., Richardson, N., eds., Sediment provenance studies in hydrocarbon exploration and production: Geological Society of London, Special Publication 386(1), p. 395-412.

Andò, S., Vignola, P., and Garzanti, E., 2011, Raman counting: a new method to determine provenance of silt: Rendiconti Lincei Scienze Fisiche e Naturali, v. 22, p. 327-347.

Anthony, E.J., 2015, Wave influence in the construction, shaping and destruction of river deltas: A review: Marine Geology, v. 361, p. 53-78.

Barrat, J.A., Keller, F., Amossé, J., Taylor, R.N., Nesbitt, R.W., and Hirata, T., 1996, Determination of rare earth elements in sixteen silicate reference samples by ICP-MS after Tm addition and ion exchange separation: Geostandards Newsletter, v. 20(1), p. 133-139.

Barrat, J.A., Zanda, B., Moynier, F., Bollinger, C., Liorzou, C., Bayon, G., 2012, Geochemistry of CI chondrites: Major and trace elements, and Cu and Zn isotopes: Geochimica et Cosmochimica Acta, v. 83, p. 79-92.

Basu, A., 1976, Petrology of Holocene fluvial sand derived from plutonic source rocks: Implications to paleoclimatic interpretation: Journal of Sedimentary Petrology, v. 46(3), p. 694-709.

Bayon, G., German, C.R., Boella, R.M., Milton, J.A., Taylor, R.N., and Nesbitt, R.W., 2002, An improved method for extracting marine sediment fractions and its application to Sr and Nd isotopic analysis: Chemical Geology, v. 187, p. 179-199.

Bea, F., Montero, P., and Ortega, M., 2006, A LA-ICP-MS evaluation of Zr reservoirs in common crustal rocks: implications for Zr and Hf geochemistry, and zircon-forming processes: The Canadian Mineralogist, v. 44(3), p. 693-714.

Beiersdorf, H., Kudrass, H.R., von Stakelberg, U., 1980, Placer deposits of ilmenite and zircon on the Zambezi shelf: Geologisches Jahrbuch, Reihe D36, 85 p.

Beilfuss, R., and dos Santos, D. 2001, Patterns of Hydrological Change in the Zambezi Delta, Mozambique. Working Paper #2. Program for the Sustainable Management of the Cahora Bassa Dam and the Lower Zambezi Valley. Baraboo, Wisconsin: International Crane Foundation, 159 p.

Beilfuss, R.D., Dutton, P., and Moore, D., 2000, Land cover and land use change in the Zambezi delta, *in* Timberlake, J., ed., Biodiversity of the Zambezi Basin Wetlands: Biodiversity Foundation for Africa, Bulawayo, Zimbabwe, v. 3, p. 31-106.

Blatt, H., 1967, Provenance determinations and recycling of sediments: Journal of Sedimentary Petrology, v. 37, p. 1031-1044.

Bolton, P., 1984, Sediment deposition in major reservoirs in the Zambezi Basin, in Challenges in African Hydrology and Water Resources: International Association of Hydrological Sciences, Publication 144, p. 559-567.

Bouvier, A., Vervoort, J.D., and Patchett, P.J., 2008, The Lu-Hf and Sm-Nd isotopic composition of CHUR: Constraints from unequilibrated chondrites and implications for the bulk composition of terrestrial planets: Earth and Planetary Science Letters, v. 273, p. 48-57.

Breitzke, M., Wiles, E., Krocker, R., Watkeys, M.K., and Jokat, W., 2017, Seafloor morphology in the Mozambique Channel: evidence for long-term persistent bottom-current flow and deep-reaching eddy activity: Marine Geophysical Research, v. 38(3), p. 241-269.

Butt, A.J., and Gould, K. 2018, 3D source-rock modelling in frontier basins: A case study from the Zambezi Delta Depression: Petroleum Geoscience, v. 24(3), p. 277-286.

Caracciolo, L., 2020, Sediment generation and sediment routing systems from a quantitative provenance analysis perspective: Review, application, and future development: Earth-Science Reviews, v. 209, n° 103226.

Castelino, J.A., Reichert, C., and Jokat, W., 2017, Response of Cenozoic turbidite system to tectonic activity and sea-level change off the Zambezi Delta: Marine Geophysical Research, v. 38(3), p.

209-226.

Collins, A.S., 2006, Madagascar and the amalgamation of Central Gondwana: Gondwana Research, v. 9(1-2), p. 3-16.

Collins, A.S., Kröner, A., Fitzsimons, I.C., and Razakamanana, T., 2003, Detrital footprint of the Mozambique ocean: U-Pb SHRIMP and Pb evaporation zircon geochronology of metasedimentary gneisses in eastern Madagascar: Tectonophysics, v. 375(1-4), p. 77-99.

Courgeon, S., Jorry, S.J., Camoin, G.F., BouDagher-Fadel, M.K., Jouet, G., Révillon, S., Bachèlery, P., Pelleter, E., Borgomano, J., Poli, E., and Droxler, A.W., 2016, Growth and demise of Cenozoic isolated carbonate platforms: New insights from the Mozambique Channel seamounts (SW Indian Ocean): Marine Geology, v. 380, p. 90-105.

Cox, K.G., 1989, The role of mantle plumes in the development of continental drainage patterns: Nature, v. 342(6252), p. 873-877.

Davies, B.R., Beilfuss, R.D., and Thoms, M.C., 2000, Cahora Bassa retrospective, 1974 - 1997: Effects of flow regulation on the Lower Zambezi River: Internationale Vereinigung für theoretische und angewandte Limnologie, Verhandlungen, v. 27(4), p. 2149-2157.

De Paolo, D.J., 1981, Neodymium isotopes in the Colorado Front Range and crust - mantle evolution in the Proterozoic: Nature, v. 291(5812), p. 193-196.

Dickinson, W.R., 1988, Provenance and sediment dispersal in relation to paleotectonics and paleogeography of sedimentary basins, *in* Kleinspehn, K.L., and Paola, C., eds., New Perspectives in Basin Analysis: Berlin, Springer, p. 3-25.

Droz, L., and Mougenot, D., 1987, Mozambique upper fan: Origin of depositional units: American Association of Petroleum Geologists, Bulletin, v. 71(11), p. 1355-1365.

Ebinger, C.E., and Scholz, C.A., 2012, Continental rift basins: the East African perspective, *in* Busby, C., and Azor, A., eds., Tectonics of Sedimentary Basins: Recent Advances: Oxford, Wiley-Blackwell, p. 185-208.

ESIA, 2011, Riversdale’s Zambezi River Barging Project, Zambezi River, Mozambique: Final

Environmental and Social Impact Assessment Report, 335 p.

Fernandes, P., Cogné, N., Chew, D.M., Rodrigues, B., Jorge, R.C.G.S., Marques, J., Jamal, D., and Vasconcelos, L., 2015, The thermal history of the Karoo Moatize - Minjova Basin, Tete Province, Mozambique: An integrated vitrinite reflectance and apatite fission track thermochronology study: Journal of African Earth Sciences, v. 112, p. 55-72.

Fierens, R., Droz, L., Toucanne, S., Raisson, F., Jouet, G., Babonneau, N., Miramontes, E., Landurain, S., and Jorry, S.J., 2019, Late Quaternary geomorphology and sedimentary processes in the Zambezi turbidite system (Mozambique Channel): Geomorphology, v. 334, p. 1-28.

Fierens, R., Toucanne, S., Droz, L., Jouet, G., Raisson, F., Jorissen, E.L., Bayon, G., Giraudeau, J., and Jorry, S., 2020, Quaternary sediment dispersal in the Zambezi turbidite system (SW Indian Ocean): Marine Geology, 428, n°106276, doi.org/10.1016/j.margeo.2020.106276.

Fierens, R., Droz, L., Jouet, G., Rabineau, M., Raisson, F., Babonneau, N., Robin, C., and Jorry, S.J., 2022, Sedimentary evolution and effects of structural controls on the development of the Zambezi mixed turbidite - contourite system (Mozambique channel, southwest Indian Ocean) since the Oligocene: Marine and Petroleum Geology, v. 138, n°105532.

Flemming, B.W., and Kudrass, H.R., 2018, Large dunes on the outer shelf off the Zambezi Delta, Mozambique: Evidence for the existence of a Mozambique Current: Geo-Marine Letters, v. 38(1), p. 95-106.

Freeman, J.J., Wang, A., Kuebler, K.E., Jolliff, B.L., and Haskin, L.A., 2008, Characterization of natural feldspars by Raman spectroscopy for future planetary exploration: The Canadian Mineralogist, v. 46(6), p. 1477-1500.

Gabriel, K.R., 1971, The biplot graphic display of matrices with application to principal component analysis: Biometrika, v. 58, p. 453-467.

Garçon, M., 2021, Episodic growth of felsic continents in the past 3.7 Ga: Science Advances, v. 7(39), eabj1807.

Garzanti, E., 1986, Source rock versus sedimentary control on the mineralogy of deltaic volcanic arenites (Upper Triassic, northern Italy): Journal of Sedimentary Petrology, v. 56(2), p. 267-275.

Garzanti, E., 2017, The maturity myth in sedimentology and provenance analysis: Journal of Sedimentary Research, v. 87, p. 353-365.

Garzanti, E., 2019, Petrographic classification of sand and sandstone: Earth-Science Reviews, v. 192, p. 545-563.

Garzanti, E., and Andò, S., 2019, Heavy Minerals for Junior Woodchucks: Minerals, v. 9(3), n° 148, doi:10.3390/min9030148.

Garzanti, E., Ando, S., and Scutella, M., 2000, Actualistic ophiolite provenance: The Cyprus case: The Journal of Geology, v. 108(2), p. 199-218.

Garzanti, E., Vezzoli, G., Ando, S., and Castiglioni, G., 2001, Petrology of rifted-margin sand (Red Sea and Gulf of Aden, Yemen): The Journal of Geology, v. 109(3), p. 277-297.

Garzanti, E., Andò, S., and Vezzoli, G., 2008, Settling equivalence of detrital minerals and grain-size dependence of sediment composition: Earth and Planetary Science Letters, v. 273, p.138-151.

Garzanti, E., Andò, S., France-Lanord, C., Vezzoli, G., Censi, P., Galy, V., and Najman, Y., 2010, Mineralogical and chemical variability of fluvial sediments: 1. Bedload sand (Ganga - Brahmaputra, Bangladesh): Earth and Planetary Science Letters, v. 299(3-4), p. 368-381.

Garzanti, E., Andó, S., France-Lanord, C., Censi, P., Vignola, P., Galy, V., and Lupker, M., 2011, Mineralogical and chemical variability of fluvial sediments: 2. Suspended-load silt (Ganga - Brahmaputra, Bangladesh): Earth and Planetary Science Letters, v. 302(1-2), p. 107-120.

Garzanti, E., Resentini, A., Vezzoli, G., Andò, S., Malusà, M., and Padoan, M., 2012, Forward compositional modelling of Alpine orogenic sediments: Sedimentary Geology, v. 280, p. 149-164.

Garzanti, E., Vermeesch, P., Padoan, M., Resentini, A., Vezzoli, G., and Andò, S., 2014a, Provenance of passive-margin sand (Southern Africa): The Journal of Geology, v. 122, p. 17-42.

Garzanti, E., Padoan, M., Setti, M., López-Galindo, A., and Villa, I.M., 2014b, Provenance versus weathering control on the composition of tropical river mud (southern Africa): Chemical Geology,

v. 366, p. 61-74.

Garzanti, E., Andò, S., Padoan, M., Vezzoli, G., and El Kammar, A., 2015, The modern Nile sediment system: Processes and products: Quaternary Science Reviews, v. 130, p. 9-56.

Garzanti, E., Dinis, P., Vermeesch, P., Andò, S., Hahn, A., Huvi, J., Limonta, M., Padoan, M., Resentini, A., Rittner, M., and Vezzoli, G., 2018a, Dynamic uplift, recycling, and climate control on the petrology of passive-margin sand (Angola): Sedimentary Geology, v. 375, p. 86-104.

Garzanti, E., Vermeesch, P., Rittner, M., and Simmons, M., 2018b, The zircon story of the Nile: Time-structure maps of source rocks and discontinuous propagation of detrital signals: Basin Research, v. 30(6), p. 1098-1117.

Garzanti, E., Andò, S., and Vezzoli, G., 2020, Provenance of Cenozoic Indus Fan sediments (IODP Sites U1456 and U1457): Journal of Sedimentary Research, v. 90(9), p. 1114-1127.

Garzanti, E., Pastore, G., Resentini, A., Vezzoli, G., Vermeesch, P., Ncube, L., Van Niekerk, H-G., Jouet, G., and Dall'Asta, M., 2021a, The Segmented Zambezi Sedimentary System from Source to Sink 1. Sand Petrology and Heavy Minerals: The Journal of Geology, v. 129(4), p. 343-369.

Garzanti, E., Bayon, G., Dennielou, B., Barbarano, M., Limonta, M., and Vezzoli, G., 2021b, The Congo deep-sea fan: Mineralogical, REE, and Nd-isotope variability in quartzose passive-margin sand: Journal of Sedimentary Research, v. 91(5), p. 433-450.

Garzanti, E., Bayon, G., Dinis, P., Vermeesch, P., Pastore, G., Resentini, A., Barbarano, M., Ncube, L., and Van Niekerk, H.J., 2022a, The Segmented Zambezi Sedimentary System from Source to Sink: 2. Geochemistry, Clay Minerals, and Detrital Geochronology: The Journal of Geology, v. 130(3), p. 171-208.

Garzanti, E., Pastore, G., Stone, A., Vainer, S., Vermeesch, P., and Resentini, A., 2022b, Provenance of Kalahari sand: Paleoweathering and recycling in a linked fluvial - eolian system: Earth-Science Reviews, v. 224, n°103867, doi.org/10.1016/j.earscirev.2021.103867.

Goscombe, B., Foster, D.A., Gray, D., and Wade, B. 2020, Assembly of central Gondwana along the Zambezi Belt: Metamorphic response and basement reactivation during the Kuunga Orogeny:

Gondwana Research, v. 80, p. 410-465.

Graham, W.A.P., 1930, A textural and petrographic study of the Cambrian sandstones of Minnesota: The Journal of Geology, v. 38, p. 696-716.

Griffin, W.L., Powell, W.J., Pearson, N.J., and O'Reilly, S.Y. 2008, GLITTER: Data reduction software for laser ablation ICP-MS, *in* Sylvester, P., ed., Laser ablation-ICP-MS in the Earth Sciences: Current practices and outstanding issues: Mineralogical Association of Canada, Short Course Series 40, p. 204-207.

Gumbricht, T., McCarthy, T.S., and Merry, C.L., 2001, The topography of the Okavango Delta, Botswana, and its tectonic and sedimentological implications: South African Journal of Geology, v. 104(3), p. 243-264.

Hall, I.R. et al. (28 co-authors), 2016, International Ocean Discovery Program; Expedition 361 Preliminary Report; South African Climates (Agulhas LGM Density Profile); 30 January-31 March 2016: College Station, Texas (International Ocean Discovery Program), doi.org/10.14379/iodp.pr.361.2016.

Hall, I.R. et al. (28 co-authors), 2017, Site U1477, *in* Hall, I.R., Hemming, S.R., LeVay, L.J., and the Expedition 361 Scientists, South African Climates (Agulhas LGM Density Profile). Proceedings of the International Ocean Discovery Program, 361: College Station, Texas (International Ocean Discovery Program), doi.org/10.14379/iodp.proc.361.106.2017

Hay, W.W., 1998, Detrital sediment fluxes from continents to oceans: Chemical Geology, v. 145(3-4), p. 287-323.

Hessler, A.M., and Fildani, A., 2019, Deep-sea fans: Tapping into Earth's changing landscapes: Journal of Sedimentary Research, v. 89(11), p. 1171-1179.

Hoguane, A.M., Gammelsrød, T., Mazzilli, S., Antonio, M.H., and da Silva, N.B.F., 2020, The hydrodynamics of the Bons Sinais Estuary: The value of simple hydrodynamic tidal models in understanding circulation in estuaries of central Mozambique: Regional Studies in Marine Science, v. 37, n° 101352.

Hubert, J.F., 1962, A zircon – tourmaline - rutile maturity index and the interdependence of the composition of heavy mineral assemblages with the gross composition and texture of sandstones: Journal of Sedimentary Petrology, v. 32, p. 440-450.

Ingersoll, R.V., and Suczek, C.A., 1979, Petrology and provenance of Neogene sand from Nicobar and Bengal fans, DSDP sites 211 and 218: Journal of Sedimentary Petrology, v. 49(4), p.1217-1228.

Ingersoll, R.V., Bullard, T.F., Ford, R.L., Grimm, J.P., Pickle, J.D., and Sares, S.W., 1984, The effect of grain size on detrital modes: A test of the Gazzi-Dickinson point-counting method: Journal of Sedimentary Petrology, v. 54, p. 103-116.

Jackson, S.E., Pearson, N.J., Griffin, W.L., and Belousova, E.A., 2004, The application of laser ablation - inductively coupled plasma - mass spectrometry to in situ U-Pb zircon geochronology: Chemical Geology, v. 211, p. 47-69.

Johnsson, M.J., 1993, The system controlling the composition of clastic sediments, *in* Johnsson, M.J., and Basu, A., eds., Processes Controlling the Composition of Clastic Sediments: Geological Society of America, Special Paper 284, p. 1-19.

Jouet, G., and Deville, E., 2015, PAMELA-MOZ04 cruise, RV *Pourquoi pas*, doi.org/10.17600/15000700.

Key, R.M., Cotterill, F.P.D., and Moore, A.E., 2015, The Zambezi River: An archive of tectonic events linked to the amalgamation and disruption of Gondwana and subsequent evolution of the African plate: South African Journal of Geology, v. 118(4), p. 425-438.

Kinabo, B.D., Atekwana, E.A., Hogan, J.P., Modisi, M.P., Wheaton, D.D., and Kampunzu, A.B., 2007, Early structural development of the Okavango rift zone, NW Botswana: Journal of African Earth Sciences, v. 48(2-3), p. 125-136.

Kolla, V., Kostecki, J.A., Henderson, L., and Hess, L., 1980a, Morphology and Quaternary sedimentation of the Mozambique Fan and environs, southwestern Indian Oceans: Sedimentology, v. 27(4), p. 357-378.

Kolla, V., Eittreim, S., Sullivan, L., Kostecki, J.A., and Burckle, L.H., 1980b, Current-controlled, abyssal microtopography and sedimentation in Mozambique Basin, southwest Indian Ocean: Marine Geology, v. 34(3-4), p. 171-206.

Kröner, A., Hegner, E., Collins, A.S., Windley, B.F., Brewer, T.S., Razakamanana, T., and Pidgeon, R.T., 2000, Age and magmatic history of the Antananarivo Block, central Madagascar, as derived from zircon geochronology and Nd isotopic systematics: American Journal of Science, v. 300(4), p. 251-288.

Kruskal. J.B., and Wish, M., 1978, Three-way multidimensional scaling, *in* Kruskal, J.B., and Wish, M., eds., Multidimensional Scaling: Sage Publications, Thousand Oaks, Quantitative Applications in the Social Sciences, p. 60-72.

Kunz, M.J., Anselmetti, F.S., Wüest, A., Wehrli, B., Vollenweider, A., Thüring, S., and Senn, D.B., 2011, Sediment accumulation and carbon, nitrogen, and phosphorus deposition in the large tropical reservoir Lake Kariba (Zambia/Zimbabwe): Journal of Geophysical Research, Biogeosciences, v. 116(G3), n° G03003, doi:10.1029/2010JG001538.

Leinweber, V.T., and Jokat, W., 2012, The Jurassic history of the Africa-Antarctica corridor — new constraints from magnetic data on the conjugate continental margins: Tectonophysics, v. 530, p. 87-101.

Ludwig, K.R.,1998, On the treatment of concordant uranium - lead ages: Geochimica et Cosmochimica Acta, v. 62(4), p. 665-676.

Lünsdorf, N.K., and Lünsdorf, J.O., 2016, Evaluating Raman spectra of carbonaceous matter by automated, iterative curve-fitting: International Journal of Coal Geology, v. 160-161, p. 51-62.

Lünsdorf, N.K., Kalies, J., Ahlers, P., Dunkl, I., and von Eynatten, H., 2019, Semi-automated heavy-mineral analysis by Raman spectroscopy: Minerals, v. 9(7), n° 385.

Malkowski, M.A., Sharman, G.R., Johnstone, S.A., Grove, M.J., Kimbrough, D.L., and Graham, S.A., 2019, Dilution and propagation of provenance trends in sand and mud: Geochemistry and detrital zircon geochronology of modern sediment from central California (USA): American Journal of

Science, v. 319(10), p. 846-902.

Malkowski, M.A., Johnstone, S.A., Sharman, G.R., White, C.J., Scheirer, D.S., and Barth, G.A., 2022, Continental shelves as detrital mixers: U-Pb and Lu-Hf detrital zircon provenance of the Pleistocene - Holocene Bering Sea and its margin: The Depositional Record, v. 8, doi:10.1002/dep2.203.

Marsaglia, K.M., and Ingersoll, R.V., 1992, Compositional trends in arc-related, deep-marine sand and sandstone: A reassessment of magmatic-arc provenance: Geological Society of America, Bulletin, v. 104(12), p. 1637-1649.

Marsaglia, K.M., Barragan, J.G.C., Padilla, I., and Milliken, K.L., 1996, 11. Evolution of the Iberian passive margin as reflected in sand provenance, *in* Whitmarsh, R.B., Sawyer, D.S., Klaus, A., and Masson, D.G., eds., Proceedings of the Ocean Drilling Program, Scientific Results, v. 149, p. 269-280.

McDonough, W.F., and Sun, S.S., 1995, The composition of the Earth: Chemical Geology, v. 120(3-4), p. 223-253.

Mikhailov, V.N., Kravtsova, V.I., and Isupova, M.V., 2015, Impact of reservoirs on the hydrological regime and morphology of the lower reaches and delta of the Zambezi River (Mozambique): Water Resources, v. 42(2), p. 170-185.

Milliman, J.D., and Farnsworth, K.L., 2011, River Discharge to the Coastal Ocean: A Global Synthesis: Cambridge University Press, Cambridge, NY., 384 p.

Miramontes, E., Penven, P., Fierens, R., Droz, L., Toucanne, S., Jorry, S.J., Jouet, G., Pastor, L., Jacinto, R.S., Gaillot, A., and Giraudeau, J., 2019, The influence of bottom currents on the Zambezi Valley morphology (Mozambique Channel, SW Indian Ocean): In situ current observations and hydrodynamic modelling: Marine Geology, v. 410, p. 42-55.

Mitchell, N.C., 2006, Morphologies of knickpoints in submarine canyons: Geological Society of America, Bulletin, v. 118(5-6), p. 589-605.

Moore, A.E., and Larkin, P.A., 2001, Drainage evolution in south-central Africa since the breakup of Gondwana: South African Journal of Geology, v. 104(1), p. 47-68.

Moore, A.E., Cotterill, F.P.D., Main, M.P.L., and Williams, H.B., 2007, The Zambezi River, *in* Gupta, A., ed., Large Rivers: Geomorphology and Management: Chichester, Wiley, p. 311-332.

Nesbitt, H.W., Fedo, C.M., and Young, G.M., 1997, Quartz and feldspar stability, steady and non-steady-state weathering, and petrogenesis of siliciclastic sands and muds: The Journal of Geology, v. 105(2), p. 173-192.

Odom, I.E., Doe, T.W., and Dott, R.H., 1976, Nature of feldspar - grain size relations in some quartz-rich sandstones: Journal of Sedimentary Petrology, v. 46, p. 862-870.

Pickering, K., Carter, A., Andò, S., Garzanti, E., Limonta, M., Vezzoli, G., and Milliken, K.L., 2020, Deciphering relationships between the Nicobar and Bengal submarine fans, Indian Ocean: Earth and Planetary Science Letters, v. 544, n° 116329, doi.org/10.1016/j.epsl.2020.116329.

Ponte, J.P., Robin, C., Guillocheau, F., Popescu, S., Suc, J.P., Dall’Asta, M., Melinte-Dobrinescu, M.C., Bubik, M., Dupont, G., and Gaillot, J. 2019, The Zambezi delta (Mozambique Channel, East Africa): High resolution dating combining bio-orbital and seismic stratigraphies to determine climate (palaeoprecipitation) and tectonic controls on a passive margin: Marine and Petroleum Geology, v. 105, p. 293-312.

Railsback, L.B., Gibbard, P.L., Head, M.J., Voarintsoa, N.R.G., and Toucanne, S., 2015, An optimized scheme of lettered marine isotope substages for the last 1.0 million years, and the climatostratigraphic nature of isotope stages and substages: Quaternary Science Reviews, v. 111, p. 94-106.

Resentini, A., Goren, L., Castelltort, S., and Garzanti, E., 2017, Partitioning sediment flux by provenance and tracing erosion patterns in Taiwan: Journal of Geophysical Research, Earth Surface, v. 122(7), p. 1430-1454.

Rimington, N., Cramp, A., and Morton, A., 2000, Amazon Fan sands: Implications for provenance: Marine and Petroleum Geology, v. 17(2), p. 267-284.

Rodrigues, S., Hernández-Molina, F.J., Fonnesu, M., Miramontes, E., Rebesco, M., and Campbell, D.C., 2022, A new classification system for mixed (turbidite - contourite) depositional systems: Examples, conceptual models and diagnostic criteria for modern and ancient records: Earth-Science Reviews, 230, n°104030.

Ronco, P., Fasolato, G., Nones, M., and Di Silvio, G., 2010, Morphological effects of damming on lower Zambezi River: Geomorphology, v. 115(1-2), p. 43-55.

Rubey, W.W., 1933, The size-distribution of heavy minerals within a water-laid sandstone: Journal of Sedimentary Petrology, v. 3, p. 3-29.

Rudnick, R.L., and Gao, S., 2003, Composition of the continental crust, *in* Rudnick, R.L., Holland, H.D., and Turekian, K., eds., Treatise on Geochemistry, v. 3, The Crust: Elsevier Pergamon, Oxford, p. 1-64.

Schulz, H., Lückge, A., Emeis, K.C., and Mackensen, A. 2011, Variability of Holocene to Late Pleistocene Zambezi riverine sedimentation at the upper continental slope off Mozambique, 15° - 21° S: Marine Geology, v. 286, p. 21-34.

Sete, C.I., Ruby, J., and Dove, V., 2002, Seasonal variation of tides, currents, salinity and temperature along the coast of Mozambique: Instituto Nacional de Hidrografia e Navegacao, Maputo, 72 p., http://hdl.handle.net/1834/188

Sharman, G.R., Covault, J.A., Stockli, D.F., Sickmann, Z.T., Malkowski, M.A., and Johnstone, S.A., 2021, Detrital signals of coastal erosion and fluvial sediment supply during glacio-eustatic sea-level rise, Southern California, USA: Geology, v. 49(12), p. 1501-1505.

Sickmann, Z.T., Chheda, T.D., Capaldi, T.N., Thomson, K.D., Paull, C.K., and Graham, S.A., 2019, Using provenance analysis in an Anthropocene natural laboratory: Quaternary Science Reviews, v. 221, n°105890.

Simpson, E.S.W., and Shipboard Scientific Party, 1974, Sites 243 and 244, *in* Simpson, E., and Schlich, R., eds., Initial Reports of the Deep Sea Drilling Project, Leg 25: U.S. Government Printing Office, Washington, D.C, p. 177-186, doi:10.2973/dsdp.proc.25.106.1974.

Sláma, J., Košler, J., Condon, D.J., Crowley, J.L., Gerdes, A., Hanchar, J.M., Horstwood, M.S., Morris, G.A., Nasdala, L., Norberg, N., and Schaltegger, U., 2008, Plešovice zircon — a new natural reference material for U-Pb and Hf isotopic microanalysis: Chemical Geology, v. 249, p. 1-35.

Tanaka, T., Togashi, S., Kamioka, H., Amakawa, H., Kagami, H., Hamamoto, T., Yuhara, M., Orihashi, Y., Yoneda, S., Shimizu, H., Kunimaru, T., Takahashi, K., Yanagi, T., Nakano. T., Fujimaki, H., Shinjo, R., Asahara, Y., Tanimizu, M., and Dragusanu, C., 2000, JNdi-1: a neodymium isotopic reference in consistency with LaJolla neodymium: Chemical Geology, v. 168(3-4), p. 279-281.

Taylor, S.R., and Mclennan, S.M., 1995, The geochemical evolution of the continental crust: Reviews of Geophysics, v. 33, p. 241-265.

Thayer, P.A., Roberts, H.H., Bouma, A.H., and Coleman, J.M., 1986, 22. Sedimentology and petrology of Mississippi Fan depositional environments, *in* Bouma, A.H., Coleman, J.M., Meyer, A.W. et al., eds., Washington, D.C., U.S. Government Printing Office: Initial Reports of the Deep Sea Drilling Project, v. 96, p. 489-503.

Thompson, J.O., Moulin, M., Aslanian, D., De Clarens, P., and Guillocheau, F., 2019, New starting point for the Indian Ocean: Second phase of breakup for Gondwana: Earth-Science Reviews, v. 191, p. 26-56.

Thomson, K.D., Stockli, D.F., and Fildani, A., 2022, Anthropogenic impact on sediment transfer in the upper Missouri River catchment detected by detrital zircon analysis. Geological Society of America, Bulletin, doi.org/10.1130/B36217.1

Todd, T.W., 1968, Paleoclimatology and the relative stability of feldspar minerals under atmospheric conditions: Journal of Sedimentarty Petrology, v. 38, p. 832-844.

van der Lubbe, J.J.L., Tjallingii, R., Prins, M.A., Brummer, G.J.A., Jung, S.J.A., Kroon, D., and Schneider, R.R., 2014, Sedimentation patterns off the Zambezi River over the last 20,000 years: Marine Geology, v. 355, p. 189-201.

Vermeesch, P., 2013, Multi-sample comparison of detrital age distributions: Chemical Geology, v.

341, p. 140-146.

Vermeesch, P. 2018, IsoplotR: A free and open toolbox for geochronology: Geoscience Frontiers, v. 9, p. 1479-1493.

Vermeesch, P., 2021, On the treatment of discordant detrital zircon U-Pb data: Geochronology, v. 3(1), p. 247-257.

Vermeesch, P., and Garzanti, E., 2015, Making geological sense of ‘Big Data’ in sedimentary provenance analysis: Chemical Geology, v. 409, p. 20-27.

Vermeesch, P., Resentini, A., and Garzanti, E., 2016, An R package for statistical provenance analysis: Sedimentary Geology, v. 336, p. 14-25.

Vermeesch, P., Rittner, M., Petrou, E., Omma, J., Mattinson, C., and Garzanti, E., 2017, High throughput petrochronology and sedimentary provenance analysis by automated phase mapping and LAICPMS: Geochemistry, Geophysics, Geosystems, v. 18, p. 4096-4109.

Vezzoli, G., Garzanti, E., Limonta, M., Andò, S., and Yang, S., 2016, Erosion patterns in the Changjiang (Yangtze River) catchment revealed by bulk-sample versus single-mineral provenance budgets: Geomorphology, v. 261, p. 177-192.

Walford, H.L., White, N.J., and Sydow, J.C., 2005, Solid sediment load history of the Zambezi Delta: Earth and Planetary Science Letters, v. 238(1-2), p. 49-63.

Wang, X., Griffin, W.L., and Chen, J., 2010, Hf contents and Zr/Hf ratios in granitic zircons: Geochemical Journal, v. 44(1), p. 65-72.

Wellington, J. 1955, Southern Africa: A Geographical Study. 1. Physical Geography, Climate, Vegetation, and Soils: Hydrography: Cambridge, Cambridge University Press, 528 p.

Weltje, G.J., 1997, End-member modeling of compositional data: Numerical-statistical algorithms for solving the explicit mixing problem: Mathematical Geology, v. 29(4), p. 503-549.

Weltje, G.J., and von Eynatten, H., 2004, Quantitative provenance analysis of sediments: Review and outlook: Sedimentary Geology, v. 171(1-4), p. 1-11.

Weyer, S., Münker, C., Rehkämper, M., and Mezger, K., 2002, Determination of ultra-low Nb, Ta, Zr and Hf concentrations and the chondritic Zr/Hf and Nb/Ta ratios by isotope dilution analyses with multiple collector ICP-MS: Chemical Geology, v. 187(3-4), p. 295-313.

Wiles, E., Green, A., Watkeys, M., and Jokat, W., 2017a, The Zambezi Channel: A new perspective on submarine channel evolution at low latitudes: Geomorphology, v. 286, p. 121-132.

Wiles, E., Green, A.N., Watkeys, M.K., and Jokat, W., 2017b, Zambezi continental margin: Compartmentalized sediment transfer routes to the abyssal Mozambique Channel: Marine Geophysical Research, v. 38(3), p. 227-240.

Wittmann, H., Oelze, M., Gaillardet, J., Garzanti, E., and von Blanckenburg, F. 2020, A global rate of denudation from cosmogenic nuclides in the Earth's largest rivers: Earth-Science Reviews, v. 204, n°103147.

Wu, F., Liu, X., Ji, W., Wang, J., and Yang, L., 2017, Highly fractionated granites: Recognition and research: Science China Earth Sciences, 60(7), p. 1201-1219.

Zindorf, M., Rooze, J., Meile, C., März, C., Jouet, G., Newton, R., Brandily, C., and Pastor, L., 2021, The evolution of early diagenetic processes at the Mozambique margin during the last glacial - interglacial transition: Geochimica et Cosmochimica Acta, v. 300, p. 79-94.

Zuffa, G.G., 1985, Optical analyses of arenites: Influence of methodology on compositional results, *in* Zuffa, G.G., ed., Provenance of Arenites: Dordrecht, Reidel Publishing Company, NATO ASI Series, v. 148, p. 165-189.

Zuffa, G.G., Normark, W.R., Serra, F., and Brunner, C.A., 2000, Turbidite megabeds in an oceanic rift valley recording jökulhlaups of late Pleistocene glacial lakes of the western United States: The Journal of Geology, v. 108(3), p. 253-274.

Figure 1

Click here to access/download;Figure;Figure 1 ZambeFan Location.jpg

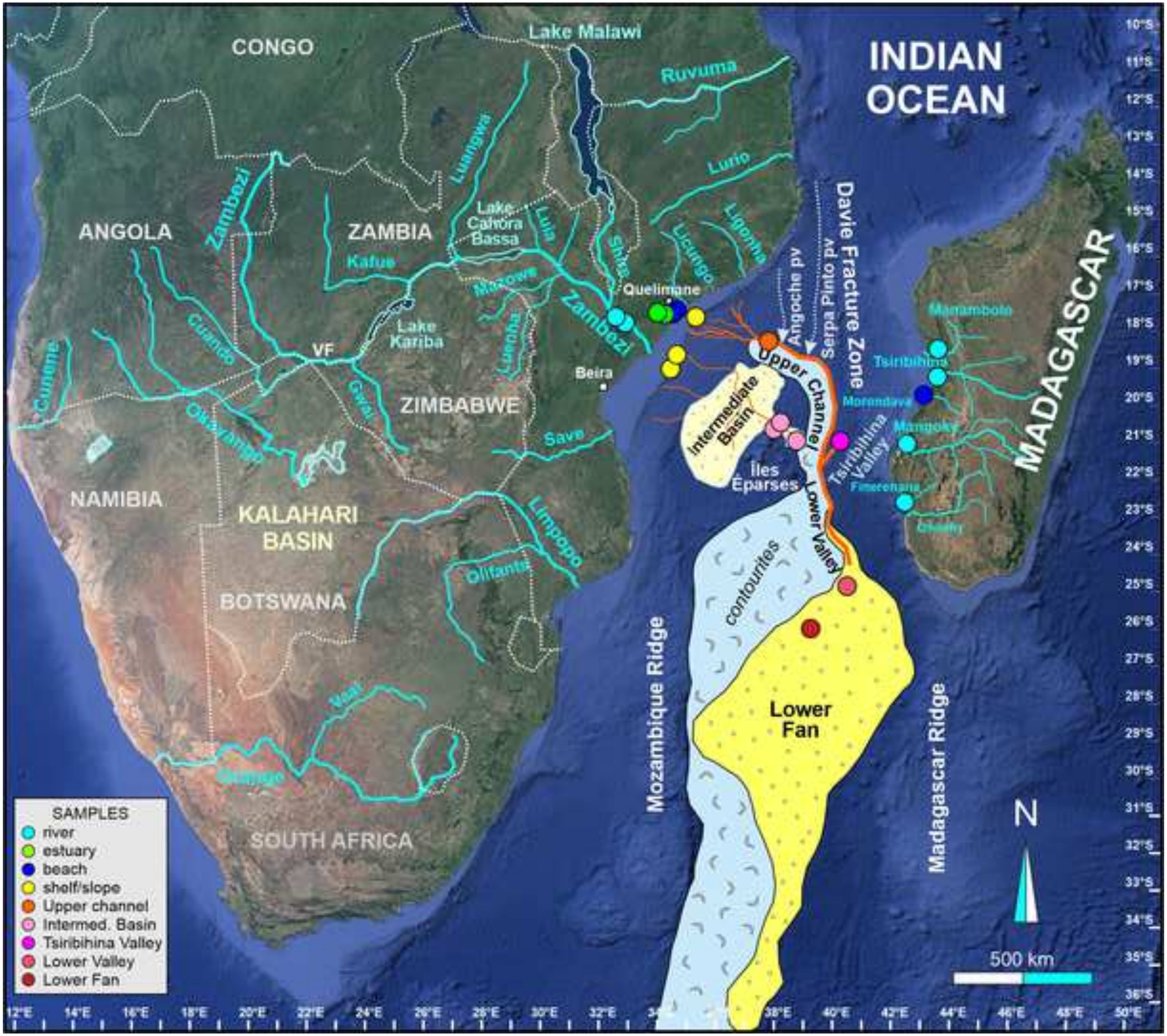

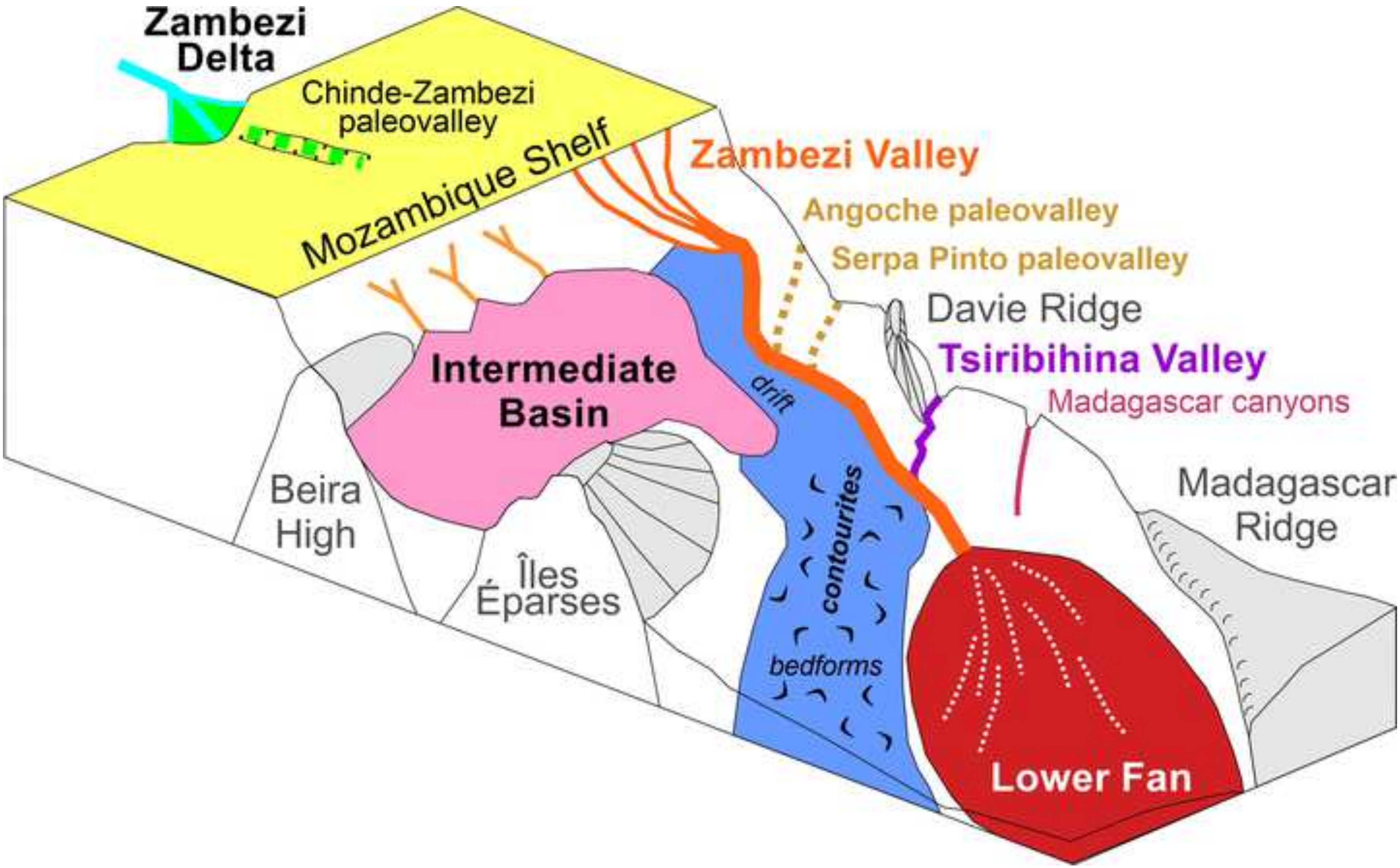
Zambezi Delta
Chinde-Zambezi paleovalley
Mozambique Shelf
Zambezi Valley
Angoche paleovalley
Serpa Pinto paleovalley
Davie Ridge
Tsiribihina Valley
Madagascar canyons
Intermediate Basin
drift
contourites
bedforms
Beira High
Îles Éparses
Madagascar Ridge
Lower Fan

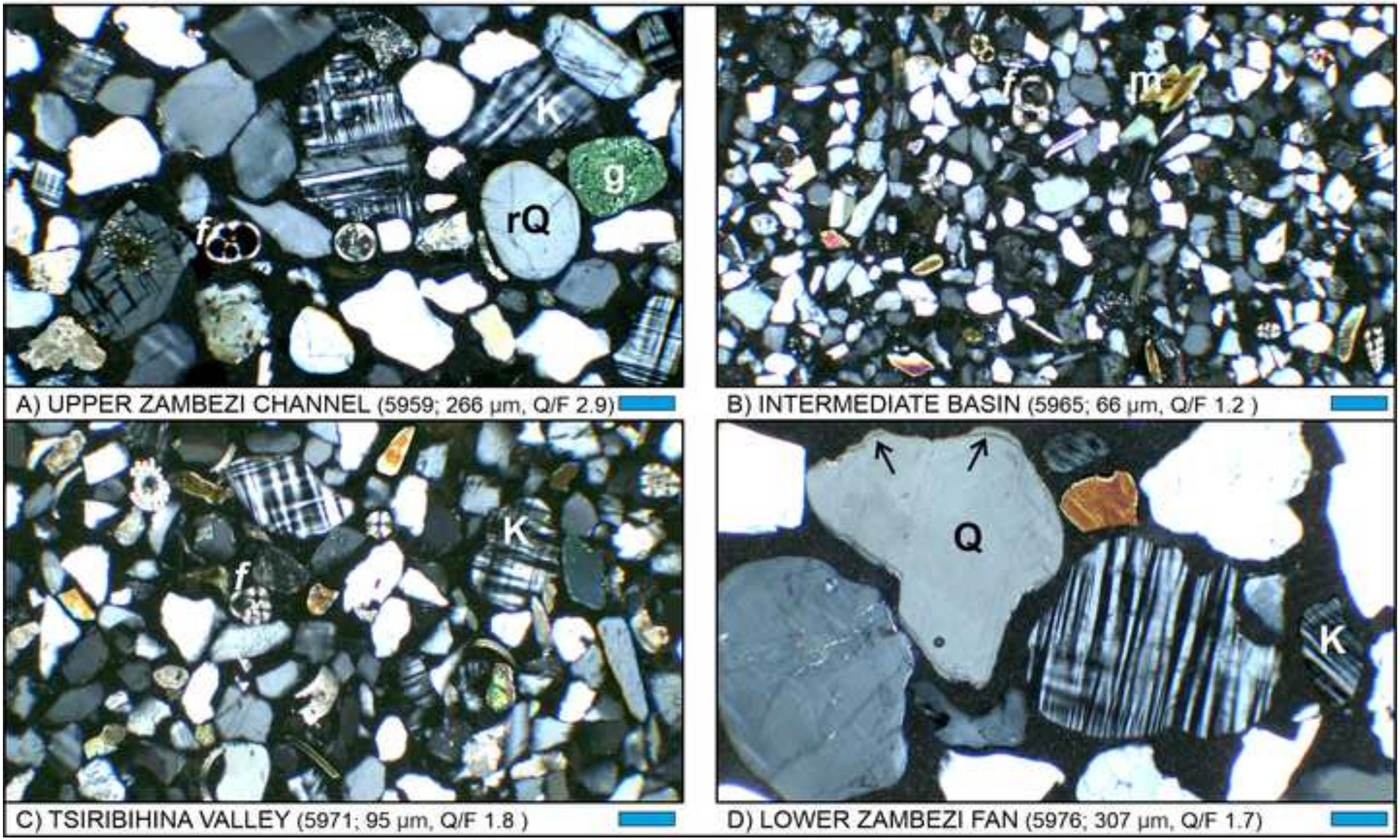
k
g
rQ
f
m
f
K
f
Q
K
A) UPPER ZAMBEZI CHANNEL (5959; 266 µm, Q/F 2.9)
B) INTERMEDIATE BASIN (5965; 66 µm, Q/F 1.2)
C) TSIRIBIHINA VALLEY (5971; 95 µm, Q/F 1.8)
D) LOWER ZAMBEZI FAN (5976; 307 µm, Q/F 1.7)

Figure 4

Click here to access/download;Figure;Figure 4 ZambeFan PTHM Plots.jpg

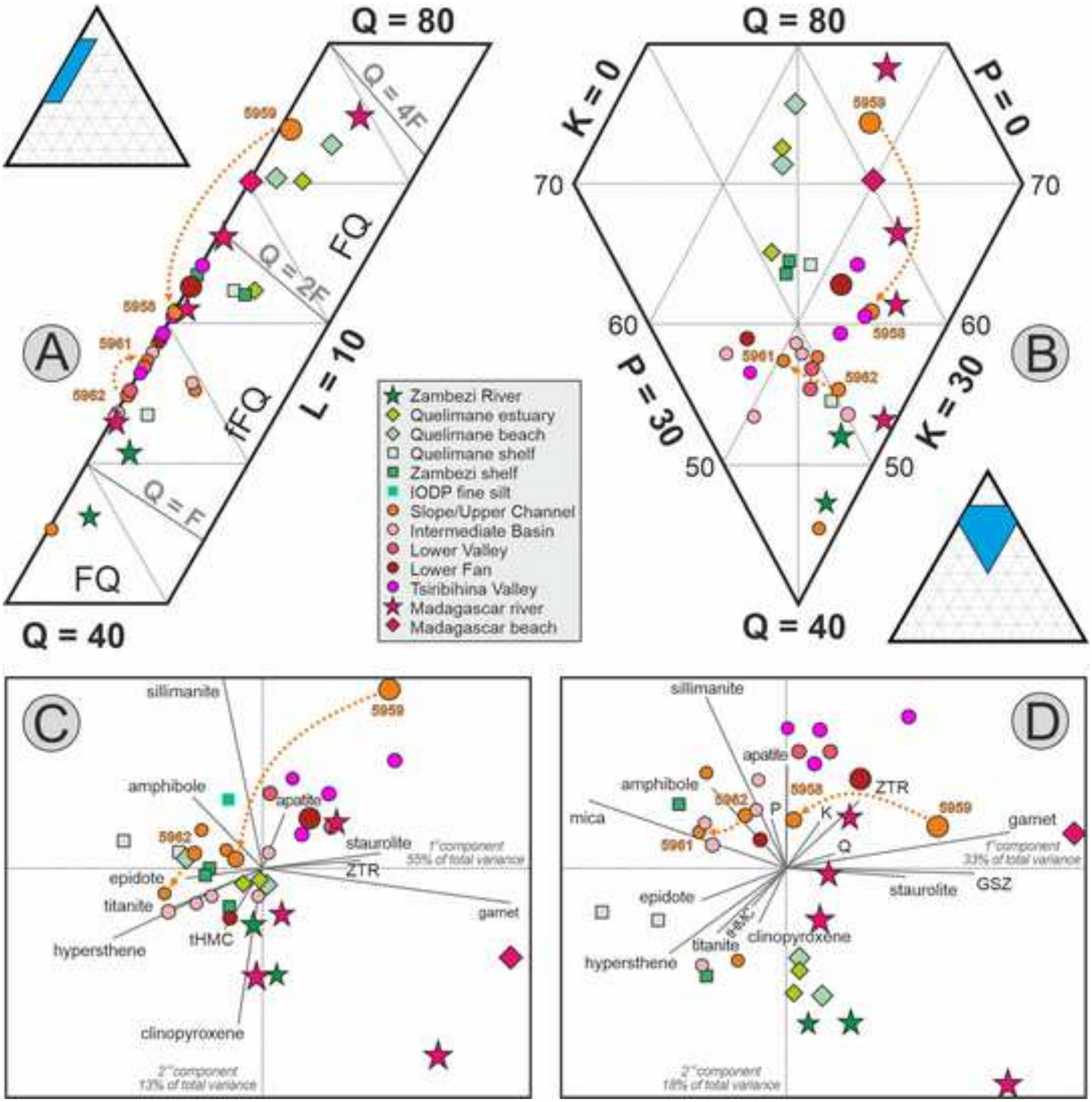

Figure 5

Click here to access/download;Figure;Figure 5 ZambeFan REE.jpg

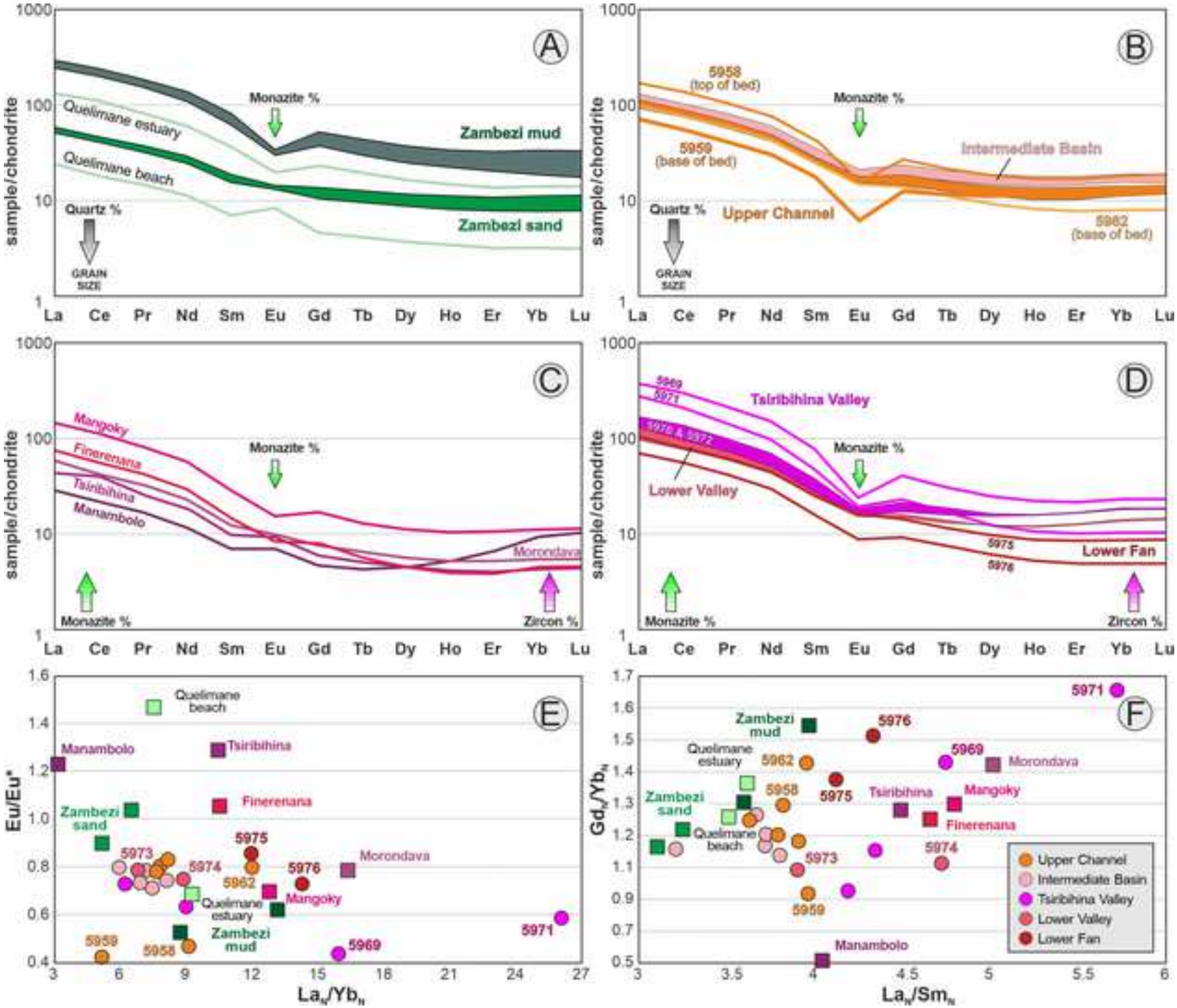

Figure 6

Click here to access/download;Figure;Figure 6 ZambeFan Nd Isotope.jpg

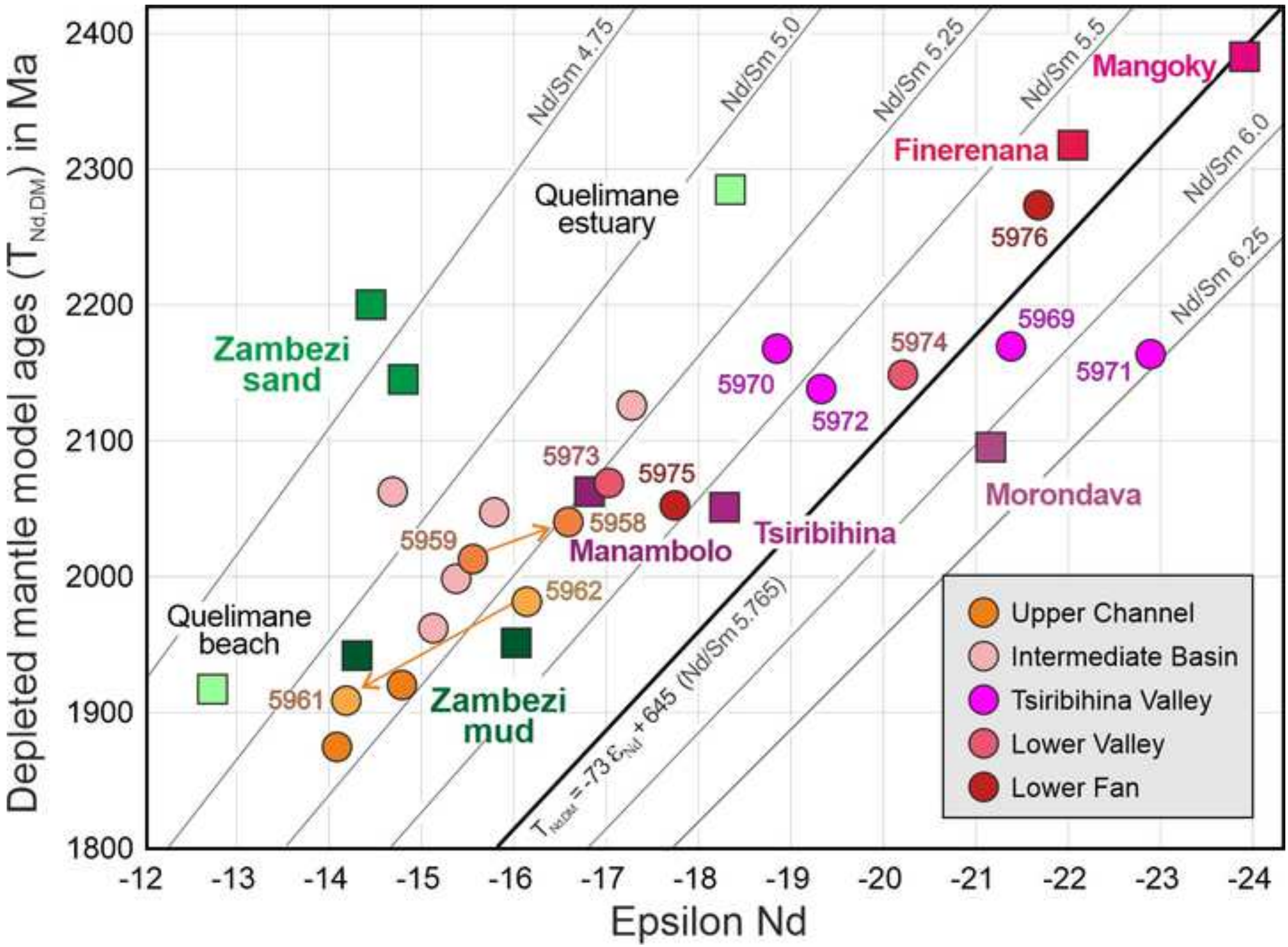

Figure 7

Click here to access/download;Figure;Figure 7 ZambeFan KDE.jpg

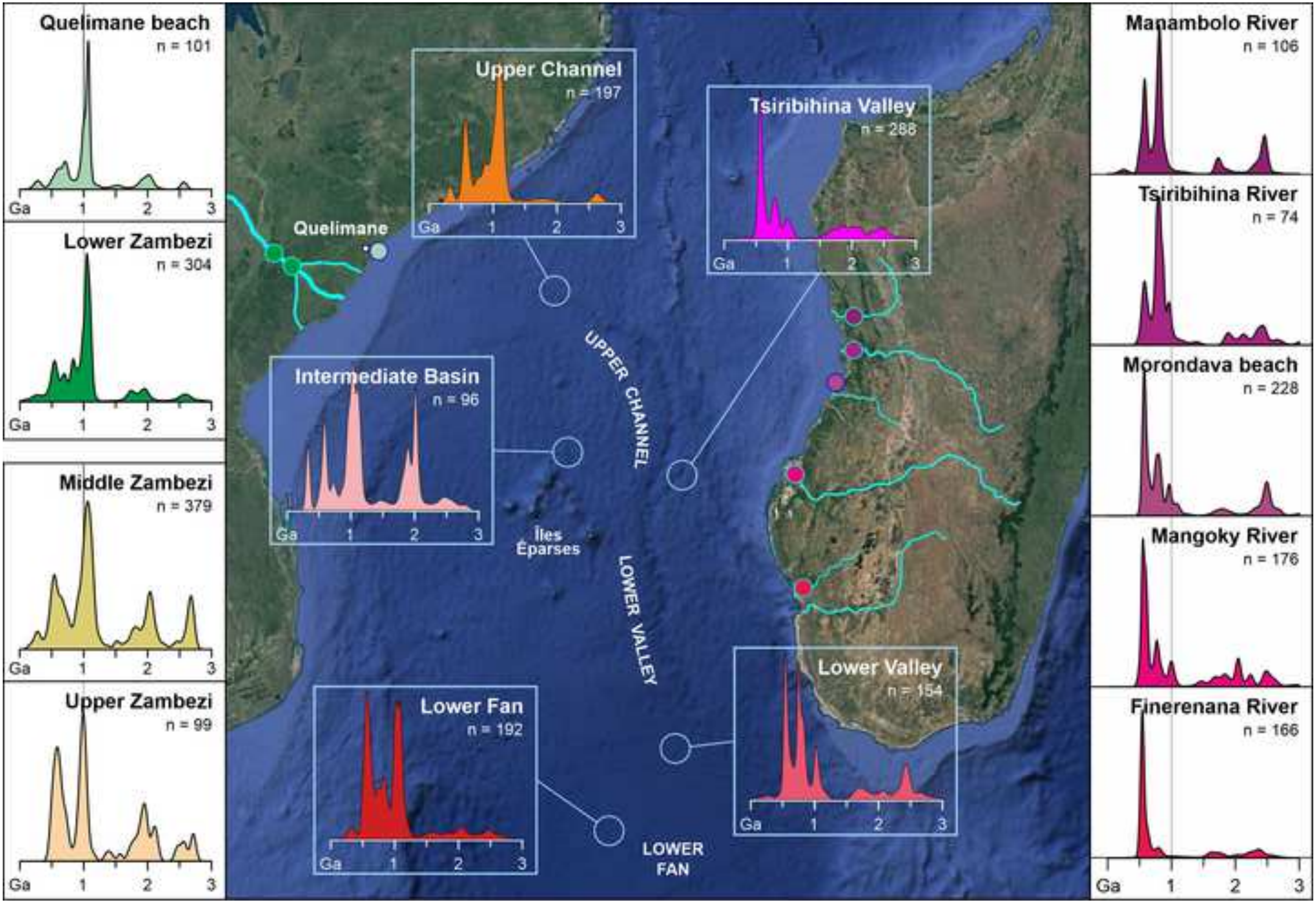

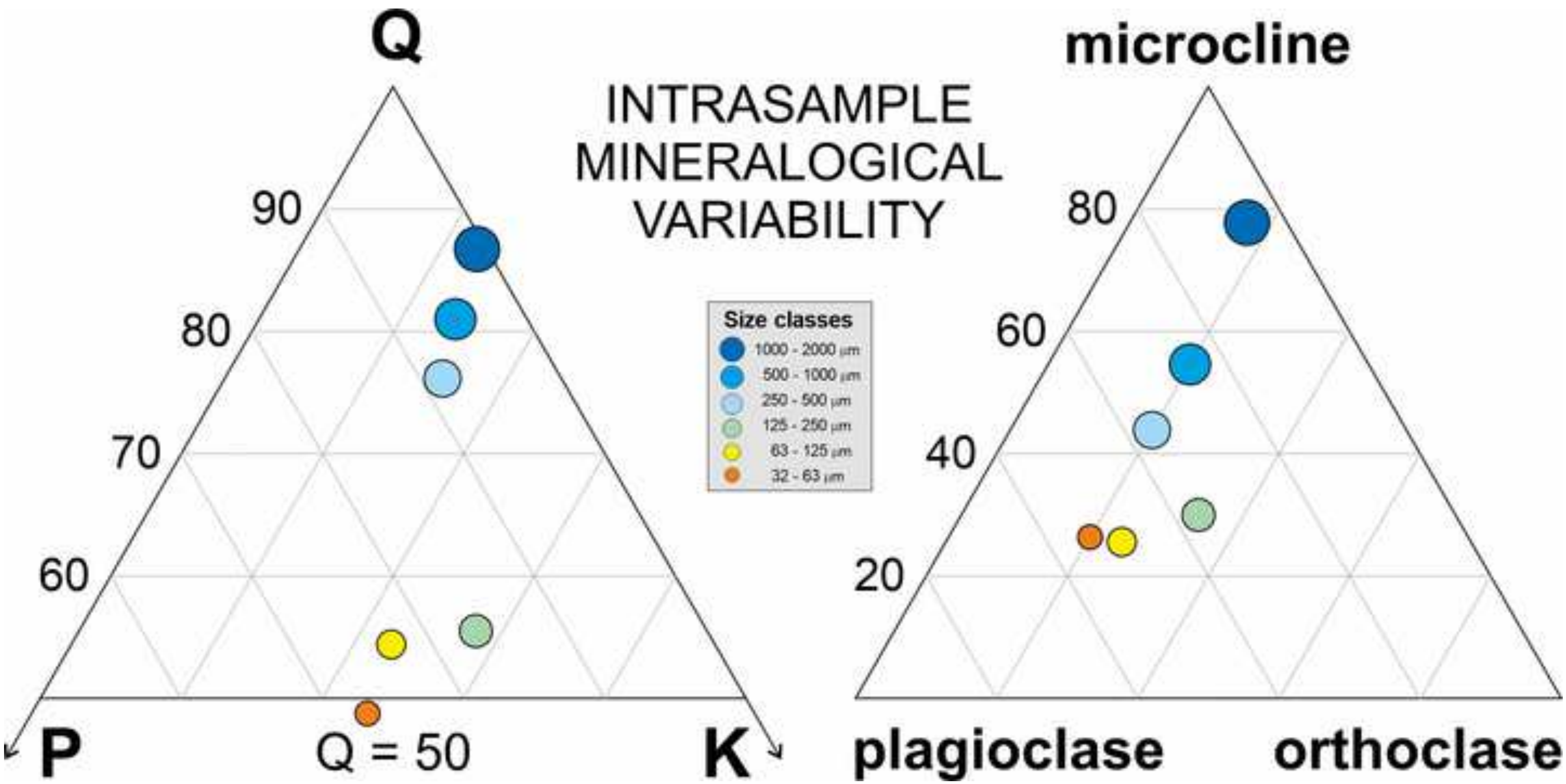
Q
INTRASAMPLE
MINERALOGICAL
VARIABILITY
microcline
90
80
70
60
80
60
40
20
Size classes
1000 - 2000 μm
500 - 1000 μm
250 - 500 μm
125 - 250 μm
63 - 125 μm
32 - 63 μm
P
Q = 50
K
plagioclase
orthoclase

Figure 9

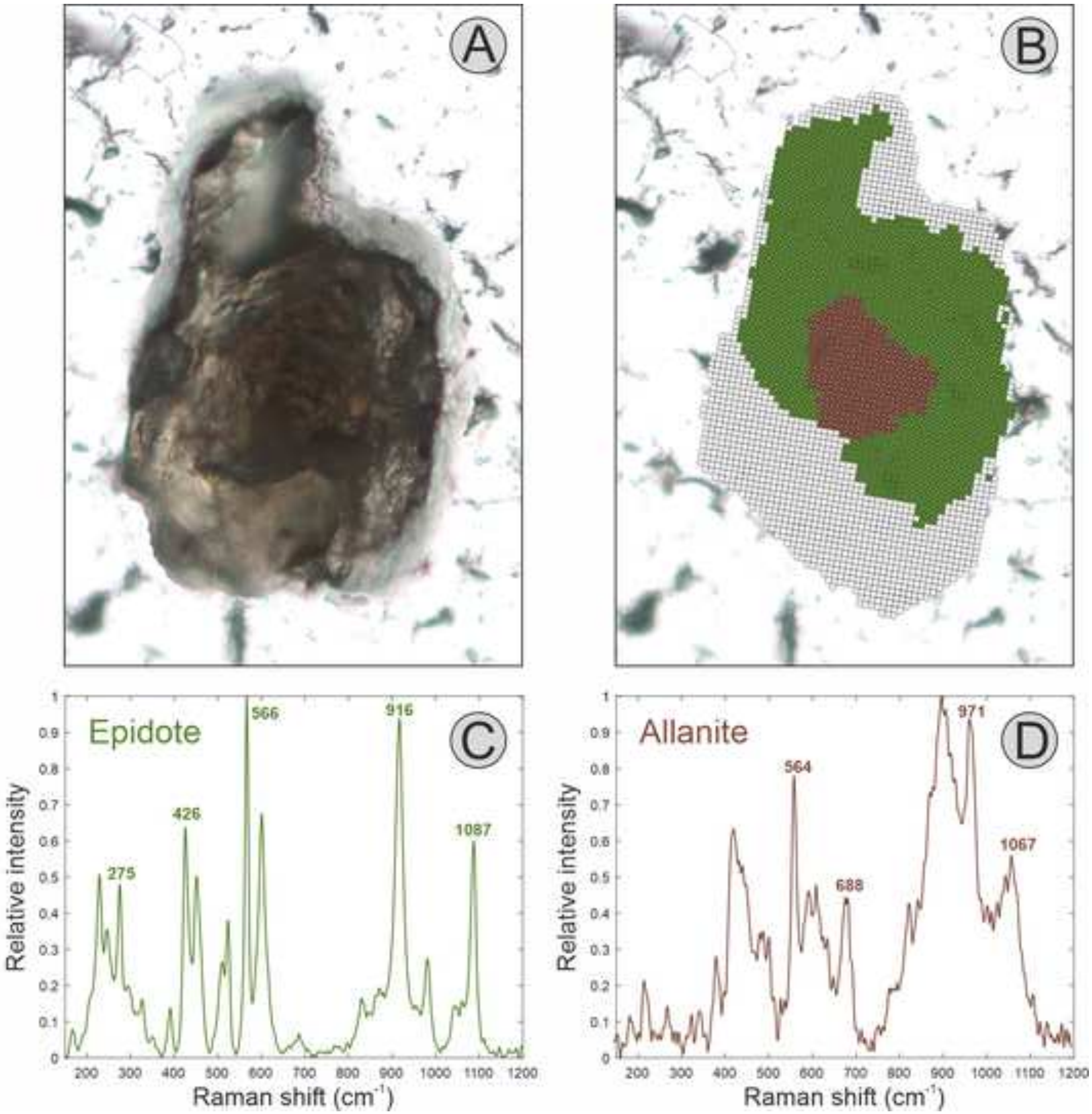
A
B
C
D
Epidote
566
916
426
1087
275
Relative intensity
Raman shift (cm^{-1})
Allanite
971
564
1067
688
Relative intensity
Raman shift (cm^{-1})

Figure 10

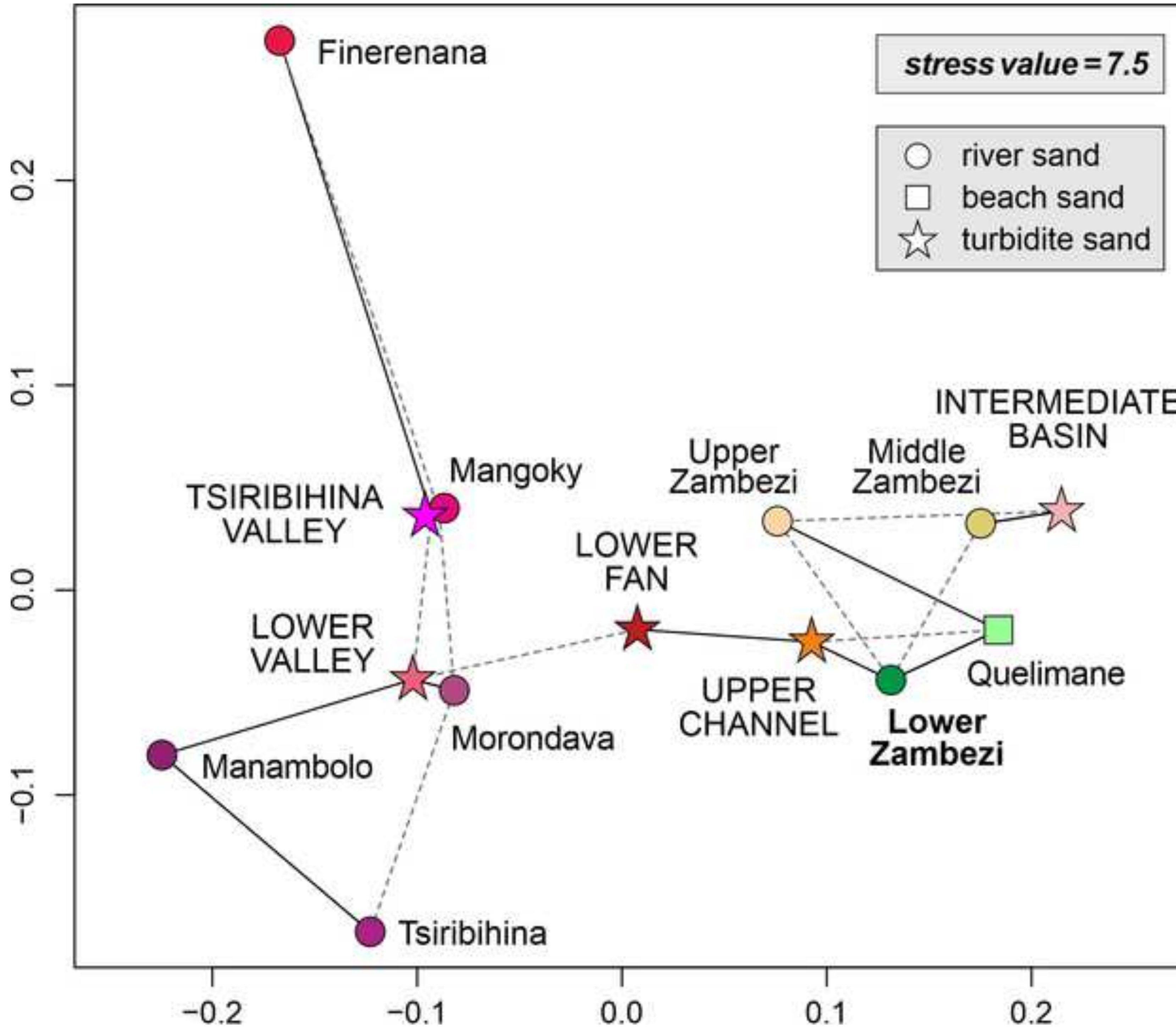

stress value = 7.5
river sand
beach sand
turbidite sand
Finerenana
Mangoky
TSIRIBIHINA VALLEY
LOWER VALLEY
Morondava
Manambolo
Tsiribihina
LOWER FAN
UPPER CHANNEL
Upper Zambezi
Middle Zambezi
INTERMEDIATE BASIN
Quelimane
Lower Zambezi
0.2
0.1
0.0
−0.1
−0.2
−0.1
0.0
0.1
0.2

Figure 11

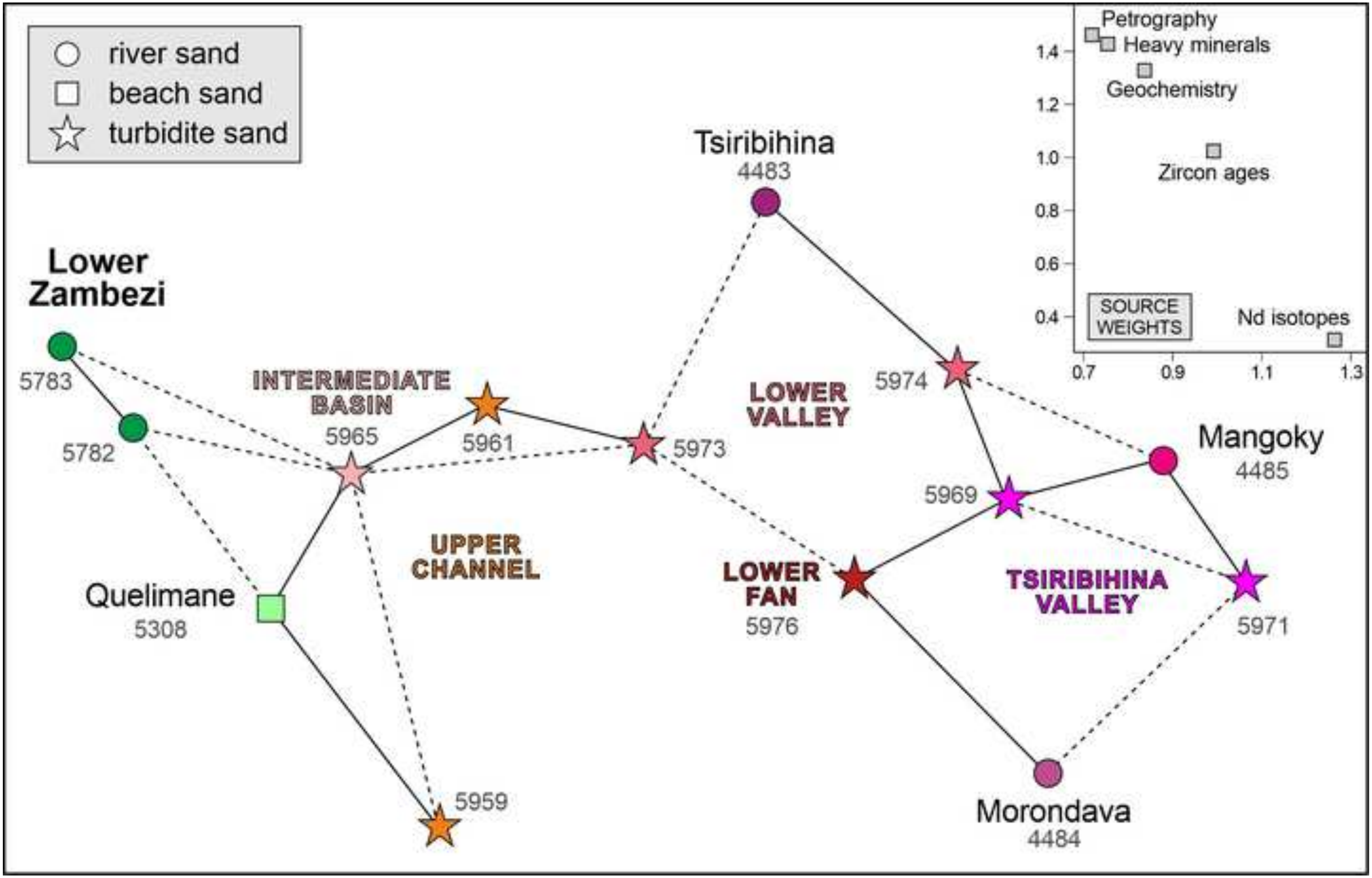

river sand
beach sand
turbidite sand
Lower Zambezi
5783
5782
Quelimane
5308
INTERMEDIATE BASIN
5965
5961
UPPER CHANNEL
5959
Tsiribihina
4483
5973
LOWER VALLEY
5974
LOWER FAN
5976
5969
Mangoky
4485
TSIRIBIHINA VALLEY
5971
Morondava
4484
Petrography
Heavy minerals
Geochemistry
Zircon ages
SOURCE WEIGHTS
Nd isotopes
1.4
1.2
1.0
0.8
0.6
0.4
0.7
0.9
1.1
1.3

Figure 12 Click here to access/download;Figure;Figure 12 ZambeFan Summary.jpg

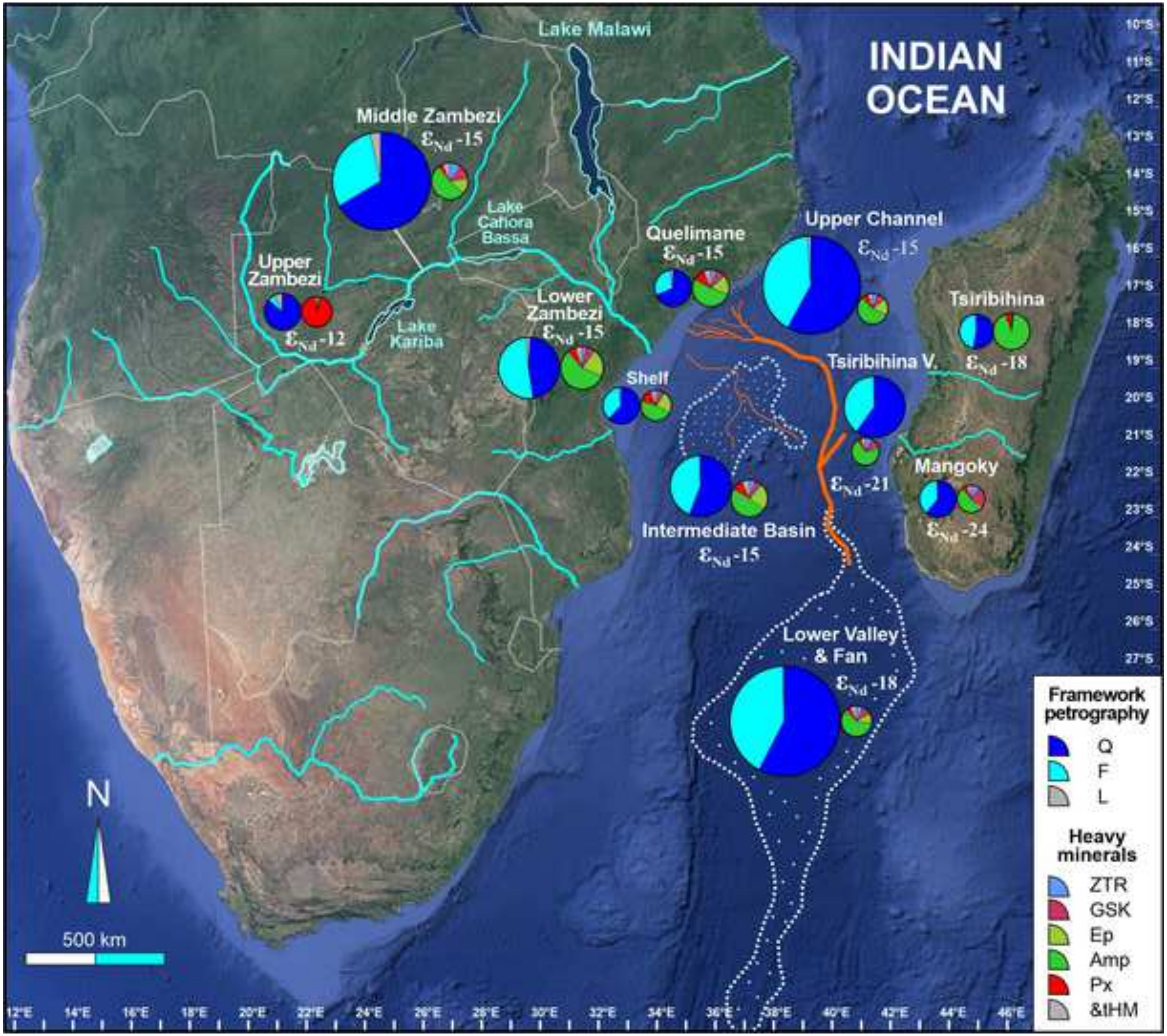

Table 1

Click here to access/download;Table;Table 1 ZambeFan Cores.xlsx

Sample	Cruise	Core	Sampled interval	Latitude	Longitude	Water depth	Isotope stage	Age	Grain size	Unit	International Geo Sample Number
5958	PAMELA-MOZ4	CSF20	S1 29-30 cm	18°26.786'S	39°55.896'E	- 2501 m	MIS1	< 15 ka	127 µm	Upper Channel	http://igsn.org/BFBGX-128005
5959	PAMELA-MOZ4	CSF20	S1 34-35 cm	18°26.786'S	39°55.896'E	- 2501 m	MIS1	< 15 ka	266 µm	Upper Channel	http://igsn.org/BFBGX-128005
5960	PAMELA-MOZ4	CSF20	S5 464-465 cm	18°26.786'S	39°55.896'E	- 2501 m	MIS4	60-70 ka	59 µm	Upper Channel	http://igsn.org/BFBGX-128005
5961	PAMELA-MOZ4	CSF20	S8 715-716 cm	18°26.786'S	39°55.896'E	- 2501 m	MIS5	70-130 ka	60 µm	Upper Channel	http://igsn.org/BFBGX-128005
5962	PAMELA-MOZ4	CSF20	S8 719-720 cm	18°26.786'S	39°55.896'E	- 2501 m	MIS5	70-130 ka	93 µm	Upper Channel	http://igsn.org/BFBGX-128005
5963	PAMELA-MOZ4	CSF20	S10 935-936 cm	18°26.786'S	39°55.896'E	- 2501 m	MIS6	130-190 ka	60 µm	Upper Channel	http://igsn.org/BFBGX-128005
5964	PAMELA-MOZ1	KS26	S7 653-655 cm	21°16.434'S	39°55.863'E	- 3095 m	MIS6	130-190 ka	54 µm	Intermediate Basin	http://igsn.org/BFBGX-127682
5965	PAMELA-MOZ4	CS22	S10 884-886 cm	21°16.441'S	39°55.878'E	- 3099 m	MIS8	245-280 ka	66 µm	Intermediate Basin	http://igsn.org/BFBGX-128007
5966	PAMELA-MOZ4	CS22	S15 1359-1360 cm	21°16.441'S	39°55.878'E	- 3099 m	MIS12	425-480 ka	55 µm	Intermediate Basin	http://igsn.org/BFBGX-128007
5967	PAMELA-MOZ2	KS05	S1 58-59 cm	21°27.606'S	40°43.075'E	- 3099 m	MIS1	< 15 ka	58 µm	Intermediate Basin	http://igsn.org/BFBGX-127456
5968	PAMELA-MOZ2	KS05	S5 488-489 cm	21°27.606'S	40°43.075'E	- 3099 m	MIS6	130-190 ka	54 µm	Intermediate Basin	http://igsn.org/BFBGX-127456
5969	PAMELA-MOZ1	KSF24	S2 143-145 cm	21°31.100'S	41°51.672'E	- 3089 m	MIS 5a	70-85 ka	72 µm	Tsiribihina Valley	http://igsn.org/BFBGX-127680
5970	PAMELA-MOZ1	KSF24	S4 388-390 cm	21°31.100'S	41°51.672'E	- 3089 m	MIS 6	130-190 ka	80 µm	Tsiribihina Valley	http://igsn.org/BFBGX-127680
5971	PAMELA-MOZ1	KSF24	S6 528-529 cm	21°31.100'S	41°51.672'E	- 3089 m	MIS 8	245-280 ka	95 µm	Tsiribihina Valley	http://igsn.org/BFBGX-127680
5972	PAMELA-MOZ1	KSF24	S6 577-579 cm	21°31.100'S	41°51.672'E	- 3089 m	MIS 8/9	ca 280 ka	57 µm	Tsiribihina Valley	http://igsn.org/BFBGX-127680
5973	PAMELA-MOZ2	KS11	S1 5-6 cm	25°33.989'S	41°36.989'E	- 4131 m	MIS1-2 ?	ca 15 ka	70 µm	Lower Valley	http://igsn.org/BFBGX-127461
5974	PAMELA-MOZ2	KS11	S4 318-320 cm	25°33.989'S	41°36.989'E	- 4131 m	MIS6	130-190 ka	70 µm	Lower Valley	http://igsn.org/BFBGX-127461
5975	PAMELA-MOZ4	CS25	S2 152-153 cm	26°37.318'S	40°42.748'E	- 4388 m	n.d.	> 500 ka ?	79 µm	Lower Fan	http://igsn.org/BFBGX-128010
5976	PAMELA-MOZ4	CS25	S4 280-281 cm	26°37.318'S	40°42.748'E	- 4388 m	n.d.	> 500 ka ?	307 µm	Lower Fan	http://igsn.org/BFBGX-128010

Table 2

Click here to access/download;Table;Table 2 ZambeFan PTHM.xlsx

Unit	n°	GSZ ϕ	Q	F	L	P/F%	tHMC	ZTR	Ep	Grt	SKA	Amp	Px	&tHM	
Lower Zambezi River	1	3.7	46	52	2	46	7.7	5	24	3	3	58	4	3	100.0
Lower Zambezi River	1	2.1	51	47	2	44	5.0	2	18	3	4	58	8	7	100.0
Quelimane estuary	1	3.0	66	30	4	54	6.5	6	18	3	3	51	12	6	100.0
Quelimane beaches	1	2.3	72	26	3	52	4.8	4	16	4	4	56	9	6	100.0
Quelimane shelf	2	3.4	58	40	2	46	2.8	5	24	0	4	47	15	6	100.0
Zambezi shelf	4	3.5	63	35	2	52	2.9	4	25	2	4	48	11	6	100.0
Upper channel	4	3.9	53	46	1	48	2.5	4	19	1	4	59	8	5	100.0
Upper channel	1	3.0	61	39	0	37	1.8	6	19	2	4	56	7	7	100.0
Upper channel	1	1.9	74	25	1	31	0.8	10	12	14	8	52	0	3	100.0
Intermediate Basin	5	4.1	56	43	1	52	4.4	5	24	3	4	49	9	7	100.0
Lower Valley	2	3.8	56	44	0	48	2.6	8	11	5	5	58	5	9	100.0
Lower Fan	1	3.7	59	41	0	58	2.8	5	16	3	1	66	7	4	100.0
Lower Fan	1	1.7	63	37	0	42	2.2	8	6	7	6	61	4	7	100.0
Tsiribihina Valley	4	3.7	60	40	0	44	1.9	8	4	7	5	67	4	6	100.0
N Madagascar rivers	2	1.8	60	40	0	34	2.8	2	1	1	1	84	9	2	100.0
Madagascar beach	1	1.9	70	30	0	33	0.5	23	6	55	1	1	8	7	100.0
S Madagascar rivers	2	1.8	68	29	3	27	1.9	9	4	43	2	25	14	3	100.0

Table 3

Unit	n°	GSZ ϕ	Fe_2O_3 wt%	MgO wt%	CaO wt%	TiO_2 wt%	Sr ppm	Ba ppm	Sc ppm	Y ppm	Th ppm	Zr ppm	Hf ppm	Co ppm	La ppm	Nd ppm	Sm ppm	Gd ppm	Yb ppm	Eu/ Eu*	Zr/Hf	ε_{Nd}	$T_{Nd,CHUR}$ Ma	$T_{Nd,DM}$ Ma
Lower Zambezi mud	2	< 5	9.1	1.8	1.1	1.4	113	477	21	43	32	475	13	18	64	57	11.0	9.1	4.4	0.57	35.7	-15.2	1470	1947
Lower Zambezi sand	1	3.7	2.3	0.7	2.2	0.6	199	628	7	19	5	272	6	5	14	13	2.9	2.8	1.9	0.89	44.0	-14.5	1685	2200.2
Lower Zambezi sand	1	2.1	2.0	0.6	2.1	0.5	197	622	6	13	4	232	5	5	12	11	2.4	2.1	1.3	1.04	45.8	-14.8	1643	2145.4
Quelimane estuary	1	3.0	3.0	0.7	1.7	1.5	171	589	7	24	13	314	9	6	31	28	5.6	4.7	2.4	0.68	36.3	-18.3	1855	2285
Quelimane beach	1	2.3	1.0	0.3	1.1	0.2	161	641	3	5	2	49	1	2	6	5	1.1	1.0	0.5	1.47	36.3	-12.7	1380	1917
Upper channel	4	3.9	2.6	0.8	1.9	0.7	225	806	7	19	10	466	12	7	24	21	4.0	3.4	2.0	0.80	38.3	-14.8	1439	1921
Upper channel	1	3.0	2.0	0.4	1.6	0.9	180	722	6	29	22	1134	28	5	39	35	6.7	5.5	3.0	0.46	40.4	-16.6	1588	2040.3
Upper channel	1	1.9	1.6	0.1	0.9	0.7	103	499	2	22	9	597	12	2	17	14	2.7	2.6	2.3	0.42	48.2	-15.6	1540	2013.1
Intermediate Basin	5	4.1	2.7	0.9	2.2	1.0	220	705	9	26	12	620	16	7	28	25	4.9	4.3	2.8	0.75	38.8	-15.7	1566	2039
Lower Valley	2	3.8	1.6	0.6	1.4	0.6	278	1191	5	21	13	717	18	4	26	22	4.0	3.2	2.4	0.76	40.0	-18.6	1690	2109
Lower Fan	1	3.7	1.9	0.8	1.8	0.5	235	836	6	15	10	423	11	5	24	21	3.9	3.0	1.5	0.86	39.2	-17.7	1622	2052.5
Lower Fan	1	1.7	n.d.	0.2	1.0	0.3	131	563	2	9	7	311	8	2	16	14	2.5	1.9	0.8	0.73	41.2	-21.7	1899	2273.7
Tsiribihina Valley	4	3.7	1.9	0.6	1.3	0.7	268	1211	6	27	26	953	24	5	54	42	7.3	5.3	3.0	0.59	39.6	-20.6	1772	2160
N Madagascar rivers	2	1.8	n.d.	0.4	1.3	0.4	247	1118	3	8	4	369	9	n.d.	9	7	1.3	1.1	1.1	1.26	42.2	-17.6	1622	2057
Madagascar beach	1	1.9	n.d.	0.1	0.6	0.4	134	756	2	7	7	408	10	n.d.	17	14	2.3	1.6	0.8	0.78	42.9	-21.2	1720	2095
S Madagascar rivers	2	1.8	n.d.	0.3	1.0	0.5	166	744	4	13	11	293	7	n.d.	24	18	3.2	2.5	1.4	0.87	41.0	-23.0	1992	2350

Appendix A TAbles

Click here to access/download;Appendices;Appendix A ZambeFan Tables.xls

River/Core	Site	Sample	Country	Year	Label	Provided by	Latitude	Longitude	Elevation	Drainage	Age	Note
LOWER ZAMBEZI RIVER												
Zambezi	Chimuara	S5782	Mozambique	2019	Lower Zambezi 5	L.Ncube-E.Van Niekerk	17°48'16" S	35°23'55" E	28 m	Indian Ocean	Modern	
Zambezi	Chupanga	S5783	Mozambique	2019	Lower Zambezi 6	L.Ncube-E.Van Niekerk	18°01'37" S	35°36'34" E	13 m	Indian Ocean	Modern	
NORTHERN ZAMBEZI DELTA												
Bons Sinais	Quelimane	S5306	Mozambique	2017	MD1-BS4	Celso de Carvalho Matsinhe	17°52'54" S	36°52'05" E	1 m	Indian Ocean	Modern	
Bons Sinais estuary	Migazela	S5307	Mozambique	2017	MI3-BS9	Celso de Carvalho Matsinhe	17°59'44" S	36°57'05" E	7 m	Indian Ocean	Modern	
beach sand	Praia da Madal	S5308	Mozambique	2017	MA3	Celso de Carvalho Matsinhe	17°58'28" S	37°01'14" E	3 m	Indian Ocean	Modern	
beach sand	Zalala	S5309	Mozambique	2017	ZSB3	Celso de Carvalho Matsinhe	17°50'19" S	37°07'32" E	1 m	Indian Ocean	Modern	
ZAMBEZI SHELF AND SLOPE										**Site**		
MOZ4-CS14/1 *	S1/20W 21-26 cm	CS14/1	Indian Ocean	2015	MOZ141	Pamela MOZ-04	17°57.307 S	37°42.548 E	-181 m	offshore Quelimane	4.3 ka	
MOZ4-CS14/3 *	S3/20W 1602-1607	CS14/3	Indian Ocean	2015	MOZ143	Pamela MOZ-04	17°57.308 S	37°42.549 E	-181 m	offshore Quelimane	15.9 ka	
MOZ4-CS17/1 *	S1/34W 52-57 cm	CS17/1	Indian Ocean	2015	MOZ171	Pamela MOZ-04	19°12.801 S	37°02.879 E	-550 m	offshore Zambezi Delta	4.0 ka	
MOZ4-CS17/8 *	S8/34W 702-707 c	CS17/8	Indian Ocean	2015	MOZ178	Pamela MOZ-04	19°12.802 S	37°02.880 E	-550 m	offshore Zambezi Delta	14.6 ka	
MOZ4-CS17/27 *	S27/34W 2402-240	CS17/27	Indian Ocean	2015	MOZ1727	Pamela MOZ-04	19°12.803 S	37°02.881 E	-550 m	offshore Zambezi Delta	24.1 ka	
U1477B	1H1A 0-1cm	77B1	Indian Ocean	2016	Hole 1477B	IODP Exp 361	19°21.2822' S	36°54.8958' E	-429 m	offshore Zambezi Delta	ca 10 ka	
ZAMBEZI VALLEY & FAN		° Research vessel L'Atalante		* Research vessel Pourquoi Pas?								
MOZ4-CSF20 *	S1 29-30 cm	S5958	Indian Ocean	2015	CSF20-1a	Pamela MOZ-04	18°26.786'S	39°55.896'E	- 2501 m	Slope-upper channel	MIS1	same turbidite bed
MOZ4-CSF20 *	S1 34-35 cm	S5959	Indian Ocean	2015	CSF20-1b	Pamela MOZ-04	18°26.786'S	39°55.896'E	- 2501 m	Slope-upper channel	MIS1	
MOZ4-CSF20 *	S5 464-465 cm	S5960	Indian Ocean	2015	CSF20-5	Pamela MOZ-04	18°26.786'S	39°55.896'E	- 2501 m	Slope-upper channel	MIS4	
MOZ4-CSF20 *	S8 715-716 cm	S5961	Indian Ocean	2015	CSF20-8a	Pamela MOZ-04	18°26.786'S	39°55.896'E	- 2501 m	Slope-upper channel	MIS5	same turbidite bed
MOZ4-CSF20 *	S8 719-720 cm	S5962	Indian Ocean	2015	CSF20-8b	Pamela MOZ-04	18°26.786'S	39°55.896'E	- 2501 m	Slope-upper channel	MIS5	
MOZ4-CSF20 *	S10 935-936 cm	S5963	Indian Ocean	2015	CSF20-10	Pamela MOZ-04	18°26.786'S	39°55.896'E	- 2501 m	Slope-upper channel	MIS6	**Nd analysis**
MOZ1-KS26 °	S7 653-655 cm	S5964	Indian Ocean	2014	KS26-7	Pamela MOZ-01	21°16.434'S	39°55.863'E	- 3095 m	Intermediate Basin	MIS6	660 cm
MOZ4-CS22 *	S10 884-886 cm	S5965	Indian Ocean	2015	CS22-10	Pamela MOZ-04	21°16.441'S	39°55.878'E	- 3099 m	Intermediate Basin	MIS8	862 cm
MOZ4-CS22 *	S15 1359-1360 cm	S5966	Indian Ocean	2015	CS22-15	Pamela MOZ-04	21°16.441'S	39°55.878'E	- 3099 m	Intermediate Basin	MIS12	1353 cm
MOZ2-KS05 °	S1 58-59 cm	S5967	Indian Ocean	2014	KS5-1	Pamela MOZ-02	21°27.606'S	40°43.075'E	- 3099 m	Intermediate Basin	MIS1	49 cm
MOZ2-KS05 °	S5 488-489 cm	S5968	Indian Ocean	2014	KS5-5	Pamela MOZ-02	21°27.606'S	40°43.075'E	- 3099 m	Intermediate Basin	MIS6	470 cm
MOZ2-KS11 °	S1 5-6 cm	S5973	Indian Ocean	2014	KS11-1	Pamela MOZ-02	25°33.989'S	41°36.989'E	- 4131 m	Lower valley outlet	MIS1-2 ?	
MOZ2-KS11 °	S4 318-320 cm	S5974	Indian Ocean	2014	KS11-4	Pamela MOZ-02	25°33.989'S	41°36.989'E	- 4131 m	Lower valley outlet	MIS6	
MOZ4-CS25 *	S2 152-153 cm	S5975	Indian Ocean	2015	CS25-2	Pamela MOZ-04	26°37.318'S	40°42.748'E	- 4388 m	Zambezi lower fan	> 500 ka ?	
MOZ4-CS25 *	S4 280-281 cm	S5976	Indian Ocean	2015	CS25-4	Pamela MOZ-04	26°37.318'S	40°42.748'E	- 4388 m	Zambezi lower fan	> 500 ka ?	
TSIRIBIHINA VALLEY												
MOZ1-KSF24 °	S2 143-145 cm	S5969	Indian Ocean	2014	KSF24-2	Pamela MOZ-01	21°31.100'S	41°51.672'E	- 3089 m	Tsiribihina Valley	MIS 5a	
MOZ1-KSF24 °	S4 388-390 cm	S5970	Indian Ocean	2014	KSF24-4	Pamela MOZ-01	21°31.100'S	41°51.672'E	- 3089 m	Tsiribihina Valley	MIS 6	
MOZ1-KSF24 °	S6 528-529 cm	S5971	Indian Ocean	2014	KSF24-6a	Pamela MOZ-01	21°31.100'S	41°51.672'E	- 3089 m	Tsiribihina Valley	MIS 8	
MOZ1-KSF24 °	S6 577-579 cm	S5972	Indian Ocean	2014	KSF24-6b	Pamela MOZ-01	21°31.100'S	41°51.672'E	- 3089 m	Tsiribihina Valley	MIS 8/9	
MADAGASCAR RIVERS & BEACH												
Manambolo	Bekopaka	S4481	Madagascar	2012		Marta Padoan	19°08'38" S	44°48'44" E	51 m	Mozambique Channel	Modern	
Tsiribihina	Belo su Tsiribihina	S4483	Madagascar	2012		Marta Padoan	19°42'45" S	44°34'37" E	6 m	Mozambique Channel	Modern	
beach sand	Morondava	S4484	Madagascar	2012		Marta Padoan	20°17'18" S	44°16'32" E	1 m	Mozambique Channel	Modern	
Mangoky	Tanambao	S4485	Madagascar	2012		Marta Padoan	21°49'53" S	43°52'32" E	43 m	Mozambique Channel	Modern	
Finerenana	Tulear	S1138	Madagascar	1999		Archive	23°18'14" S	43°39'40" E	7 m	Mozambique Channel	Modern	

Sample	Label	Site	<15	15-32	32-63	63-125	125-250	250-500	0.5-1	1-2	> 2	total	Gran size		Sorting	Skewness	Kurtosis
ZAMBEZI VALLEY & FAN			μm	μm	μm	μm	μm	μm	mm	mm	mm		μm	phi	σϕ	Sk	Ku
S5958	CSF20-1a	Upper channel	5%	3%	13%	31%	27%	16%	4%	0%	0%	100.0%	127	3.0	1.1	-0.2	-0.6
S5959	CSF20-1b	Upper channel	4%	1%	3%	4%	16%	65%	7%	0%	0%	100.0%	266	1.9	1.0	1.6	2.5
S5960	CSF20-5	Upper channel	17%	9%	34%	39%	1%	0%	0%	0%	0%	100.0%	59	4.1	0.6	0.1	-1.2
S5961	CSF20-8a	Upper channel	3%	10%	52%	34%	1%	0%	0%	0%	0%	100.0%	60	4.0	0.6	-0.4	-0.7
S5962	CSF20-8b	Upper channel	5%	5%	10%	57%	22%	2%	0%	0%	0%	100.0%	93	3.4	0.7	0.1	0.4
S5963	CSF20-10	Upper channel	12%	10%	42%	32%	3%	1%	0%	0%	0%	100.0%	60	4.1	0.7	-0.6	0.3
S5964	KS26-7	Intermediate Basin	13%	24%	53%	9%	0%	0%	0%	0%	0%	100.0%	54	4.2	0.6	-0.5	-1.0
S5965	CS22-10	Intermediate Basin	1%	5%	42%	51%	1%	0%	0%	0%	0%	100.0%	66	3.9	0.5	-0.3	0.3
S5966	CS22-15	Intermediate Basin	14%	22%	48%	15%	1%	0%	0%	0%	0%	100.0%	55	4.2	0.6	-0.5	-0.3
S5967	KS5-1	Intermediate Basin	11%	17%	48%	21%	2%	1%	0%	0%	0%	100.0%	58	4.1	0.7	-0.9	1.5
S5968	KS5-5	Intermediate Basin	11%	22%	57%	10%	0%	0%	0%	0%	0%	100.0%	54	4.2	0.5	-0.7	0.1
S5973	KS11-1	Lower valley	4%	6%	32%	53%	4%	0%	0%	0%	0%	100.0%	70	3.8	0.6	0.0	-0.1
S5974	KS11-4	Lower valley	9%	7%	23%	58%	3%	0%	0%	0%	0%	100.0%	70	3.8	0.6	0.4	0.1
S5975	CS25-2	Lower Fan	8%	5%	15%	62%	8%	1%	1%	0%	0%	100.0%	79	3.7	0.7	-0.5	3.0
S5976	CS25-4	Lower Fan	1%	1%	3%	10%	23%	24%	26%	12%	0%	100.0%	307	1.7	1.2	0.7	-0.4
TSIRIBIHINA VALLEY																	
S5969	KSF24-2	Tsiribihina Valley	3%	8%	29%	56%	4%	0%	0%	0%	0%	100.0%	72	3.8	0.6	0.1	0.2
S5970	KSF24-4	Tsiribihina Valley	3%	5%	20%	63%	9%	1%	0%	0%	0%	100.0%	80	3.6	0.6	0.0	0.7
S5971	KSF24-6a	Tsiribihina Valley	13%	4%	7%	40%	33%	2%	0%	0%	0%	100.0%	95	3.4	0.9	0.3	-0.4
S5972	KSF24-6b	Tsiribihina Valley	16%	13%	40%	29%	1%	0%	0%	0%	0%	100.0%	57	4.1	0.6	-0.3	-0.4

River / Erg	Site	Sample	Age	GSZ (μm)	Analized Class	Operator	Q	K	P	Lvf	Lvm	Lc	Lh	Lp	Lms	Lmv	Lmf	Lmb	Lu	mica	HM		Q/F	Qp/Q %	P/F %	Mic*/F %	bt/mica	classification	Q	F	L	Q	P	K
LOWER ZAMBEZI RIVER																																		
Zambezi	Chimuara	S5782	Modern	235	63-2000	A.Resentini	45	24	18	0	0	0	0	0	0	1	1	0	0	1	10	100.0	1.1	7	44	21	n.d.	feldspar-rich feldspatho-quartzose	51	47	2	52	21	27
Zambezi	Chupanga	S5783	Modern	75	63-2000	A.Resentini	39	23	20	0	0	0	0	0	0	0	1	1	0	5	11	100.0	0.9	4	46	15	63%	quartzo-feldspathic	46	52	2	47	24	28
NORTHERN ZAMBEZI DELTA																																		
Bons Sinais	Quelimane	S5306	Modern	130	63-2000	G.Vezzoli	61	11	12	0	0	0	0	1	1	0	1	0	0	3	10	100.0	2.6	4	54	15	100%	feldspatho-quartzose	70	27	3	73	15	13
Bons Sinais estuary	Migazela	S5307	Modern	125	63-2000	G.Vezzoli	55	13	16	0	1	0	0	1	1	1	0	0	0	2	9	100.0	1.9	5	55	17	67%	feldspar-rich feldspatho-quartzose	62	33	4	65	19	16
beach sand	Praia da Madal	S5308	Modern	200	63-2000	G.Vezzoli	69	11	11	1	0	0	0	1	2	0	0	0	0	2	4	100.0	3.1	2	51	23	71%	feldspatho-quartzose	73	23	4	76	12	12
beach sand	Zalala	S5309	Modern	210	63-2000	G.Vezzoli	68	13	15	0	1	0	0	0	0	0	0	0	0	0	3	100.0	2.5	4	53	23	n.d.	feldspatho-quartzose	70	28	2	71	15	13
ZAMBEZI SHELF AND SLOPE																																		
MOZ 4-CS14/1 S1/20W 21-26 cm		CS14/1	4.3 ka	85	>63	G.Vezzoli	43	13	11	0	0	0	0	0	1	0	0	0	0	29	2	100.0	1.8	5	47	14	86%	feldspar-rich feldspatho-quartzose	62	35	3	64	17	19
MOZ 4-CS14/3 S3/20W 1602-1607 cm		CS14/3	15.9 ka	100	>63	G.Vezzoli	37	17	14	0	0	0	0	0	0	0	1	0	0	29	2	100.0	1.2	7	45	14	88%	feldspar-rich feldspatho-quartzose	54	45	2	55	20	25
MOZ 4-CS17/1 S1/34W 52-57 cm		CS17/1	4.0 ka	80	>63	G.Vezzoli	56	15	16	0	0	0	0	0	1	0	1	0	0	7	3	100.0	1.8	7	52	12	70%	feldspar-rich feldspatho-quartzose	62	34	4	65	18	17
MOZ4-CS17/27 S27/34W 2402-2407cm		CS17/27	24.1 ka	95	>63	G.Vezzoli	52	14	15	0	0	0	0	0	0	0	0	0	0	15	4	100.0	1.7	2	52	9	76%	feldspar-rich feldspatho-quartzose	64	36	0	64	19	17
ZAMBEZI VALLEY & FAN																																		
MOZ4-CSF20-1a	Upper channel	S5958	MIS1	127	>63	A.Resentini	57	23	14	0	0	0	0	0	0	0	0	0	0	2	4	100.0	1.6	2	37	30	100%	feldspar-rich feldspatho-quartzose	61	39	0	61	15	25
MOZ4-CSF20-1b	Upper channel	S5959	MIS1	266	>63	A.Resentini	69	16	7	0	0	1	0	0	0	0	0	0	0	1	6	100.0	2.9	1	31	38	n.d.	feldspatho-quartzose	74	25	1	74	8	18
MOZ4-CSF20-5	Upper channel	S5960	MIS4	59	>63	A.Resentini	35	22	20	0	0	0	0	0	0	0	0	0	0	14	8	100.0	0.8	4	47	18	80%	quartzo-feldspathic	45	55	0	45	26	29
MOZ4-CSF20-8a	Upper channel	S5961	MIS5	60	>63	A.Resentini	50	18	19	0	0	0	0	0	0	0	0	0	0	6	7	100.0	1.3	4	52	12	72%	feldspar-rich feldspatho-quartzose	57	43	0	57	22	20
MOZ4-CSF20-8b	Upper channel	S5962	MIS5	93	>63	A.Resentini	51	23	19	0	0	0	0	0	0	0	0	0	0	3	5	100.0	1.2	1	45	23	20%	feldspar-rich feldspatho-quartzose	55	45	0	55	20	25
MOZ4-CSF20-10	Upper channel	S5963	MIS6	60	>63	A.Resentini	47	19	16	0	0	0	0	0	1	0	2	0	0	9	5	100.0	1.4	3	47	17	48%	feldspar-rich feldspatho-quartzose	55	41	4	58	20	23
MOZ1-KS26-7	Intermediate Basin	S5964	MIS6	54	>63	A.Resentini	38	11	17	0	0	0	0	0	0	0	3	0	0	26	5	100.0	1.4	2	61	18	52%	feldspar-rich feldspatho-quartzose	56	41	4	58	26	16
MOZ4-CS22-10	Intermediate Basin	S5965	MIS8	66	>63	A.Resentini	44	22	16	0	0	0	0	0	0	0	0	0	0	5	14	100.0	1.2	4	43	22	59%	feldspar-rich feldspatho-quartzose	54	46	0	54	20	27
MOZ4-CS22-15	Intermediate Basin	S5966	MIS12	55	>63	A.Resentini	49	18	17	0	0	0	0	0	0	0	0	0	0	11	5	100.0	1.4	2	49	22	58%	feldspar-rich feldspatho-quartzose	58	42	0	58	21	21
MOZ2-KS5-1	Intermediate Basin	S5967	MIS1	58	>63	A.Resentini	46	16	16	0	0	0	0	0	0	0	0	0	0	16	6	100.0	1.4	2	50	22	44%	feldspar-rich feldspatho-quartzose	59	41	0	59	21	21
MOZ2-KS5-5	Intermediate Basin	S5968	MIS6	54	>63	A.Resentini	44	17	22	0	0	0	0	0	0	0	0	0	0	12	6	100.0	1.1	2	56	20	59%	feldspar-rich feldspatho-quartzose	53	47	0	53	26	20
MOZ2-KS11-1	Lower valley	S5973	MIS1-2 ?	70	>63	A.Resentini	51	20	18	0	0	0	0	0	0	0	0	0	0	4	7	100.0	1.3	1	48	19	67%	feldspar-rich feldspatho-quartzose	57	43	0	57	21	23
MOZ2-KS11-4	Lower valley	S5974	MIS6	70	>63	A.Resentini	51	22	20	0	0	0	0	0	0	0	0	0	0	2	5	100.0	1.2	2	48	18	80%	feldspar-rich feldspatho-quartzose	55	45	0	55	21	23
MOZ4-CS25-2	Lower Fan	S5975	> 500 ka ?	79	>63	A.Resentini	53	15	21	0	0	0	0	0	0	0	0	0	0	6	5	100.0	1.4	3	58	15	61%	feldspar-rich feldspatho-quartzose	59	41	0	59	24	17
MOZ4-CS25-4	Lower Fan	S5976	> 500 ka ?	307	>63	A.Resentini	56	19	14	0	0	0	0	0	0	0	0	0	0	2	8	100.0	1.7	4	42	15	57%	feldspar-rich feldspatho-quartzose	63	37	0	63	16	22
TSIRIBIHINA VALLEY																																		
MOZ1-KSF24	Tsiribihina Valley	S5969	MIS 5a	72	>63	A.Resentini	52	20	15	0	0	0	0	0	0	0	0	0	0	7	5	100.0	1.5	1	43	18	48%	feldspar-rich feldspatho-quartzose	59	41	0	59	17	23
MOZ1-KSF24	Tsiribihina Valley	S5970	MIS 6	80	>63	A.Resentini	56	22	14	0	0	0	0	0	0	0	0	0	0	4	3	100.0	1.5	2	39	24	83%	feldspar-rich feldspatho-quartzose	61	39	0	61	15	24
MOZ1-KSF24	Tsiribihina Valley	S5971	MIS 8	95	>63	A.Resentini	61	21	13	0	0	0	0	0	0	0	0	0	0	1	3	100.0	1.8	3	39	12	50%	feldspar-rich feldspatho-quartzose	64	36	0	64	14	22
MOZ1-KSF24	Tsiribihina Valley	S5972	MIS 8/9	57	>63	A.Resentini	51	17	22	0	0	0	0	0	0	0	0	0	0	5	5	100.0	1.3	1	57	17	57%	feldspar-rich feldspatho-quartzose	57	43	0	57	25	19
MADAGASCAR RIVER & BEACH																																		
Manambolo	Bekopaka	S4481	Modern	330	bulk	A.Resentini	62	22	9	0	0	0	0	0	0	0	0	0	0	5	2	100.0	2.0	9	30	22	81%	feldspatho-quartzose	66	33	0	67	10	23
Tsiribihina	Belo su Tsiribihina	S4483	Modern	245	bulk	A.Resentini	43	24	14	0	0	0	0	0	0	0	0	0	0	6	12	100.0	1.1	3	38	20	62%	feldspar-rich feldspatho-quartzose	53	47	0	53	18	29
beach sand	Morondava	S4484	Modern	260	bulk	A.Resentini	70	20	10	0	0	0	0	0	0	0	0	0	0	0	0	100.0	2.4	8	33	19	n.d.	feldspatho-quartzose	70	30	0	70	10	20
Mangoky	Tanambao	S4485	Modern	230	bulk	A.Resentini	56	23	11	0	0	0	0	0	0	0	0	0	0	5	3	100.0	1.6	7	33	14	94%	feldspar-rich feldspatho-quartzose	61	38	1	61	13	26
Finerenana	Tulear	S1138	Modern	340	bulk	G.Vezzoli	75	16	5	0	3	0	0	0	0	0	0	1	0	0	0	100.0	3.6	4	22	49	n.d.	feldspatho-quartzose	75	21	5	78	5	17

River	Site	Sample	Age	GSZ class (μm)	%weight finer	%weight class	%weight coarser	method	n° tHM counted	n° grains counted	Operator	HMC %weight	tHMC %weight	zircon	tourmaline	rutile	& Ti oxides	titanite	apatite	monazite
LOWER ZAMBEZI RIVER																				
Zambezi	Chimuara	S5782	Modern	15-500	3%	97%	0%	point	226	268	Guido Pastore	5.7	5.0	1	0	0.4	0	5	2	0
Zambezi	Chupanga	S5783	Modern	15-500	7%	93%	0%	point	210	258	Guido Pastore	8.9	7.7	4	0.5	0.5	0	3	0.5	0
NORTHERN ZAMBEZI DELTA																				
Bons Sinais	Quelimane	S5306	Modern	15-500	15%	84%	1%	point	200	291	Sergio Andò	8.5	6.2	5	4	1	0	3	2	0
Bons Sinais estuary	Migazela	S5307	Modern	15-500	2%	98%	0%	point	215	297	Sergio Andò	8.8	6.7	1	0	2	0	4	3	0.5
beach sand	Praia da Madal	S5308	Modern	15-500	1%	98%	1%	point	201	280	Sergio Andò	9.6	7.1	2	1	1	0.5	6	1	0
beach sand	Zalala	S5309	Modern	15-500	0%	99%	1%	point	205	235	Sergio Andò	2.7	2.5	0.5	2	0	0	2	2	0
ZAMBEZI SHELF AND SLOPE																				
MOZ 4-CS14/1 S1/20W 21-26 cm		CS14/1	4.3 ka	15-500	54%	45%	1%	point	202	336	Sergio Andò	3.2	2.8	1	3	0.5	0	1	3	0
MOZ 4-CS14/3 S3/20W 1602-1607 cm		CS14/3	15.9 ka	15-500	75%	25%	0%	point	202	352	Sergio Andò	3.2	2.8	0.5	3	1	1	2	2	0
MOZ 4-CS17/1 S1/34W 52-57 cm		CS17/1	4.0 ka	15-500	56%	44%	0%	point	203	278	Sergio Andò	5.3	4.4	1	1	0	0	5	2	0
MOZ 4-CS17/8 S8/34W 702-707 cm		CS17/8	14.6 ka	15-500	89%	11%	0%	point	205	505	Sergio Andò	2.4	2.0	1	3	1	1	3	1	0
MOZ 4-CS17/27 S27/34W 2402-2407 cm		CS17/27	24.1 ka	15-500	78%	22%	0%	point	205	328	Sergio Andò	4.4	3.8	0.5	0.5	1	1	3	1	0
U1477B 1H1A 0-1cm		77B1	ca 10 ka	> 5	60%	40%	0%	point	202	515	Marta Barbarano	3.1	1.6	4	0	1	0.5	3	1	0
ZAMBEZI VALLEY & FAN																				
MOZ4-CSF20-1a	Upper channel	S5958	MIS1	15-500	5%	91%	4%	point	214	415	Marta Barbarano	2.4	1.8	4	0	2	0	5	1	0
MOZ4-CSF20-1b	Upper channel	S5959	MIS1	15-500	4%	90%	7%	point	202	458	Marta Barbarano	1.7	0.8	5	2	2	0	2	0.5	0.5
MOZ4-CSF20-5	Upper channel	S5960	MIS4	15-500	16%	84%	0%	point	204	332	Marta Barbarano	3.0	2.4	2	1	0.5	0	0.5	1	0
MOZ4-CSF20-8a	Upper channel	S5961	MIS5	15-500	3%	97%	0%	point	201	277	Marta Barbarano	4.6	4.1	1	0	1	1	2	1	0
MOZ4-CSF20-8b	Upper channel	S5962	MIS5	15-500	4%	96%	0%	point	207	337	Marta Barbarano	1.6	1.3	3	1	0	0.5	4	1	0.5
MOZ4-CSF20-10	Upper channel	S5963	MIS6	15-500	11%	89%	0%	point	206	302	Marta Barbarano	2.4	2.1	2	1	0	1	3	2	0
MOZ1-KS26-7	Intermediate Basin	S5964	MIS6	15-500	12%	88%	0%	point	222	315	Marta Barbarano	5.2	4.2	3	1	0.5	2	4	1	0.5
MOZ4-CS22-10	Intermediate Basin	S5965	MIS8	15-500	1%	99%	0%	point	204	271	Marta Barbarano	8.1	6.5	1	2	0	1	4	2	0.5
MOZ4-CS22-15	Intermediate Basin	S5966	MIS12	15-500	14%	86%	0%	point	202	305	Marta Barbarano	5.3	4.2	4	3	0.5	0	4	0.5	0.5
MOZ2-KS5-1	Intermediate Basin	S5967	MIS1	15-500	10%	90%	0%	point	204	286	Marta Barbarano	3.8	3.1	2	1	0.5	0.5	4	1	0
MOZ2-KS5-5	Intermediate Basin	S5968	MIS6	15-500	10%	90%	0%	point	202	320	Marta Barbarano	5.4	4.1	2	2	0	0.5	3	3	0.5
MOZ2-KS11-1	Lower valley	S5973	MIS1-2 ?	15-500	4%	96%	0%	point	204	304	Marta Barbarano	2.9	2.2	4	2	0.5	1	3	5	0
MOZ2-KS11-4	Lower valley	S5974	MIS6	15-500	9%	91%	0%	point	208	310	Marta Barbarano	3.9	3.0	3	4	1	0.5	3	2	1
MOZ4-CS25-2	Lower Fan	S5975	> 500 ka	15-500	8%	91%	1%	point	200	289	Marta Barbarano	3.1	2.8	4	1	0	0	3	1	0
MOZ4-CS25-4	Lower Fan	S5976	> 500 ka	15-500	1%	61%	38%	point	202	269	Marta Barbarano	2.6	2.2	6	1	0.5	0.5	4	1	0.5
TSIRIBIHINA VALLEY																				
MOZ1-KSF24	Tsiribihina Valley	S5969	MIS 5a	15-500	3%	97%	0%	point	200	321	Marta Barbarano	2.9	2.3	8	1	1	4	2	4	0
MOZ1-KSF24	Tsiribihina Valley	S5970	MIS 6	15-500	3%	97%	0%	point	202	319	Marta Barbarano	2.6	2.0	4	3	1	0.5	1	1	0.5
MOZ1-KSF24	Tsiribihina Valley	S5971	MIS 8	15-500	13%	87%	0%	point	203	302	Marta Barbarano	1.7	1.4	4	2	0	1	0	3	1
MOZ1-KSF24	Tsiribihina Valley	S5972	MIS 8/9	15-500	15%	85%	0%	point	203	327	Marta Barbarano	2.5	2.0	3	3	1	1	1	1	1
MADAGASCAR RIVER & BEACH																				
Manambolo	Bekopaka	S4481	Modern	15-500	0%	82%	18%	point	202	343	Marta Barbarano	3.4	2.3	2	0.5	1	0.5	1	0.5	0
Tsiribihina	Belo su Tsiribihina	S4483	Modern	15-500	0%	100%	0%	point	204	250	Marta Barbarano	3.8	3.3	0.5	0	0.5	0	0	0.5	0
beach sand	Morondava	S4484	Modern	15-500	0%	100%	0%	point	209	639	Marta Barbarano	1.3	0.5	16	2	5	0.5	0	6	0.5
Mangoky	Tanambao	S4485	Modern	15-500	1%	91%	3%	point	212	310	Marta Barbarano	3.3	2.5	6	2	2	1	0.5	3	0
Finerenana	Tulear	S1138	Modern	63-250	2%	36%	62%	area	237	693	Marta Padoan	2.7	1.4	6	0.4	0.4	0	2	0	0

River	Sample	epidote	garnet	staurolite	andalusite	kyanite	sillimanite	amphibole	clinopyroxene	enstatite	hypersthene	olivine	spinel	other tHM	Total	ZTR	ACI	MMI	Sil.I	% transparent	% opaque	% Fe oxides	% Ti oxides	% turbid HM	% rock fragments	% soil/turbid	% glaucony	% chlorite	% biotite	% carbonates	% light minerals	Total
LOWER ZAMBEZI RIVER																																
Zambezi	S5782	18	3	3	0	1	0.4	58	4	0	4	0	0	0	100.0	2	38	55	n.d.	84%	12%	0%	0%	0%	2.6%	0%	0.0%	0%	0%	0%	1%	100%
Zambezi	S5783	24	3	1	0	2	0	58	3	0	1	0	0	0	100.0	5	26	50	n.d.	81%	12%	2%	0%	0%	1.2%	0%	0.0%	0%	3%	0%	0%	100%
NORTHERN ZAMBEZI DELTA																																
Bons Sinais	S5306	22	3	0.5	0	1	2	47	11	0	1	0	0	0	100.0	10	11	79	100	69%	25%	2%	1%	0%	0.0%	0%	0.0%	0%	3%	0%	0%	100%
Bons Sinais estuary	S5307	15	4	1	0	0	2	54	7	0	4	0	0	0	100.0	3	5	86	100	72%	23%	2%	0%	0%	0.0%	0%	0.0%	0%	2%	0%	0%	100%
beach sand	S5308	16	6	0.5	0	1	2	54	6	0	1	0	0	0	100.0	4	2	79	100	72%	25%	1%	1%	0%	0.0%	0%	0.0%	1%	1%	0%	0%	100%
beach sand	S5309	17	1	0	0	2	3	59	7	0	4	0	0	0	100.0	3	11	82	64	87%	6%	3%	0%	0%	0.0%	0%	0.0%	0%	2%	0%	1%	100%
ZAMBEZI SHELF AND SLOPE																																
MOZ 4-CS14/1 S1/20W 21-26 cm	CS14/1	28	0.5	0	0	0	3	45	13	0	1	0	0	0.5	100.0	4	8	86	100	60%	8%	2%	4%	0%	0.0%	0%	0.0%	3%	20%	2%	1%	100%
MOZ 4-CS14/3 S3/20W 1602-1607 cm	CS14/3	20	0	0	0	0.5	4	48	14	0.5	1	0	0	0	100.0	5	4	95	100	57%	9%	9%	0%	0%	0.3%	0%	2.0%	2%	17%	3%	0%	100%
MOZ 4-CS17/1 S1/34W 52-57 cm	CS17/1	23	2	0.5	0	1	4	43	12	0	3	0	0	0	100.0	3	4	85	100	73%	14%	1%	4%	0%	0.0%	0%	0.0%	1%	6%	0%	0%	100%
MOZ 4-CS17/8 S8/34W 702-707 cm	CS17/8	22	4	0	0	1	1	45	12	0	3	0	0	0	100.0	6	7	80	n.d.	41%	8%	33%	1%	0%	0.2%	0%	0.0%	1%	7%	9%	1%	100%
MOZ 4-CS17/27 S27/34W 2402-2407 cm	CS17/27	25	2	0	0	0	2	51	10	0	1	0	0	1	100.0	2	4	100	100	63%	9%	18%	0%	0%	0.0%	0%	0.0%	2%	6%	3%	0%	100%
U1477B 1H1A 0-1cm	77B1	28	1	0	0	0.5	4	52	2	0	0.5	0	0	0	100.0	5	28	94	75	39%	36%	1%	2%	0%	0.0%	1%	0.0%	0%	8%	13%	0%	100%
ZAMBEZI VALLEY & FAN																																
MOZ4-CSF20-1a	S5958	19	2	0.5	1	0.5	2	56	6	0	1	0	0.5	0	100.0	6	17	78	100	52%	19%	1%	14%	0%	0.7%	1%	0.0%	0%	0%	13%	0%	100%
MOZ4-CSF20-1b	S5959	12	14	1	0.5	1	5	52	0	0	0	0	0	0	100.0	10	21	82	82	44%	48%	3%	4%	0%	0.0%	0%	0.0%	0%	1%	1%	0%	100%
MOZ4-CSF20-5	S5960	19	1	0	0	1	3	62	5	0	2	0	0.5	0	100.0	3	17	85	100	61%	14%	1%	1%	0%	1.5%	5%	0.0%	0%	9%	8%	0%	100%
MOZ4-CSF20-8a	S5961	19	0.5	0	0	1	1	56	11	0	2	0	0	0	100.0	3	17	75	n.d.	73%	7%	1%	4%	0%	1.1%	4%	0.0%	2%	4%	1%	1%	100%
MOZ4-CSF20-8b	S5962	20	2	0	0	1	3	54	5	0	4	0	0	0	100.0	4	15	85	100	61%	15%	1%	6%	0%	0.3%	1%	0.0%	0%	3%	12%	0%	100%
MOZ4-CSF20-10	S5963	19	2	0	0.5	0.5	1	63	2	0	1	0	0	0	100.0	4	16	80	n.d.	68%	9%	0%	2%	0%	0.0%	1%	0.0%	1%	13%	6%	0%	100%
MOZ1-KS26-7	S5964	24	2	0	0.5	0.5	1	52	7	0	1	0	0	0	100.0	5	14	80	n.d.	70%	15%	1%	3%	0%	0.0%	3%	0.0%	0%	4%	2%	0%	100%
MOZ4-CS22-10	S5965	21	1	0	0.5	1	1	51	6	0	5	0	0	0	100.0	4	21	67	n.d.	75%	16%	2%	0%	0%	0.0%	3%	0.0%	0%	2%	1%	0%	100%
MOZ4-CS22-15	S5966	22	4	0	0	1	1	49	8	0	0.5	0	0	0	100.0	8	22	80	n.d.	66%	18%	1%	5%	0%	0.3%	1%	0.0%	0%	4%	3%	2%	100%
MOZ2-KS5-1	S5967	26	2	0	0	3	1	47	8	0.5	3	0	0	0	100.0	3	25	67	n.d.	71%	13%	2%	2%	1%	1.7%	2%	0.0%	0%	2%	4%	0%	100%
MOZ2-KS5-5	S5968	25	5	0.5	0	2	3	44	5	0	1	0	0	0	100.0	5	17	77	100	63%	19%	1%	3%	0%	0.0%	1%	0.0%	1%	7%	5%	0%	100%
MOZ2-KS11-1	S5973	12	6	0.5	0	0.5	2	56	6	0	0	0	0	0	100.0	7	17	83	100	67%	20%	0%	1%	1%	0.3%	2%	0.0%	0%	8%	0%	1%	100%
MOZ2-KS11-4	S5974	10	4	0	0	0	6	60	3	0	0.5	0	0	0.5	100.0	9	16	93	100	67%	20%	1%	1%	1%	0.0%	4%	0.0%	0%	6%	0%	0%	100%
MOZ4-CS25-2	S5975	16	3	0	0	0.5	0.5	66	4	0	3	0	0	0	100.0	5	19	n.d.	n.d.	69%	6%	2%	2%	1%	0.3%	3%	0.0%	0%	14%	0%	1%	100%
MOZ4-CS25-4	S5976	6	7	1	0	1	4	61	3	0	1	0	0	0	100.0	8	29	83	100	75%	16%	1%	1%	0%	0.0%	2%	0.0%	0%	5%	0%	0%	100%
TSIRIBIHINA VALLEY																																
MOZ1-KSF24	S5969	2	7	0.5	0	0.5	5	63	4	0	0.5	0	0	0	100.0	10	20	91	100	62%	19%	0%	2%	1%	0.3%	4%	0%	0%	10%	1%	0%	100%
MOZ1-KSF24	S5970	4	2	0	0	0.5	1	76	4	0	0	0	0	0	100.0	8	21	n.d.	n.d.	63%	18%	0%	4%	1%	0%	4%	0%	0%	4%	3%	2%	100%
MOZ1-KSF24	S5971	3	16	1	0	1	4	60	2	0	0.5	0	0	0	100.0	6	34	82	100	67%	13%	0.3%	4%	0.3%	0%	2%	0%	0.3%	12%	1%	0%	100%
MOZ1-KSF24	S5972	5	2	0	0	1	5	71	4	0	0	0	0	0	100.0	7	14	92	100	62%	14%	0%	3%	1%	0.3%	4%	0.3%	0%	13%	3%	0%	100%
MADAGASCAR RIVER & BEACH																																
Manambolo	S4481	1	1	0	1	1	0	76	12	0	0.5	0	0	0	100.0	4	19	n.d.	n.d.	59%	29%	0%	1%	0%	0.6%	6%	0%	0%	3%	0.3%	0.3%	100%
Tsiribihina	S4483	0.5	0.5	0	0	0	0	92	5	0.5	0	0	0	0	100.0	1	16	n.d.	n.d.	82%	9%	2%	2%	0%	0.4%	3%	0%	0%	0.4%	0%	2%	100%
beach sand	S4484	6	55	0.5	0	0.5	0	1	8	0	0	0	0	0	100.0	23	n.d.	n.d.	n.d.	34%	34%	0%	3%	0%	28%	0%	0%	0%	0%	0%	1%	100%
Mangoky	S4485	5	20	0	0	0.5	4	48	6	0	1	0	0	0	100.0	10	34	95	100	33%	62%	0.6%	1%	0%	0%	0.6%	0%	0%	0%	0%	3%	100%
Finerenana	S1138	3	65	0	0	0	0	2	22	0	0	0	0	0	100.0	7	n.d.	n.d.	n.d.	68%	21%	0.3%	1%	0%	0%	1%	0%	0%	7%	0.3%	0.3%	100%

Sample	class	density	% class	n°Q+F	n° points	quartz	microcline	orthoclase	albite	Ca-plagioclase	phyllosilicate	carbonate	heavy minerals	others		Q	P	K		Mic	Or	Pl	
Zambezi Lower Fan			Operator: Marta Barbarano																				
L5976	1000-2000	<2.90 g/cm^3	12%	136	137	86	10	2	0	0.7	0	0	0.7	0	100.0	87	1	13	100.0	78	17	6	100.0
L5976	500-1000	<2.90 g/cm^3	26%	162	162	81	10	4	2	3	0	0	0	0	100.0	81	5	14	100.0	55	19	26	100.0
L5976	250-500	<2.90 g/cm^3	24%	199	199	76	11	5	3	6	0	0	0	0	100.0	76	9	16	100.0	44	21	35	100.0
L5976	125-250	<2.90 g/cm^3	23%	202	210	53	13	14	6	10	1	0.5	0.5	1	100.0	55	16	28	100.0	30	33	37	100.0
L5976	63-125	<2.90 g/cm^3	10%	205	221	50	11	10	7	14	5	1	0.9	0	100.0	54	23	23	100.0	26	24	50	100.0
L5976	32-63	<2.90 g/cm^3	3%	216	253	42	11	9	5	18	9	4	0.4	1	100.0	49	27	24	100.0	26	21	53	100.0
			97.4%			**70**	**11**	**7**	**3**	**7**	**1**	**0.4**	**0.3**	**0.4**	100.0	**71**	**10**	**19**	100.0	**39**	**25**	**35**	100.0

Full sample label	Site	Sample	Age	GSZ (µm)	Class (µm)	n° QF counted	n° grains counted	quartz	albite	Ca-plagioclase	orthoclase	microcline	mica	heavy minerals	carbonate	total	Q	P	K	total	Mic	Or	Pl	total
Operator: Alberto Resentini / Marta Barbarano																								
MOZ4-CSF20-1a	Upper channel	L5958	MIS1	127	15-500	423	658	41.5	11.2	1.5	3.0	7.0	0.0	0.0	35.7	100.0	64.5	19.9	15.6	100.0	30.7	13.3	56.0	100.0
MOZ4-CSF20-1b	Upper channel	L5959	MIS1	266	15-500	1300	1427	66.0	9.0	1.1	3.4	11.6	0.1	0.3	8.5	100.0	72.5	11.1	16.5	100.0	46.4	13.4	40.2	100.0
MOZ4-CSF20-8a	Upper channel	L5961	MIS5	60	15-500	3387	3599	52.8	23.0	2.7	6.7	8.9	0.2	0.5	5.2	100.0	56.1	27.3	16.6	100.0	21.6	16.2	62.2	100.0
MOZ4-CS22-10	Intermediate Basin	L5965	MIS8	66	15-500	1667	1725	72.2	13.2	1.0	5.6	4.6	0.0	0.6	2.8	100.0	74.7	14.7	10.6	100.0	19.0	23.0	58.1	100.0
MOZ2-KS5-5	Intermediate Basin	L5968	MIS6	54	15-500	2128	2262	53.7	21.8	1.3	8.0	9.2	0.4	0.6	5.0	100.0	57.0	24.6	18.4	100.0	22.9	19.9	57.2	100.0
MOZ1-KSF24-2	Tsiribihina Valley	L5969	MIS5a	72	15-500	2774	3004	42.7	16.1	5.6	14.7	13.2	0.1	0.3	7.2	100.0	46.2	23.5	30.2	100.0	26.6	29.6	43.8	100.0
MOZ1-KSF24-6a	Tsiribihina Valley	L5971	MIS8	95	15-500	735	974	38.7	10.0	2.7	14.8	9.3	0.3	0.3	23.9	100.0	51.3	16.7	32.0	100.0	25.4	40.2	34.4	100.0
MOZ2-KS11-1	Lower valley	L5973	MIS1-2 ?	70	15-500	2128	2320	49.3	15.9	2.8	11.8	12.0	0.1	0.2	8.0	100.0	53.7	20.3	26.0	100.0	28.3	27.8	43.9	100.0
MOZ2-KS11-4	Lower valley	L5974	MIS6	70	15-500	2905	3048	42.2	21.8	1.1	15.1	15.2	0.1	0.1	4.5	100.0	44.2	24.0	31.8	100.0	28.6	28.3	43.0	100.0
MOZ4-CS25-2	Lower fan	L5975	> 500 ka	79	15-500	2907	3121	45.9	22.1	2.4	10.6	12.2	0.3	0.4	6.2	100.0	49.3	26.3	24.4	100.0	25.8	22.4	51.8	100.0
MOZ4-CS25-4	Lower fan	L5976	> 500 ka	307	15-500	1931	1990	58.5	17.1	2.1	8.7	10.7	0.2	0.5	2.4	100.0	60.3	19.7	19.9	100.0	27.7	22.6	49.7	100.0

Full sample label	Site	Sample	Age	GSZ (µm)	Class (µm)	%weight			n° tHM counted	n° grains counted	zircon	tourmaline	rutile	titanite	apatite	monazite	barite	epidote	prehnite	garnet	staurolite	andalusite	kyanite	sillimanite	amphibole	clinopyroxene	enstatite	hypersthene	olivine	spinel	Total	total tHM	opaques	Fe oxides	Ti oxides	mica	carbonate	light minerals		ZTR
Operator: Alberto Resentini / Guido Pastore						finer	class	coarser																																
MOZ4-CSF20-1a	Upper channel	H5958	MIS1	127	15-500	5%	91%	4%	753	1259	8.8	2.8	3.2	7.3	2.1	0.7	0.0	30.3	0.0	2.9	0.3	0.7	0.4	0.4	30.5	8.6	0.0	1.1	0.0	0.0	100.0	60%	9%	22%	1%	3%	4%	2%	100.0%	15
MOZ4-CSF20-1b	Upper channel	H5959	MIS1	266	15-500	4%	90%	7%	481	680	8.9	1.7	6.4	2.5	2.3	1.5	0.0	21.6	0.0	8.7	0.8	0.6	1.0	1.2	40.7	0.8	0.0	0.8	0.0	0.2	100.0	71%	24%	0%	0%	1%	2%	3%	100.0%	17
MOZ4-CSF20-8a	Upper channel	H5961	MIS5	60	15-500	3%	97%	0%	1809	2157	1.3	2.0	3.1	5.3	4.1	0.1	0.0	22.3	0.1	0.8	0.2	0.4	0.4	1.5	39.9	15.8	0.1	2.8	0.0	0.0	100.0	84%	2%	5%	0%	5%	1%	3%	100.0%	6
MOZ4-CS22-10	Intermediate Basin	H5965	MIS8	66	15-500	1%	99%	0%	1890	2280	1.4	2.1	1.6	6.5	5.6	0.1	0.0	23.8	0.0	2.3	0.3	0.8	0.5	1.5	40.1	11.5	0.3	1.7	0.1	0.0	100.0	83%	3%	4%	1%	6%	0%	3%	100.0%	5
MOZ2-KS5-5	Intermediate Basin	H5968	MIS6	54	15-500	10%	90%	0%	1555	1968	1.2	1.6	3.8	6.0	2.6	0.1	0.0	29.5	0.0	2.1	0.2	0.3	0.8	1.5	40.3	8.8	0.4	1.0	0.0	0.0	100.0	79%	1%	11%	0%	4%	1%	3%	100.0%	7
MOZ1-KSF24-2	Tsiribihina Valley	H5969	MIS5a	72	15-500	3%	97%	0%	1722	2200	8.9	4.9	5.6	2.7	5.0	2.4	0.1	6.3	0.0	6.0	0.2	3.6	0.5	4.7	41.5	7.1	0.1	0.3	0.0	0.1	100.0	78%	3%	7%	2%	8%	0%	1%	100.0%	19
MOZ1-KSF24-6a	Tsiribihina Valley	H5971	MIS8	95	15-500	13%	87%	0%	1121	1426	10.3	3.9	4.7	2.9	4.7	3.6	0.0	3.9	0.0	11.3	0.8	10.5	0.0	3.6	33.1	6.2	0.1	0.2	0.0	0.1	100.0	79%	5%	6%	3%	6%	1%	1%	100.0%	19
MOZ2-KS11-1	Lower valley	H5973	MIS1-2?	70	15-500	4%	96%	0%	1707	2059	4.5	4.6	3.7	4.5	4.3	0.7	0.0	15.6	0.1	4.3	0.4	0.2	0.4	2.3	44.3	8.3	0.1	1.4	0.0	0.1	100.0	83%	3%	3%	2%	6%	0%	2%	100.0%	13
MOZ2-KS11-4	Lower valley	H5974	MIS6	70	15-500	9%	91%	0%	1414	2034	5.4	4.5	4.6	5.0	4.2	1.2	0.1	15.3	0.0	2.8	0.3	1.7	0.4	1.4	45.4	6.5	0.1	1.0	0.0	0.1	100.0	70%	7%	13%	1%	8%	0%	1%	100.0%	14
MOZ4-CS25-2	Lower fan	H5975	>500 ka?	79	15-500	8%	91%	1%	1588	1963	1.3	1.8	3.0	5.2	4.4	0.1	0.0	21.2	0.0	2.8	0.3	0.3	0.6	1.0	51.3	6.0	0.3	0.4	0.0	0.1	100.0	81%	4%	3%	0%	9%	0%	2%	100.0%	6
MOZ4-CS25-4	Lower fan	H5976	>500 ka?	307	15-500	1%	61%	38%	1075	1405	5.5	2.3	4.8	6.0	3.8	1.5	0.1	15.3	0.0	6.9	0.1	4.0	0.7	1.9	42.3	3.9	0.5	0.3	0.0	0.1	100.0	77%	6%	6%	1%	8%	0%	2%	100.0%	13

GRANULOMETRIC DISTRIBUTION OF REE-BEARING MINERALS

	H5858			H5859				H5861			H5865			H5868		
	32-63	63-125	125-250	32-63	63-125	125-25(	250-500	15-32	32-63	63-125	32-63	63-125	125-250	15-32	32-63	63-125
Allanite																
Monazite		5			2	5			1		1				1	
Zircon	6	60		3	18	21	1	1	19	3	23	4		11	6	1
Titanite	5	45	5	2	5	3	2	1	63	31	76	46		24	59	10
Apatite	1	13	2	1	3	7			56	18	64	40	1	7	33	1

	H5869				H5871			H5873				H5874				H5875				H5876			
	15-32	32-63	63-125	125-250	32-63	63-125	125-250	15-32	32-63	63-125	125-250	15-32	32-63	63-125	125-250	15-32	32-63	63-125	125-250	32-63	63-125	125-25(	250-500
Allanite																							
Monazite		33	9		20	19	1		9	3			9	8			1			5	11		
Zircon	4	117	32		37	78	1		48	27	2	1	48	26	1	1	16	3		13	38	7	1
Titanite		35	11	1	5	18	9		36	41			29	40	2		35	46	1	6	37	21	
Apatite		52	34		6	31	16	1	31	41	1		22	37	1		28	42		6	33	2	

Sample	Label	Site	Digested by	Age	GSZ sample (µm)	GSZ class (µm)	Analysed class (wt%)	Fe_2O_3 (wt%)	MgO (wt%)	CaO (wt%)	TiO_2 (wt%)	Sr ppm	Ba ppm	Sc ppm	Y ppm	Th ppm	Zr ppm	Hf ppm	Co ppm	La ppm	Ce ppm	Pr ppm	Nd ppm	Sm ppm	Eu ppm	Gd ppm	Tb ppm	Dy ppm	Ho ppm	Er ppm	Yb ppm	Lu ppm	La_N/Yb_N	La_N/Sm_N	Gd_N/Yb_N	Gd_N/Ho_N	Ho_N/Yb_N	Ce/Ce*	Eu/Eu*	Measured Sm/Nd	Theoretical $^{147}Sm/^{144}Nd$	$^{143}Nd/^{144}Nd$	2σ	ε_{Nd}	2σ	$T_{Nd,CHUR}$ (Ma)	$T_{Nd,DM}$ (Ma)
ZAMBEZI RIVER MUD																			CI chondrite (Barrat et al. 2012)	0.24	0.60	0.09	0.46	0.15	0.06	0.21	0.04	0.25	0.06	0.17	0.17	0.02									0.6049					0.00000000000654	
m5782	Zambezi River	Chimuara	HF-HCl-HNO_3	Modern	220	< 32 wet	2.2%	9.78	1.85	0.71	1.20	99	518	22	32	21	178	5	18.7	58	118	14	51	9	1.7	7.5	1.1	6.3	1.3	3.3	3.1	0.4	13.2	4.0	2.0	1.6	1.2	1.02	0.62	0.186	0.1124	0.511808	0.000004	-16.03	0.07	1495	1951
m5783	Zambezi River	Chupanga	HF-HCl-HNO_3	Modern	75	< 32 wet	12.7%	8.48	1.84	1.46	1.64	128	436	21	55	44	772	21	17.7	69	143	17	64	13	2.0	10.6	1.6	9.5	1.9	5.4	5.7	0.8	8.7	3.6	1.5	1.5	1.0	1.02	0.52	0.196	0.1188	0.511897	0.000005	-14.30	0.09	1446	1943
ZAMBEZI RIVER & DELTA SAND																																															
S5782	Zambezi River	Chimuara	Alkaline fusion	Modern	220	63-2000 we	95.1%	1.97	0.63	2.11	0.53	197	622	6	13	4	232	5	5.3	12	24	3	11	2	0.8	2.1	0.4	2.2	0.5	1.3	1.3	0.2	6.5	3.3	1.3	1.3	1.0	0.99	1.04	0.208	0.1258	0.511871	0.000006	-14.81	0.12	1643	2145
S5783	Zambezi River	Chupanga	Alkaline fusion	Modern	75	63-2000 we	69.5%	2.29	0.72	2.23	0.64	199	628	7	19	5	272	6	5.4	14	28	3	13	3	0.8	2.8	0.5	3.0	0.6	1.8	1.9	0.3	5.2	3.1	1.2	1.2	1.0	0.98	0.89	0.213	0.1291	0.511889	0.000003	-14.45	0.05	1685	2200
S5307	Quelimane estuary	Migazela	HF-HCl-HNO_3	Modern	125	Bulk sand	100%	2.99	0.66	1.69	1.47	171	589	7	24	13	314	9	5.9	31	65	7	28	6	1.2	4.7	0.7	4.1	0.8	2.2	2.4	0.3	9.3	3.6	1.6	1.6	1.0	1.04	0.68	0.197	0.1190	0.511690	0.000004	-18.34	0.08	1855	2285
S5309	Quelimane beach	Zalala	HF-HCl-HNO_3	Modern	210	Bulk sand	100%	1.02	0.32	1.08	0.23	161	641	3	5	2	49	1	2.4	6	11	1	5	1	0.5	1.0	0.2	0.9	0.2	0.5	0.5	0.1	7.5	3.5	1.4	1.4	1.0	0.94	1.47	0.205	0.1240	0.511977	0.000011	-12.74	0.22	1380	1917
ZAMBEZI VALLEY & FAN																																															
S5958	MOZ4_CSF20_S1_29-30	Upper channel	Alkaline fusion	MIS1	127	> 2	>> 95%	1.98	0.42	1.63	0.89	180	722	6	29	22	1134	28	5.0	39	82	9	35	7	0.9	5.5	0.8	4.7	1.0	2.8	3.0	0.5	9.2	3.8	1.5	1.6	0.9	1.04	0.46	0.1894	0.1146	0.511780	0.000005	-16.59	0.09	1588	2040
S5959	MOZ4_CSF20_S1_34-35	Upper channel	Alkaline fusion	MIS1	266	> 2	>> 96%	1.59	0.10	0.91	0.65	103	499	2	22	9	597	12	1.7	17	33	4	14	3	0.4	2.6	0.4	2.9	0.7	2.1	2.3	0.3	5.2	4.0	0.9	1.1	0.9	1.01	0.42	0.1937	0.1172	0.511832	0.000005	-15.56	0.11	1540	2013
S5960	MOZ4_CSF20_S5_464-465	Upper channel	Alkaline fusion	MIS4	59	> 2	>> 83%	n.d.	0.78	1.93	0.66	250	925	7	24	11	517	13	6.9	26	52	6	23	4	1.0	3.7	0.6	3.6	0.8	2.3	2.4	0.4	7.7	3.9	1.3	1.3	0.9	1.01	0.78	0.1914	0.1158	0.511872	0.000005	-14.79	0.10	1438	1920
S5961	MOZ4_CSF20_S8_715-716	Upper channel	Alkaline fusion	MIS5	60	> 2	>> 97%	2.70	1.04	2.15	0.81	214	672	9	22	10	518	13	7.7	25	49	6	23	4	1.1	3.9	0.6	3.6	0.7	2.2	2.3	0.3	7.8	3.6	1.4	1.4	1.0	0.99	0.80	0.1946	0.1177	0.511903	0.000005	-14.19	0.09	1413	1909
S5962	MOZ4_CSF20_S8_719-720	Upper channel	Alkaline fusion	MIS5	93	> 2	>> 96%	3.03	0.74	1.79	0.55	212	788	6	14	10	319	8	7.8	23	46	5	20	4	0.9	2.9	0.4	2.4	0.5	1.3	1.4	0.2	12.0	4.0	1.8	1.7	1.0	1.01	0.80	0.1874	0.1134	0.511802	0.000004	-16.14	0.08	1525	1981
S5963	MOZ4_CSF20_S10_935-936	Upper channel	Alkaline fusion	MIS6	60	> 2	>> 88%	2.00	0.61	1.81	0.59	224	840	6	17	10	509	14	5.6	22	44	5	19	4	0.9	3.0	0.5	2.8	0.6	1.7	1.9	0.3	8.2	3.8	1.3	1.4	0.9	1.02	0.83	0.1924	0.1164	0.511908	0.000006	-14.09	0.11	1380	1874
S5964	MOZ1_KS26_S7-653-655	Intermediate Basin	Alkaline fusion	MIS6	54	> 2	>> 87%	2.50	0.83	2.06	0.97	206	697	8	25	13	655	17	6.9	28	57	7	25	5	1.1	4.3	0.7	4.1	0.9	2.5	2.7	0.4	7.5	3.7	1.3	1.4	0.9	1.00	0.71	0.1950	0.1180	0.511821	0.000005	-15.79	0.10	1577	2048
S5965	MOZ2_CS22_S10_884-886	Intermediate Basin	Alkaline fusion	MIS8	66	> 2	> 99%	2.44	0.81	2.43	0.98	229	672	9	25	11	609	16	6.5	23	47	6	23	5	1.1	4.1	0.7	4.0	0.9	2.5	2.7	0.4	6.0	3.2	1.2	1.3	0.9	0.99	0.79	0.2030	0.1228	0.511877	0.000004	-14.69	0.08	1564	2063
S5966	MOZ2_CS22_S15_1359-136(	Intermediate Basin	Alkaline fusion	MIS12	55	> 2	>> 86%	2.69	0.92	2.31	1.07	232	716	9	30	12	631	17	7.6	31	61	7	28	5	1.2	4.9	0.8	4.8	1.0	3.0	3.2	0.5	7.0	3.7	1.2	1.3	0.9	0.99	0.74	0.1938	0.1172	0.511842	0.000005	-15.38	0.09	1522	1998
S5967	MOZ2_KS05_S1_58-59	Intermediate Basin	Alkaline fusion	MIS1	58	> 2	>> 89%	2.82	0.94	2.33	0.97	226	711	9	25	12	668	17	7.4	30	61	7	28	5	1.2	4.6	0.7	4.1	0.8	2.5	2.6	0.4	8.1	3.7	1.4	1.5	1.0	1.01	0.74	0.1916	0.1159	0.511744	0.000005	-17.28	0.10	1682	2126
S5968	MOZ2_KS05_S5_488-489	Intermediate Basin	Alkaline fusion	MIS6	54	> 2	>> 89%	3.06	1.06	1.99	0.89	208	730	9	24	11	539	14	8.4	26	49	6	23	4	1.0	3.7	0.6	3.8	0.8	2.5	2.6	0.4	7.0	3.8	1.2	1.3	0.9	0.96	0.78	0.1925	0.1164	0.511854	0.000004	-15.13	0.07	1484	1962
S5973	MOZ2_KS11_S1_5-6	Lower valley	Alkaline fusion	MIS1-2 ?	70	> 2	>> 96%	1.59	0.53	1.43	0.62	252	1127	5	20	10	599	16	4.2	23	46	5	20	4	0.9	3.1	0.5	3.1	0.7	2.1	2.3	0.3	6.9	3.9	1.1	1.3	0.9	1.02	0.78	0.1889	0.1142	0.511757	0.000005	-17.03	0.09	1624	2069
S5974	MOZ2_KS11_S4_318-320	Lower valley	Alkaline fusion	MIS6	70	> 2	>> 91%	1.66	0.63	1.46	0.61	304	1256	5	21	16	836	20	4.3	30	57	7	24	4	0.9	3.3	0.5	3.2	0.7	2.1	2.4	0.4	8.9	4.7	1.1	1.3	0.9	0.99	0.74	0.1758	0.1063	0.511594	0.000004	-20.21	0.08	1756	2149
S5975	MOZ4_CS25_S2_152-153	Lower fan	Alkaline fusion	> 500 ka	79	> 2	>> 92%	1.90	0.83	1.79	0.49	235	836	6	15	10	423	11	4.9	24	47	6	21	4	1.0	3.0	0.4	2.5	0.5	1.4	1.5	0.2	12.0	4.1	1.7	1.6	1.0	0.98	0.86	0.1831	0.1108	0.511721	0.000004	-17.74	0.08	1622	2052
S5976	MOZ4_CS25_S4_280-281	Lower fan	Alkaline fusion	> 500 ka	307	> 2	> 99%	n.d.	0.20	0.96	0.34	131	563	2	9	7	311	8	2.0	16	33	4	14	2	0.5	1.9	0.3	1.6	0.3	0.8	0.8	0.1	14.3	4.3	1.9	1.7	1.1	1.03	0.73	0.1771	0.1071	0.511519	0.000049	-21.68	0.96	1899	2274
TSIRIBIHINA VALLEY																																															
S5969	MOZ1_KSF24_S2_143-145	Tsiribihina Valley	Alkaline fusion	MIS 5a	72	> 2	>> 97%	1.79	0.55	1.35	0.87	274	1241	6	37	41	1449	36	4.5	87	178	19	70	12	1.4	8.4	1.2	6.3	1.3	3.6	3.9	0.6	15.9	4.8	1.8	1.8	1.0	1.06	0.43	0.1705	0.1031	0.511534	0.000006	-21.38	0.12	1794	2169
S5970	MOZ1_KSF24_S4_388-390	Tsiribihina Valley	Alkaline fusion	MIS 6	80	> 2	>> 97%	1.85	0.64	1.23	0.63	274	1248	5	26	13	760	19	5.4	26	52	6	22	4	0.9	3.5	0.6	3.9	0.9	2.7	3.0	0.5	6.2	4.2	0.9	1.1	0.9	1.01	0.72	0.1854	0.1122	0.511664	0.000004	-18.85	0.09	1752	2168
S5971	MOZ1_KSF24_S6_528-529	Tsiribihina Valley	Alkaline fusion	MIS 8	95	> 2	>> 87%	2.01	0.59	1.16	0.53	249	1190	6	18	32	686	17	5.1	64	125	13	45	7	1.1	4.8	0.6	3.2	0.6	1.7	1.8	0.3	26.1	5.7	2.2	2.2	1.0	1.05	0.59	0.1611	0.0974	0.511457	0.000004	-22.89	0.09	1809	2164
S5972	MOZ1_KSF24_S6_577-579	Tsiribihina Valley	Alkaline fusion	MIS 8/9	57	> 2	>> 84%	2.06	0.75	1.34	0.76	274	1167	6	27	18	917	24	6.2	40	83	9	33	6	1.1	4.6	0.7	4.3	0.9	2.8	3.1	0.5	9.0	4.4	1.2	1.4	0.9	1.07	0.63	0.1802	0.1090	0.511639	0.000005	-19.33	0.10	1732	2138

THE ZAMBEZI DEEP-SEA FAN: MINERALOGICAL, REE, Zr/Hf, Nd-ISOTOPE, AND ZIRCON-AGE VARIABILITY IN FELDSPAR-RICH PASSIVE-MARGIN TURBIDITES

Eduardo Garzanti, Germain Bayon, Pieter Vermeesch, Marta Barbarano,
Guido Pastore, Alberto Resentini, Bernard Dennielou, Gwenael Jouet

APPENDIX A

Table A1. Sample information. Location of the studied sediment samples in the Zambezi sediment-routing system from land to the deep sea. MIS = Marine Isotope Stages.

Table A2. Grain size. Data obtained by wet sieving on 19 turbidite samples from the Zambezi submarine channel and deep-sea fan.

Table A3. Sand petrography. GSZ = median grain size (in microns), determined by wet sieving (19 turbidite samples from the Zambezi submarine channel and deep-sea fan) or in thin section by ranking sand samples from coarsest to finest followed by visual comparison with in-house standards sieved at 0.25 ϕ sieve interval. Q = quartz (Qp = polycrystalline); F = feldspars (K = K-feldspar; P = plagioclase; Mic* = cross-hatched microcline); L= aphanitic lithic grains (Lvf = felsic volcanic; Lvm = mafic and intermediate volcanic; Lc = carbonate; Lh = chert; Lp = pelite; Lms = low-rank metasedimentary; Lmv = low-rank metavolcanic; Lmf = high-rank metapelite, metapsammite, and metafelsite; Lmb = high-rank metabasite; Lu = ultramafic); bt = biotite; HM = heavy minerals; n.d. = not determined. Sand classification scheme after Garzanti (2019). QFL and QPK parameters after Dickinson and Suczek (1979).

Table A4. Heavy minerals. GSZ = grain size. HM = heavy minerals; tHM = transparent heavy minerals; HMC and tHMC = heavy-mineral and transparent-heavy-mineral concentration; n.d. = not determined. The ZTR index (sum of zircon, tourmaline, and rutile over total transparent heavy minerals; Hubert 1962) evaluates the "chemical durability" of the detrital assemblage. The Metasedimentary Minerals Index MMI and the Amphibole Colour Index ACI vary from 0 in detritus from low-grade to lowermost medium-grade rocks yielding exclusively chloritoid and blue/green amphibole to 100 in detritus from granulite-facies or volcanic rocks yielding exclusively sillimanite and brown hornblende or oxy-hornblende and are used to estimate the average metamorphic grade of source rocks and provenance of amphibole grains. The Sillimanite index Sil.I varies from 0 in detritus from upper amphibolite facies metasediments yielding only fibrolitic sillimanite to 100 in detritus from granulite facies metasediments yielding only prismatic sillimanite (Andò and Garzanti, 2014; Garzanti and Andò, 2019).

Table A5. Intrasample tectosilicate variability. Grain-size-dependent intrasample variability of relative tectosilicate abundances was determined by manual Raman grain counting of the low-density fraction (L; < 2.90 g/cm^3) of Zambezi Lower Fan sample 5976. Q = quartz; F = feldspars (K = K-feldspar; Mic = microcline; Or = orthoclase; P, Pl = plagioclase).

Table A6. Mineralogy of the low-density fraction (L; < 2.90 g/cm^3). Data determined by semi-automated Raman counting of 11 selected turbidite samples from the Zambezi submarine channel and deep-sea fan. Q = quartz; F = feldspars (K = K-feldspar; Mic = microcline; Or = orthoclase; P, Pl = plagioclase).

Table A7. Mineralogy of the dense fraction (H; > 2.90 g/cm^3). Data determined by semi-automated Raman counting of 11 selected turbidite samples from the Zambezi submarine channel and deep-sea fan; tHM = transparent heavy minerals; ZTR = zircon + tourmaline + rutile.

Table A8. Elemental and isotope geochemistry. Data obtained at the Pôle Spectrométrie Océan (Plouzané, France) from 30 selected samples from the Zambezi sediment-routing system (n.d. = not determined). Concentration of selected major and trace-elements (including Rare Earth Elements, REE) were determined using a Thermo Scientific Element XR sector field ICP-MS, using the Tm addition method (Barrat et al. 1996). Rare Earth Element concentrations are normalized to CI carbonaceous chondrites according to values in Barrat et al. (2012). Neodymium isotopes were measured using a Thermo Scientific Neptune multi-collector ICP-MS, after Nd purification by conventional ion chromatography. Epsilon Nd values were calculated using the present-day chondritic (CHUR) value of $^{143}Nd/^{144}Nd = 0.512630$ (Bouvier et al. 2008) and neodymium depleted mantle model ages ($T_{Nd,DM}$) following the approach described in De Paolo (1981), using measured Sm and Nd concentrations ($^{147}Sm/^{144}Nd = Sm/Nd \times 0.6049$) and present-day depleted mantle values of $^{143}Nd/^{144}Nd = 0.513073$ and $^{147}Sm/^{144}Nd = 0.21083$ (Garçon, 2021).

FORWARD MIXING CALCULATIONS

Terrigenous sediments are complex mixtures of single detrital minerals and rock fragments supplied in various proportions by numerous different end-member sources (e.g., rivers or source-rock domains). If the compositional signatures of detritus in each end-member source are known accurately, then the relative contribution of each source (provenance budget) can be quantified mathematically with forward mixing models (Draper and Smith 1981; Weltje, 1997). The forward mixing model calculates a row vector of compositional data (with columns representing variables) as a non-negative linear combination between a matrix of fixed end-member compositions (with rows representing observations and columns representing variables) and a row vector of coefficients representing the proportional contribution of each end member to the observation.

Several assumptions are made to derive a forward model from a series of compositions (Weltje and Prins 2003): 1) the order of the compositional variables or categories is irrelevant (permutation invariance); 2) the observed compositional variation reflects linear mixing or an analogous process with a superposed measurement error; 3) end-member compositions are fixed; 4) end-member compositions are as close as possible to observed compositions. The accuracy of forward-modelling calculations based on integrated petrographic and heavy-mineral modes depends on how distinct and precisely assessed the end-member signatures of each potential source are. For a detailed illustration of several different practical applications the specifically interested reader is referred to Garzanti et al. (2005, 2007, 2012) and Resentini et al. (2017).

2.1 Compositional data

Geological data are often presented in percentages that represent relative contributions of the single variables to a whole (i.e. closed data; Chayes, 1971). This means that the relevant information is contained only in the ratios between variables of the data (i.e., compositions; Pawlowsky-Glahn and Egozcue, 2006). Compositional data are by definition vectors in which each variable (component) is positive, and all components sum to a constant c, which is usually chosen as 1 or 100.

The sample space for compositional data with D variables is not the real space R^D, but the simplex S^D (Aitchison, 1986):

(1) $$S^D = \left\{ x = [x_1, x_2, \ldots, x_D]; \quad x_i > 0; \quad i = 1, 2, \ldots, D; \quad \sum_{i=1}^{D} x_i = c \right\}.$$

Karl Pearson (1897) first highlighted problems that arise with the analysis of such compositional datasets. The obvious and natural properties of compositional data are in fact in contradiction with most methods of standard multivariate statistics. Principal-component analysis, for instance, may lead to questionable results if directly applied to compositional data. In order to perform standard statistics, a family of logratio transformations from the simplex to the standard Euclidean space were introduced (Aitchison, 1986; Egozcue et al., 2003; Buccianti et al., 2006).

2.2 The mixing model

The forward mixing model (regression model) stipulates a linear relationship between a dependent variable (also called a response variable) and a set of explanatory variables (also called independent variables, or covariates). The relationship is stochastic, in the sense that the model is not exact, but subject to random variation, as expressed in an error term (also called disturbance term).

Let y be the row vector of compositional data with D columns representing variables, X a matrix of end-member compositions with n rows representing observations and D columns representing variables, and β a row vector of coefficients with $q = n$ columns representing the proportional contribution of the end members to the observation. In matrix notation, a forward mixing model can be expressed as

(2) $$y = \beta X + e.$$

The row vector y consists of a non-negative linear combination β of q end-member compositions, and e is the row vector of errors with D columns representing variables.

In order to solve the linear-regression problem, we must determine an estimation of the row vector β describing a functional linear relation b between a matrix of end-member compositions X and an output row vector y. The solution of equation (2) consists in the calculation of the row vector of coefficients b such that

(3) $$\hat{y} = bX,$$

where   is a row vector of calculated compositional data with D columns representing variables. This equation represents a forward mixing model (or "perfect mixing"). The model parameters are subject to the following non-negativity and constant-sum constraints

(4) $$\sum_{k=1}^{q} b_k = 1, \qquad b_k \geq 0,$$

(5) $$\sum_{j=1}^{D} x_{kj} = 1, \qquad x_{kj} \geq 0.$$

It follows from equations (4) and (5) that

(6) $$\sum_{j=1}^{D} \hat{y}_j = c, \qquad \hat{y}_j \geq 0,$$

and thus

(7) $$\sum_{j=1}^{D} e_j = 0.$$

The goodness of fit of the forward mixing model can be assessed by the coefficient of multiple correlation R

(8) $$R = \sqrt{1-(RSS/TSS)},$$

where RSS is the residual sum of squares

(9) $$RSS = \sum_i (y_i - \hat{y}_i)^2,$$

and TSS is the total sum of squares

(10) $$TSS = \sum_i (y_i - \bar{y})^2.$$

The coefficient R departs from a decomposition of the total sum of squares into the “explained” sum of squares (the sum of squares of predicted values, in deviations from the mean) and the residual sum of squares. R is a measure of the extent to which the total variation of the dependent variable is explained by the forward model. The R statistic takes on a value between 0 and 1. A value of R close to 1, suggesting that the model explains well the variation in the dependent variable, is obviously important if one wishes to use the model for predictive or forecasting purposes.

APPENDIX B

Detrital-zircon geochronology. U-Pb ages of zircon grains in the studied sediment samples from the Zambezi sedimentary system (analyses made at the London Geochronology Centre, University College London).

CITED REFERENCES

Aitchison, J., 1986. The statistical analysis of compositional data. Chapman and Hall, London.

Andó, S., Morton, A., Garzanti, E., 2014. Metamorphic grade of source rocks revealed by chemical fingerprints of detrital amphibole and garnet. In: Scott, R., Smyth. H., Morton, A., Richardson, N. (Eds.), Sediment provenance studies in hydrocarbon exploration and production. Geological Society London, Special Publication 386, pp. 351-371.

Barrat, J.A., Keller, F., Amossé, J., Taylor, R.N., Nesbitt, R.W., Hirata, T., 1996. Determination of rare earth elements in sixteen silicate reference samples by ICP- MS after Tm addition and ion exchange separation. Geostandards Newsletter 20(1), 133-139.

Barrat, J.A., Zanda, B., Moynier, F., Bollinger, C., Liorzou, C., Bayon, G., 2012. Geochemistry of CI chondrites: major and trace elements, and Cu and Zn isotopes. Geochimica et Cosmochimica Acta 83, 79–92.

Bouvier, A., Vervoort, J.D., Patchett, P.J., 2008. The Lu–Hf and Sm–Nd isotopic composition of CHUR: constraints from unequilibrated chondrites and implications for the bulk composition of terrestrial planets. Earth and Planetary Science Letters 273, 48–57.

Buccianti, A., Mateu-Figueras, G., Pawlowsky-Glahn, V. (Eds.), 2006. Compositional Data Analysis in the Geosciences: From Theory to Practice. Geological Society, Special Publications 264, London.

Chayes, F. (1971). Ratio correlation: A manual for students of petrology and geochemistry. Univ. Chicago Press, Chicago (USA), 99 p.

Dickinson, W.R., Suczek, C.A., 1979. Plate tectonics and sandstone compositions. American Association of Petroleum Geologists Bulletin, 63(12), 2164-2182.

Draper, N., Smith, H. 1981. Applied regression analysis (2nd ed.). New York, Wiley, 709 p.

Egozcue, J. J., Pawlowsky-Glahn, V., Mateu-Figueraz, G., Barceló-Vidal, C., 2003. Isometric logratio transformations for compositional data analysis. Math. Geol. 35, 279-300.

Garçon, M., 2021. Episodic growth of felsic continents in the past 3.7 Ga. Science Advances 7(39), p.eabj1807.

Garzanti, E., 2019. Petrographic classification of sand and sandstone. Earth-Science Reviews 192, 545-563.

Garzanti, E., Andò, S., 2019. Heavy Minerals for Junior Woodchucks. Minerals 9(3), 148, doi:10.3390/min9030148.

Garzanti, E., Resentini, A., Vezzoli, G., Andò, S., Malusà, M., Padoan, M., 2012. Forward compositional modelling of Alpine orogenic sediments. Sedimentary Geology 280, 149-164.

Garzanti, E., Vezzoli, G., Andò, S., Lavé, J., Attal, M., France-Lanord, C., DeCelles, P., 2007. Quantifying sand provenance and erosion (Marsyandi River, Nepal Himalaya). Earth and Planetary Science Letters 258(3-4), 500-515.

Garzanti, E., Vezzoli, G., Andò, S., Paparella, P., Clift, P.D., 2005. Petrology of Indus River sands: a key to interpret erosion history of the Western Himalayan Syntaxis. Earth and Planetary Science Letters 229(3-4), 287-302.

Hubert, J.F., 1962. A zircon-tourmaline-rutile maturity index and the interdependence of the composition of heavy minerals assemblages with the gross composition and texture of sandstones. Journal of Sedimentary Petrology 32, 440-450.

Pawlowsky-Glahn, V., Egozcue, J.J., 2006. Compositional data and their analysis: an introduction. In: Buccianti, A., Mateu-Figueras, G., Pawlowsky- Glahn, V. (Eds.), Compositional data analysis in the geosciences: From theory to practice. Geological Society of London Special Publications 264, 1–10.

Pearson, K., 1897. Mathematical contributions to the theory of evolution. On a form of spurious correlation which may arise when indices are used in the measurement of organs. Proceedings of the Royal Society of London LX, 489–502.

Resentini, A., Goren, L., Castelltort, S., Garzanti, E., 2017. Partitioning the sediment flux by provenance and tracing erosion patterns in Taiwan. Journal Geophysical Research - Earth Surface 122(7), 1430-1454.

Weltje, G.J., 1997. End-member modeling of compositional data: Numerical-statistical algorithms for solving the explicit mixing problem. Mathematical Geology 29(4), 503-549.

Weltje, G.J., Prins, M.A., 2003. Muddled or mixed? Inferring palaeoclimate from size distributions of deep-sea clastics. Sedimentary Geology 162, 39–62.De Paolo, D.J., 1981. Neodymium isotopes in the Colorado Front Range and crust–mantle evolution in the Proterozoic. Nature 291(5812), 193-196.

Appendix B Zircon ages

Click here to access/download

Supplemental Material

Appendix B ZambeFan Zircon.xlsx

Ref.: Ms. No. 2022.033 Journal of Sedimentary Research
THE ZAMBEZI DEEP-SEA FAN: MINERALOGICAL, REE, Nd-ISOTOPE, AND ZIRCON-AGE VARIABILITY IN FELDSPAR-RICH PASSIVE-MARGIN TURBIDITES

I have received two detailed and thorough reviews for manuscript 2022.033, Garzanti et al THE ZAMBEZI DEEP-SEA FAN: MINERALOGICAL, REE, Nd-ISOTOPE, AND ZIRCON-AGE VARIABILITY IN FELDSPAR-RICH PASSIVE-MARGIN TURBIDITES. Personally, I very much enjoyed this manuscript – it comprises a large multi-proxy provenance dataset which has been integrated in order to present an interpretation of sand/sediment delivery from drainage systems in eastern Africa and western Madagascar into deep marine fans. It clearly has the potential to be an impactful contribution. Both reviewers have provided a number of suggestions, many of these are minor in nature, but, if addressed, will help improve the flow of the manuscript. In addition, reviewer #1 raises some valid concerns in their more conservative review. Therefore, I think the authors should consider each of the points raised by both reviewers below and in annotated manuscripts and provide a response to each. I have some additional comments myself (below) and would appreciate a response to these too. As a whole, I feel that addressing these comments, suggestions and concerns amount to moderate revisions.

TEXT: Quite a number of amendments and integrations have been made, following the advice provided by both Editors and Reviewers.

FIGURES: Several new geographic names were added to Figure 1, including major African countries with political boundaries and the location of Victoria Falls. In Figure 3 we labelled several grains and added arrows to highlight the most relevant petrographic features. In panels A and B of Figure 4 we added two triangles to show which area is represented in zoomed fields and changed the color of several symbols to use the same color code in all figures (the color of Tsiribihina Valley and Lower Fan samples were slightly modified also in Figure 1 to this aim). Some additional sample labels were added to Figure 5 and Figure 6. A further legend was added to both Figure 10 and Figure 11 to clarify the meaning of symbols' shape. Finally, a final Figure 12 has been newly prepared to illustrate with pie charts the provenance budget of the Zambezi sedimentary system from the South African Plateau to the deep-sea fan.

TABLES: Information on sample ages and grain size have been added to Table 1 and fluvial and turbiditic samples with significantly different grain sizes have been indicated separately in Table 3, where a column with the Zr/Hf ratio was also added. These integrations allowed to better clarify statements in the text by making systematic reference to the appropriate data table.

The major issue raised by reviewer #1, and to a lesser extent by the second reviewer, relates to the authors assertion that the dataset can be used to show the impact of anthropogenic activity in the catchments of the major drainage systems. I share some of the reviewers concerns here and feel that, as currently presented, this might be an over-interpretation of the available data.

We agree. Taking into full account the criticism received we have clearly distinguished between direct implications versus speculation and the assumptions being made, and used more cautionary expressions in the revised version of the manuscript.

The key line is "This provenance study of pre-Anthropocene deep-sea sediments allowed us to evaluate the anthropogenic impact on natural sediment fluxes caused by the construction of large dams on the Zambezi River."

We have remodulated this and other similar claims that were over-emphasized in the submitted version of the manuscript.

However, the reviewer argues that a comparison between Pleistocene deep marine sediments, and post-dam-construction river sediment may not be sufficient to support such a statement given the numerous other factors which may have impacted sediment delivery, composition and flux over this time scale (e.g. climate fluctuation, sea level change, even pre-Anthropocene anthropogenic controls (changing land use – a point raised by reviewer 2 as well)). Many of these issues are covered in the detailed points of reviewer #1 below.

We agree that there are many potential interplaying causes and thus made due amendments and added cautionary notes to our statements. On the other hand, it must be considered that Lakes Kariba and Cahora Bassa sequester all of the sediment generated upstream, and that the sediment reaching the delta today is exclusively generated in the lower catchment. Before dam construction this was obviously not the case, and detritus generated across the large upper and middle parts of the Zambezi catchment were also fed into the submarine Zambezi sediment system. In our view, this effect plausibly overwhelmed any other additional control.

I believe there are several ways the authors can address these concerns. They can 1) strengthen their discussion and address each of the points raised below accordingly; or 2) they can downplay the potential anthropogenic impact, contend that this could be a control, but that the subtle variations could also be accounted for by other factors. To my thinking, the first option is a difficult proposition, because, as reviewer #1 argues below, it is difficult to specifically constrain relative sedimentary flux from the dataset – but the authors may have ideas on addressing this. Needless to say, these points will be key for the authors in their revision and generally there needs to be less ambiguous use of “anthropogenic” and “Anthropocene”. Reveiwer #2 has some thoughts on better wording (e.g. pre-dam, post-dam).

We agree, but Option 1 is not really viable. So we followed option 2 and discussed the critical issues in greater depth. Also we agree that pre-dam and post-dam would be far clearer terms than pre-Anthropocene and Anthropocene, and modified the text accordingly.

One critique that is consistent across both reviews relates to a lack of clarity regarding the final outcomes of the paper/project and the inherent (albeit necessary) complexity of some of the figures. I feel this could be addressed with an additional final summary figure, one that would illustrate the pathways, routes and processes across the hinterland and basin. I think this would be an excellent synthesis of the dataset and would address some of the concerns expressed by the reviewers below e.g. comment by reviewer #1 “include a figure or two that is less results-focused and more conceptual”. A simplified version of Figure 1 could be used a base to this figure perhaps?

Following this request and suggestion, we prepared a new final figure (Figure 12) that uses the same geographic/topographic background as Figure 1 and illustrates with pie charts of different size key information on sediment petrology and mineralogy (plus Nd isotope values) together with a rough provenance budget across the Zambezi segmented routing system from the South African Plateau to the Indian Ocean.

I have some additional minor comments, largely driven by my enthusiasm for and interest in the dataset/paper:

1) The Lower Fan sands comprises a (almost equal) mix of Madagascar and Zambezi sources. But, in sedimentological terms, how does this mixing take place? I appreciate that the Tsiribihina submarine valley/canyons appears to feed into that of the Zambezi – but have the authors any comment on the flux through these systems and how the mixing might physically be achieved? Unless sedimentary flux through the systems is constantly “balanced” in both “valleys”, one might anticipate that the amount of mixing, and thus the detrital signal in different turbidite beds , would vary? This might be addressed at the same time as some of the reviewer comments below?

This is a very relevant remark. Stimulated by the highly appreciated Reviewer's interest, we have added a full-dozen-lines-long paragraph to section *Mineralogical and Geochemical Variability in Space*, where we discuss the sediment-mixing issue. Homogenization by current reworking appears to be less efficient in the Tsiribihina Valley, where different turbidite beds maintain a distinct composition, than in the Lower Zambezi Valley and Fan.

2) "Durability of feldspars" is flagged as keyword and this piqued my interest. These systems have abundant fresh feldspar of variable varieties. However, there is no system-specific discussion on this. There are some great observations detailed in lines 514 – 522 and some general comments about Q/F ratios and grain size. Chemical weathering is evoked as being a controlling factor, but it is not explained how this might have varied through time in these catchment areas?

Reviewer Lawton also expressed some disappointment about this paragraph, which made us realize that subsection *Intrasample Mineralogical Variability* was not optimally structured. Therefore, we have rearranged the text into two clear steps: 1) Evidence. Tectosilicate abundance is grain-size dependent, plagioclase being finer than orthoclase, being finer than microcline, being finer than quartz. This is confirmed by what observed in other sedimentary systems, fluvial to turbiditic. 2) Interpretation. Grain-size control cannot be ascribed to hydraulic processes, all tectosilicates having similar density and shape. The size order coincides with the mechanical and chemical durability order of tectosilicates, hence selective weathering of plagioclase relative to orthoclase relative to microcline relative to quartz is consistent with evidence and represents a plausible explanation. No other cause can seemingly explain the same systematic trend, although lower density of K-feldspar and its larger size in source rocks are considered as additional factors. Evidence does not allow us to proceed further than this.

I feel it is worthy of brief comment as feldspar abundance and condition might be an indicator of chemical weathering conditions in the hinterland, or sedimentary residence time in the system?

A proper response to this query would have benefited from analyses of intrasample variability of tectosilicate abundance on river sands from southern Africa and Madagascar, which was not performed. Causes are diverse and intertwined (e.g., chemical etching and mechanical breakage are favored by both twinning and cleavability). For the time being, any further consideration at this regard would be speculative, but we hope to presently obtain new indications in a study of the Niger River, which appears to be an excellently suited place to investigate this issue in detail.

I very much look forward to reading a revision of the paper and the authors response to the comments above and below.

Thank you so much for your kind consideration and for the time dedicated to provide us with very helpful constructive advice.

Reviewer #1

Garzanti et al present the provenance results from the submarine Zambezi Fan System in the broader context of companion provenance studies from the Zambezi and Madagascar sediment routing system. The paper is relatively well-written in terms of structure and grammar, and the authors present a diverse provenance dataset from a range of depositional environments. I am left a but unclear as to why this study was done - i.e., what question was addressed, or hypothesis tested.

This study was principally done to fill up a knowledge gap: no information was previously available from the huge Zambezi submarine valley and fan. The addressed questions regard the diverse controls on sediment composition and the performed tests include technical issues (e.g., comparison between semi-automated Raman counting, manual Raman counting and point counting under the optical microscope) as well as processes (e.g., grain-size dependence of the Q/F ratios). Every new study poses challenges that allow us to grow in experience thanks to newly acquired data-based knowledge. As stated in the initial Confucius quote: ““*Roads were made for journeys, not destinations*”.

Authors note their aims are to "illustrate and discuss the variability of petrographic, heavy mineral, element geochemistry, Nd-isotope, and U-Pb detrital zircon geochronological signatures of Middle Pleistocene to Holocene turbidite deposits, highlight provenance changes in space and time, reconstruct sedimentary and geochemical budgets, and reconstruct the relative amounts of detritus supplied from Africa versus Madagascar as well as the changing contributions from different rivers of SW Madagascar." I think these are fine objectives (except for sediment budgets - more below), but I am still wondering what the key points/takeaways are from this impressive dataset that the rest of the provenance community can learn from.

We tried to better clarify our aims and the implications of our study in the revised version of the manuscript. We prepared a new final Figure 12 to illustrate with pie charts the fundamental results of provenance analysis (sediment petrology and mineralogy plus Nd isotope values). The new figure includes pictorial information on relative sediment fluxes and heavy-mineral concentration to help visualize relative contributions from Africa *versus* Madagascar and mineral fertilities all across the Zambezi sediment routing system.

Authors say: "This provenance study of pre-Anthropocene deep-sea sediments allowed us to evaluate the anthropogenic impact on natural sediment fluxes caused by the construction of large dams on the Zambezi River."
I'm not sure what the authors mean by 'evaluate the impact', but my understanding is that they have used provenance data from deep-sea fan deposits to infer the Anthropogenic changes to the Zambezi S2S system as a result of dams that were constructed in 1958 and 1974.

Yes, this was it. To clarify this issue we replaced the terms pre-Anthropocene and Anthropocene by pre-dam and post-dam throughout the manuscript, as also suggested by Reviewer Lawton.

The authors note that in the present day high-stand conditions the Mozambican shelf is disconnected from the submarine valley and that connection between the terrestrial and deep-sea systems occurred during the LGM (lines 89-91). Thus, they are comparing a Pleistocene deep-marine record with a modern on-shore system and suggesting that differences/changes are the result of anthropogenic causes (dam construction and sediment impoundment). If I am interpreting their message correctly, this is concerning for a few reasons.

The fundamental comparison here is between the composition of turbidite sand and that of river sand, rather than that of coastal sand. Although modern coastal sands are deposited during a highstand, whereas turbidites are generated chiefly during lowstands, the studied shelf sediments were deposited both during the Holocene highstand and the last glacial lowstand. No systematic compositional differences, however, could be observed. To clarify this issue we have restructured and added a full new paragraph to subsection *Mineralogical and Geochemical Variability in Time*:

“Because the studied turbidites were mostly deposited during glacial (lowstand) stages, compositional differences between lowstand and highstand deposits could be investigated only for outer shelf to uppermost slope samples. No systematic mineralogical difference, however, could be observed among sediments deposited during the last glacial lowstand, the postglacial warming and sea-level rise, and the Holocene highstand, possibly because of reworking and homogenization of sediment in coastal areas and across wide continental shelves (Sharman et al., 2021; Malkovski et al., 2022).”

The Reviewer is concerned with the fact that numerous other factors may have impacted sediment flux and composition between the Middle Pleistocene and the present, which is certainly true, and thus we used more cautionary expressions in the revised version of the manuscript. On the other hand, it must be considered that Lakes Kariba and Cahora Bassa today sequester all of the sediment generated upstream and that the sediment reaching the delta today is exclusively generated in the lower catchment. Before dam construction this was not the case and supply from the very large upper and middle parts of the catchment were fed into the submarine Zambezi sediment system as well. This effect, in our view, plausibly overwhelmed any other additional control.

1. Are the rivers of these catchments bedrock or sediment lined? Perhaps the authors can explain if/why they do not agree with the assumption that when sediment is impounded by a dam, the downstream reach of the river will re-equilibrate its sediment load by eroding its banks (if it can). Therefore, even if sediment is impounded, it's flux and provenance signature may not be expected to proportionally reflect the amount of sediment impounded. Sediment along the downstream banks will yield provenance signatures just as it did prior to dam construction.

We agree that these statements do apply in several other cases, but rather not in the case of the Zambezi River (or of the Adda River in northern Italy; Garzanti et al., 1999 Geol. Insubr.). Restoration of the original mineralogical signal we have for instance testified in studies on modern sediments generated in Cyprus Island (2000 JG) and on the Yangtze River (2016 Geomorphology). Along the Zambezi River, however, sand composition changes drastically and irreversibly downstream of Kariba Dam first and of Cahora Bassa next, largely because downstream of the dam there are no floodplains but impressive bedrock rapids (e.g., Kebrabassa means “*end of journey*” because the rapids where the Cahora Bassa Dam was constructed were impassable). As now clarified in the revised version of the manuscript, the dam effect can be dampened only in river systems where the dominant erosional *foci* are located upstream of the dams, which is not the case of the Zambezi, especially as Lake Kariba is concerned. The dam effect in the Zambezi River is evident and complete: the compositional signal is not reconstituted downstream of the dams, as illustrated in our two companion papers (2021 and 2022 JG) entitled for this reason *The Segmented Zambezi Sedimentary System.*

For a list of references on the issue, here is an excerpt from Malkowski et al., (2019 - American Journal of Science): "Although dams retain sediment, the river segment immediately downstream will be sediment deficient and erode its bed or channel margins to establish a new equilibrium sediment load (Porterfield and others, 1978; Smith and Perez-Arlucea, 2008; Schoellhamer and others, 2012; Nittrouer and Viparelli, 2014). Thus, dams enhance downstream erosion of sediments that were deposited prior to dam construction, thereby reflecting pre-dam provenance characteristics." Moreover, the authors are referred to a recent publication by Thompson et al. 2022 in GSAB where they conclude that "Dams not only reduce the sediment flux from a river but also change the locations where sediment is generated by initiating erosion in a river downstream from a dam."

This important comment led us to briefly discuss this issue by adding a new 8 lines-long paragraph in subsection *Zambezi Sediment Transport in Pre-Dam vs. Post-Dam Times,* where reference to six additional studies were made including the most recent papers by Malkovski et al. (2019) and Thomson et al. (2022).

2. Provenance changes between Pleistocene to modern day cannot be attributed explicitly to anthropogenic effects.

We agree that provenance changes cannot be exclusively attributed to dam construction and that other factors are at play, as now clarified in the revised version of the manuscript. Dam construction, however, completely disrupted the continuity of the sediment flux, and it is for this reason considered as the major cause of compositional change.

The dams were constructed in the 1950's, 60's, 70's. Can the authors exclude other potential impacts to provenance between the Pleistocene and 20th century, especially related to climate and variations in erosion of upstream catchments or coastal erosion via sea level rise (e.g., Mason et al, 2017 - EPSL; Fildani et al., 2016 - Geology, Sharman et al., 2021 - Geology)?

Although we fully agree that any geological setting is influenced by several interplaying autocyclic and allocyclic factors (including tectonics, climate, eustacy, etc.), it must be considered that Lakes Kariba and Cahora Bassa today sequester <u>all</u> of the sediment generated upstream and that the sediment reaching the delta today is exclusively generated in the lower catchment. Before dam construction this was not the case and supply from the very large upper and middle parts of the catchment were fed into the submarine Zambezi sediment system. Based on such reasoning, this effect plausibly overwhelmed any other additional control.

The study by Sharman et al. (2021), which we considered as more pertinent to the focus of our discussion than the other two articles signaled by the Reviewer, is now cited in subsection *Mineralogical and Geochemical Variability in Time.*

3. The deep-water deposits of the Zambezi appear to be mixtures of both Madagascar and African sources. Thus estimating changes in relative flux require not only to be able to "unmix", but also be able to inversely mix relative proportions of sources. Although mixture modeling of detrital provenance data has made substantial progress, it has not yet been demonstrated with a convincing degree of success (Amidon et al., 2005; Sundell and Saylor, 2017 - G3; Sharman and Johnstone, 2017 - EPSL; Malkowski et al., 2019 - AJS; Saylor et al., 2019 - EPSL).

These mentioned studies are all based on detrital-zircon geochronology data. In several papers (e.g., Vezzoli et al., 2016; Garzanti, 2016; Garzanti and Andò, 2019) we have underscored how zircon grains represent only a minimal part of the sediment flux (ca. 1/5000 of fine/medium sand on average, which represents in turn 10% or less of the total sediment flux in major rivers; e.g., Hay, 1998). Moreover, zircon is a durable mineral that can be recycled even several times, and can thus provide information only on the first igneous or metamorphic source ("protosource" of Andersen et al., 2016, 2018) rather than on the final source. Zircon, therefore, is an extraordinary carrier of provenance information only if coupled with other bulk sediment methods (e.g., petrography, heavy minerals, geochemistry), which explains the rationale we used in this Zambezi Fan paper as in the two companion Zambezi River papers (JG 2021 and 2022). Unmixing calculations have proven to be very successful in very many studies based on integrated multi-technique datasets!

This is further complicated by the fact that continental shelves serve as both capacitors and mixers of sediment (Malkowski et al., 2022 - depositional record, in press). Thus the end member sources of the deep-water Zambezi can likely be gleaned, but not sure about their relative fluxes.

This comment helped us to improve on subsection *Mineralogical and Geochemical Variability in Time*, where we better circumstantiated the difficulties in distinguish mineralogical signatures at the high-frequency scale. Reworking and mixing by sedimentary processes on a wide shelf is one of the main causes of homogenization, as now underscored also by the citation to the recent studies by Sharman et al. (2021) and Malkovski et al. (2022).

What is not clear to me is if they have independent estimates of sediment flux changes from CRN's and how much they are relying on the deepwater provenance changes to quantify these changes. If the former, then I think a comparison between CRNs and changes to provenance is potentially interesting, albeit speculative. If the latter, I do not think deep-water Pleistocene sediment should be used to quantify changes in relative sediment flux. Portions of the paper read as though they rely on approximated sediment supply estimations as their "best guess" estimates of approximated sediment flux. I am skeptical of quantitative estimations of relative sediment flux via back of the envelope estimates. Another good general reference on provenance and anthropogenic complexities is Sickmann et al (2019, Quaternary Science Reviews), which also includes many other useful references.

The acronym CRN should stand for cosmogenic radio-nuclides. If so, then the only CRN information we are aware of is from the Upper Zambezi upstream of the Cuando confluence in the Kalahari Basin. No gauged data are to the best of our knowledge available from any part of the Zambezi catchment. All information available on sediment fluxes is illustrated and discussed in detail in the companion paper published a few months ago in The Journal of Geology (https://doi.org/10.1086/719166) to which the reader is referred several times in the text.

The review paper by Sickmann et al. (2019) is now cited in the Introduction section of the revised manuscript.

Zr and Zircon budget: The authors note that their calculations suggest that as little as 40% of the Zr budget is from zircon. They speculate that the rest is caught up in phyllosilicates or as inclusions. I find this result interesting and would like to know more about where the authors think this much Zr is being stored and why. Currently there are no citations to support their explanation, but I suggest they look at Bea et al. (2006, The Canadian Mineralogist).

The excellent study by Bea et al. (2006), together with a few others that are now cited as well in the manuscript, turned out to be very useful and made us radically re-think and re-write this paragraph, focusing more specifically on grain-size control on the Zr/Hf ratio. The results confirm that in finer-grained sediment a significant portion of zirconium is contained in minerals other than zircon, presumably phyllosilicates and feldspars that have average Zr/Hf values lower than zircon and whose abundance correlates negatively with grain size.

The conclusions are mostly a summary of the results and therefore took me several re-reads to comprehend. As the reader, it is hard to pull out the key pieces of information. I suggest the authors reduce the conclusion by a third to half and focus more on key provenance conclusions as they pertain to this larger sediment routing system.

We have partly modified the CONCLUSION section — although not to the extent suggested by the Reviewer — to better clarify some of the key points concerning compositional signatures and provenance interpretations.

As previously mentioned, I suggest more caution related to last paragraph of the conclusions - or at least move to the discussion and clearly distinguish between direct implications versus speculation and the assumptions being made (i.e., "If we assume that any differences in provenance between the Pleistocene deep-water deposits and the modern river sands is exclusively a result of sediment impoundment by dams… then we can make inferences about the role that anthropogenic forcings may be imparting on this sediment routing system").

Agreed. Thanks to this suggestion we have modified one sentence in the ABSTRACT and rephrased the introduction to section TRACING SEDIMENT COMPOSITION IN TIME AND SPACE.

In their conclusions, the authors note: "Age spectra of Mangoky River and Tsiribihina Valley zircons are very similar, indicating the Mangoky River as a greater sediment contributor than the Tsiribihina River from the Madagascar side." Detrital zircon populations are not a direct reflection, or representation, of sediment supply (Qs). They are result of sediment supply and zircon abundance. Therefore, I find the conclusion statement misleading unless the authors can demonstrate that relative zircon fertility is not contributing to the discrepancy.

As illustrated above in subsection *Provenance Changes from the Madagascar Side*, and now duly clarified in the CONCLUSION section, this inference was by no means based on zircon data only, but on petrographic, heavy-mineral, elemental geochemistry, and isotope-geochemistry signatures combined. Moreover, it is corroborated by the heavy-mineral analyses of 17 additional Tsiribihina Valley samples that we have very recently analysed for another research project. We are well aware that zircon fertility is a major thorny problem (e.g., Malusà et al., 2016 GR) and this is why provenance budgets based on zircon-age data alone must be considered frail at best.

Figures: The figures presented are of sufficient quality and clarity. They are primarily a selection of the results of the study. Some of them are a bit challenging to interpret at face value.

Most figures have been modified to various degrees (as detailed below) to make them clearer and more effective, and one new final Figure 12 has been drawn.

For example:
Figure 4 shows a plot of all the results of variously zoomed in ternary diagrams. These plots take a long time to digest.

The very same difficulty was reported by Reviewer Lawton, and so we apologize if the “zoomed” fields (chiefly aimed not only at saving space but also to illustrate details that would have been lost if the entire, much larger triangular diagram was drawn) resulted to be hard to digest. As a remedy, we added two small full triangles to panels A and B of Figure 4 that show the area represented in the zoomed fields. We have also changed the color of several symbols to use the same color code in all figures.

Seemingly, a key takeaway (from the caption) is that there is an important relationship between grain size and quartz or grain size and plagioclase. I cannot see that in this plot. But the authors have made a clearer figure (Figure 8) where the reader can quickly see the relationship between grain size and composition.

Figure 4 illustrates the grain-size-dependent *intersample* and *intrabed* compositional variabilities by symbol size (increasing with sample grain size) and arrows (connecting bottom to top of same turbidite bed), as now better clarified in the caption. Figure 8, instead, illustrates the grain-size-dependent *intrasample* compositional variability (i.e., different composition of grain-size classes within the same sample). Plagioclase concentration in finer classes (Fig. 8) is indeed much more evident than plagioclase concentration in finer samples (Fig. 4).

In Figure 5 some of the subplots include arrows (up or down) with percent monazite or quartz or zircon. What do these mean and how do they relate to the data being shown? What about Monazite % is driving geochemical changes (increase in Monazite or decrease)?

We have now clarified in the caption of Figure 5 that arrows indicate the effect of increasing quartz, monazite, or zircon percentages (e.g., more quartz implies less REE content, more monazite implies steeper LREE curve and more negative Eu anomaly, more zircon implies less steep or even raising HREE curve).

I suggest experimenting with a bit more annotation on some of the later figures that have a lot of names. I had to go back and forth too many times to understand what was going on. It may be that annotation is too cluttering.

Following Reviewer's Lawton advice, we have labelled several grains and added arrows to highlight the most relevant petrographic features in Figure 3.

In Figure 4 we have added two small triangles to show the area represented in the zoomed fields of panels A and B, and changed the color of several symbols to use the same color code in all figures (the same was done for several symbols in Figure 1).

In Figure 5 and Figure 6 we have added several sample labels and in the caption of Figure 5 we have clarified the significance of the ten arrows.

Figures 7 (on which we have added a few scripts), 8, and 9 are clear and effective we believe.

A legend has been added to Figures 10 and 11 to clarify the meaning of symbols' shape. Moreover, as specifically requested by Reviewer Lawton, we have specified in the caption that all samples are plotted individually in the 3-way MDS map of Figure 11 (all sample numbers are now indicated). Instead, data were combined from 2 or 3 samples for the Middle Zambezi, Lower Zambezi, Upper Channel, Tsiribihina Valley and Lower Valley in Fig. 7 and in the MDS map of Fig. 10, as indicated in the caption of Fig. 7 (to which the caption of Fig. 11 refers).

References: The lead author is an author on ~25% of the works cited in this paper. I've never seen that before. May simply be a product of the author's experience and career, but this review includes several studies that the authors might consider reading and perhaps including in their list of references.

We are really more than happy to include references to other articles that are pertinent to the focus of our study. In the revised version of the manuscript we have added 21 new references, several of which kindly indicated by the Reviewers.

This is presumably the final chapter of a larger, more comprehensive, and integrated provenance study across the full extent of a sediment routing system. I would like to learn more about what the authors think the most important scientific findings and take-aways are regarding this provenance analysis and study area. I do not find the anthropogenic conclusions compelling without a more direct and clearer 'before and after' test. My suggestion to the journal is to return this manuscript to the authors to modify its scope, message, and presentation of the data and their provenance implications. My suggestion to the authors is to tone down the anthropogenic implications, amplify the provenance implications …..

We thank the Reviewer for stimulating us to do better. This article does come after an extensive provenance study across the Kalahari Basin and Zambezi River catchment, but we are hardly able to say "a final word" on the sedimentary system in this large area for a number of reasons, several of which underscored by the comments made by both Reviewers. One major problem is the lack of gauged sediment fluxes. Getting around this "black hole" implied a rather devious route and large uncertainties, as discussed in the previous 2022 JG paper. This has also an effect on the conclusions of the present study, and explains some disappointment expressed by the Reviewers concerning our tentative assessment of anthropogenic impact, which was one of the key goals of the research plan. We maintain that, considered that Lakes Kariba and Cahora Bassa today sequester all detritus generated upstream, sediment trapping in large reservoirs is with all likelihood the most important cause of the observed compositional differences between Pleistocene-Holocene offshore sediments and sediments supplied today by the Zambezi River to the delta. However, we do agree that other controls are potentially at play and that our statements needed to be toned down and reset to some extent.

…. and include a figure or two that is less results-focused and more conceptual (but as a byproduct of the results).

We have prepared a new final Figure 12 that illustrates with pie charts of different sizes key compositional information and the estimated proportions of sediment generated in the three main tracts of the Zambezi catchment in Africa and transferred to the Zambezi submarine valley and fan, where it mixes with detritus shed from Madagascar (mostly by the Mangoky and Tsiribihina main rivers *via* the Tsiribihina submarine valley).

Which provenance indicators were most effective vs. susceptible at detecting source inputs?

No single indicator is by itself sufficient. Provenance analysis based on a single line of investigation (e.g., zircon ages or Nd isotopes) is bounded to be unrobust. A response to this question can be provided by the newly drawn Figure 12 (illustrating petrographic, heavy-mineral, and Nd-isotope signatures) combined with Figure 7 (illustrating KDE plots of detrital-zircon ages).

How sensitive are the various provenance indicators to grain size?

Grain-size-dependent intersample and intrabed compositional variabilities are fully discussed in the text and illustrated in Figure 4, whereas grain-size-dependent intrasample compositional variability is illustrated in Figure 8 (where plagioclase is shown to concentrate in finer classes relative to orthoclase, orthoclase relative to microcline, and microcline relative to quartz).

How the results of this study differ from the other recent "companion papers" of provenance data from this system?

The companion papers only dealt with river sediments, whereas the present study is focused on the submarine Zambezi valley and fan and thus completes a multi-method research program on sediments generated in southern Africa and transferred to the sea floors of the Indian Ocean. In turn, all this is part of a larger project on African continental to deep-sea sedimentary systems, including the Congo, the Niger, the Nile, the Limpopo, and the Orange. Every system in Nature is unique, but the differences and similarities observed among these diverse African systems may help us understand better the complexity of processes of sediment generation and its various controls (i.e., source-rock lithology, grain-size, mechanical break-down, chemical weathering, hydraulic sorting, recycling).

Or what about the fact that in Figure 11, the ultimate sink (Lower Fan) more closely reflects the Madagascar (smaller drainages) than the big Zambezi? Was this expected?

No, it was definitely not expected. This is certainly one of our most unexpected results.

I look forward to seeing this comprehensive dataset published in the relatively near future.

Thank you for the time dedicated to carefully read our manuscript and for the many constructive comments that helped us to improve on the clarity and completeness of our paper.

Reviewer #2: This manuscript is an in-depth analysis of sediment compositions derived from the Zambezi River catchment of Africa and several smaller river catchments of Madagascar, and how they contribute to the enormous Zambezi submarine fan. As with other publications in this "series" by the Garzanti research group, it is enormously edifying and stimulating, and the reader comes away feeling enlightened regarding a whole new realm of sediment routing. It is appealing that the authors have approached the concept of human disruption of natural systems by dam building, an awareness that is growing rapidly as a result of studying modern sand routing systems. I think this manuscript will attract a wide readership among persons seeking better insight into controls on submarine fan deposition and size as related to catchment characteristics (in this case catchments lying on two continents), petrographers amassing databases on controls of modern sand composition, detrital zircon provenance specialists seeking to understand the limitations of maximum depositional ages, and persons interested in assessing human impact on sediment transfer and implications for coastal communities.

This is a high-quality, well written manuscript. My comments below are mainly oriented toward improving articulation of text, figures, and tables, and thereby making it easier for readers to understand the sources of many assertions in the manuscript.

Note that I made my comments on the Word version of the manuscript in track changes, but attempted not to insert or delete text so as to change the line numbers relative to the pdf version.

My Regards to the Authors,
Tim Lawton
Austin, Texas

Thank you so much for your appreciation, very careful review, and generous constructive advice.

General comments:

1. The manuscript would benefit from more extensive citations to Figures and especially Tables to permit a reader to evaluate many passages that make assertions about compositional characteristics and compositional trends in the sediment. I have noted some of these in the manuscript margin.

Sure! Systematic citations to Figures and especially to Tables 2 and 3 (particularly in sections COMPOSITIONAL SIGNATURES and COMPOSITIONAL VARIABILITY) were added to substantiate our statements and facilitate reading.

It would be useful for the Tables to have titles more descriptive than table number.

The three Tables all have a title and a caption (albeit short). A title has now been given also to all Appendix Tables whenever they are referred to in the text.

2. I made a comment about appropriate use of topic sentences to introduce paragraphs on line 317. At this point, the authors launch into a description of many different aspects of Zambezi River sand without signalling to the reader that that's what they are about to do. The topic sentence predicts a paragraph full of mineralogical compositional details, but really that's the only sentence that concerns minerals. An effective topic sentence indicates the content of the entire paragraph and, as such, should enhance reader comprehension.

The introductory sentence to section COMPOSITIONAL SIGNATURES, found a few lines above, does signal to the reader that the fundamental aim of this section is to describe compositional signatures (petrography, heavy minerals, major elements, trace elements, isotope geochemistry, and detrital-zircon geochronology). This descriptive section may be found (and largely is) boring, but descriptive parts are needed, because the description of facts is the solid base unto which interpretations are built.

The Reviewer is asking us to introduce every paragraph with a topic sentence that compositionally singles out one group of samples from the others. However, on the one hand compositional differences are generally subtle (because, as stated in the Abstract, the studied sediments are all generated from dissected rifted margins) and on the other hand multiple data from multiple sediment groups are hardly compared in one simple topic sentence. The best way by far to make such intra-group comparisons is to look at Table 2 for petrography and heavy minerals, at Table 3 for elemental and isotope geochemistry, and at Figure 7 for detrital zircon ages. Both Tables are now referred to more systematically in section COMPOSITIONAL SIGNATURES. A final comparison of compositional signatures and sediment fluxes is provided in the new Figure 12.

3. Better explanation of figure symbols. For me, the most difficult part of the manuscript was to understand the meanings of the symbols in the various figures. These need to be explained in the figure captions. There are comments on the various captions, where I was confused.

In both Figure 10 and Figure 11, we have added a further legend to indicate that circles are for river sands, squares for beach sand, and stars for turbidite sand. In panels A and B of Figure 4 we added full triangles that show the area represented in zoomed fields and changed the color of several symbols to use the same color code of all figures (Figures 4, 5, 6, 7, 10, and 11). Figure captions have also been clarified and most other figures were improved to various degrees.

4. To make the manuscript more accessible to non-Quaternary specialists (like me), indicate on Table 1 how the Quaternary stages correspond to the Marine isotope stages (I confess I had to look this abbreviation up). Maybe also write out the term MIS the first time it's used (line 160, I think).

Sure. In Table 1 we have added one column that provides the age correspondence between Marine Isotope Stages (MIS, spelled out in the table caption) after Railsback et al. (2015).

The corresponding Quaternary stage is the Chibanian (Middle Pleistocene) for most samples. Age information is provided in the first part of section SAMPLING AND ANALYTICAL METHODS. “Marine Isotope Stage” is spelled out the first time the term is met, in the first part of section SAMPLING AND ANALYTICAL METHODS (Line 157 of the submitted manuscript).

5. Mixing model algorithms should be included as excel files in supplementary material. They are as important as basic DZ and geochemical data to interested readers.

The method is by itself quite simple (it is basically a calculation of weighted averages of end-member signatures). Nevertheless, its rigorous mathematical explanation requires a couple of full pages that would be rather cumbersome to add to the main text. Therefore, in order to duly respond to this query we have: 1) added a full explanation of the mathematical rationale of the calculations in Appendix A, which contains further specific references where the founding assumptions, and limitations of the method are discussed in practical applications to modern sediments of different geological settings; 2) restructured the main text, adding a 2/3 page-long explanation of the method to section SAMPLING AND ANALYTICAL METHODS, where the specifically interested reader is referred to Appendix A for further information.

6. Please make sure that the geographic features in the early discussion of geography and drainage networks are shown on Figure 1, even if you have to abbreviate them to get everything on the figure. For example, the Kalahari Plateau, referred to many times and an important potential player in contributions of recycled sediment, is not indicated on Figure 1.

We have indicated several new geographic names in Figure 1, including the name of major African countries and the location of Victoria Falls (abbreviated VF). In the text we have replaced “Kalahari Plateau” with “South African Plateau” (or with “Kalahari Basin” were appropriate). Kalahari Basin is indicated in Figure 1.

7. I come back to the term Anthropocene several times in my text comments, questioning whether it is the correct term to apply to pre-dam as opposed to post-dam sediment yields. I suspect that anthropogenic changes in sediment yield long pre-dated building of these dams as a result of deforestation of drainage basins, grazing of domestic animals, and other agricultural practices that altered pre-human sediment discharge. At some point, experts may actually agree on when the Anthropocene began, which will potentially lead to confusion among future readers as to why you used that term specifically, especially if it begins with an atomic-era cesium layer.

We agree. In order to avoid any possible ambiguity we modified the text referring to pre-dam and post-dam sediment yields. The term Anthropocene is not used anymore throughout the manuscript.

I did not check correspondence of text citations and references. The following comments are indexed to line numbers in the manuscript word file with comments, which accompanies the review.

The correspondence between citations in the text and reference list has been thoroughly checked.

Pages 5-8: Please be sure to indicate all names (including country names and boundaries) on Figure 1. I recognize that this might make the figure too busy, but perhaps you could add a companion figure that handles the political names and leave the satellite image to handle the geographic features like plateaus, rivers, and waterfalls.

We have added several geographic names to Figure 1, including country names and boundaries.

Lines 185-196, near 193: In this passage, it would be useful to note that the QFL plot of Garzanti (2016, 2019, summarized on his table 1) is a modified version of most other QFL or QmFLt plots in that Qp is plotted with Q, but chert is plotted with L. I'm fine with this compositional paradigm, but it is neither a QmFLt nor a QtFL plot in the context of other historical ternary plots, except for Zuffa's classification. Such a notation would offer most interested readers (who might not have been following these arguments closely) a little assistance in terms of thinking about provenance implications.

Yes! In the revised version of the manuscript we have clarified that carbonate and chert grains are included in the lithic fragment population, according to Zuffa (1985).

Lines 317-321: This might seem a little picky, but the topic sentence for this paragraph describing the sediment of the Zambezi River and Shelf is a complicated description of the grain composition of the sediment. I submit it's the kind of introductory sentence that makes the reader want to skip the paragraph.

The description of compositional signatures, although admittedly boring, was organized as efficiently as we could. A scientific paper is (perhaps unfortunately) not a thriller, and the (boring) descriptive parts are needed, because the description of facts is the solid base unto which interpretations are built. No harm is done if the reader freely wants to skip it and go directly to the meat. The important thing is that data are there, also for use in future studies.

It does not signal the content of the paragraph, which also covers bulk chemistry, REE trends, and DZ age distribution, in a succinct way.

The introductory sentence to section COMPOSITIONAL SIGNATURES is to be found a few lines above, where it is specified that the fundamental aim of this section is the description of compositional signatures (petrography, heavy minerals, elemental geochemistry – now more punctually modified as *major-element and trace-element geochemistry* for further clarity –, Nd isotopes, and U-Pb age spectra).

If you were to stand back and characterize the general nature of this sediment--what makes this sediment similar to or different from the other sediment types to come, or what characteristic label you could apply to it--how would you put that in a sentence? Let the reader know the content of the paragraph in a single simple introductory sentence, and then go through the laundry list of characteristics.

This section is intended to be a pure description of facts. Its aim is to provide basic objective information. Tables and Diagrams are the best places to detect differences among sample groups directly and visually by the reader without the bias that wording may introduce.

The topic sentences for the next two paragraphs could state how those sands or silts are similar or different from the first batch. I tried writing one for the next paragraph.

Thank you for the constructive suggestion, but we prefer to mainly stick to our style here, and let the Reader free to make comparisons and check by her/himself on Figures and Tables whether differences are there, minor or sharp, significant or not significant.

Line 528. See my comment here about citing Figure 8 in the topic sentence for trends discussed later in the paragraph, which are not illustrated by Figure 8 and instead by table in an appendix.

Figure 8 does allow the reader to outline a steady mineralogical trend with marked concentration of plagioclase in the fine tail of the size distribution relative to quartz. For further clarity we have also addressed the interested reader to the database upon which Fig. 8 is drawn, provided in full in Appendix Table A5.

This is just an example, but it's a case of a table buried in the long list of untitled appendix tables that documents the trends noted in the final two sentences of the paragraph. I think this table may be destined, without a title, for a long appendix. It would be better as a table in the text, or at least cited as Appendix Tablexx in the text.

Not to encumber the manuscript too much with a data table we chose this last option and made reference also to Appendix TableA5 *Intrasample tectosilicate variability*.

The appendix table would be more effective if it had a title.

This is a nice suggestion, thanks. Now all Appendix Tables quoted in the text have their own title.

Lines 529-542: It appears that what you're saying in a roundabout way here is that the observed tendency for Q/F to increase with grain size, whether in continental or deep-marine deposits (this should probably be the first sentence of the paragraph) might be related to durability of quartz over feldspar, or to inherent crystal size differences in the source region. But you don't know which of these factors causes it in the Zambezi-Madagascar system. It seems like if it's been reported from a couple of other places (e.g., Marsaglia et al., 1996; Garzanti et al., 2021), maybe it's the more universal process of weathering that is the underlying factor, and not provenance grain size differences. At present, the final sentence is general and unexplained; therefore, a bit disappointing.

This comment made us realize that this paragraph was not optimally organized. Therefore, following the Reviewer's suggestion, we have restructured the text changing the order of statements to make the narrative more logical and fluent.

Circa line 689: You consistently use the terms "Anthropocene" and "pre-Anthropocene" to refer to post-dam construction and pre-dam construction sediment yields, respectively, in this part of the manuscript. I submit that Anthopocene (whatever that means and whenever it started in Africa) sediment yields probably were a result of the onset of human agricultural activity and deforestation (particularly in Madagascar perhaps, where there are apparently no dams), long before those dams were constructed. Therefore, the "Anthropocene" may have temporarily (pre-dam) increased sediment yields. The point of this diatribe is to suggest that perhaps the modifiers "pre-dam" and "post-dam" would be more accurate for indicating what you refer to here, which are sediment-yield effects directly tied to the construction of the dams.

Indeed. Pre-dam and post-dam are far clearer terms. We thus changed the text accordingly. The term Anthropocene is not used anymore through the manuscript.

Line 712: Comment copied here, because this is important: These days when mixing calculations are performed, it's typical to include the algorithm in the supplemental data, or at least include the data in a table. There is no citation to such here, but it would be useful to include such information. Otherwise, the reader is simply taking the preceding paragraph discussion on faith.

To duly respond to this query we have: 1) added a full explanation of the mathematical rationale of the calculations in Appendix A, which contains further specific references where the founding assumptions and limitations of the method are discussed in practical applications to modern sediments of different geological settings; 2) restructured the main text, adding a 2/3 of a page-long explanation of the method to section SAMPLING AND ANALYTICAL METHODS, where the specifically interested reader is referred to Appendix A for further information.

Lines 812-814: That Madagascar has been such a major contributor of sediment is an interesting conclusion that really comes through clearly for the first time here. A quick look at the sizes of the drainage basins, the Intermediate Basin, and the Lower Fan makes this all the more astonishing from a mass balance perspective and makes one wonder if there might not be other factors other than upstream sediment trapping at play here: inadequate sampling of such a huge system, short-term climatic deterioration, anthopogenic sediment flux from Madagascar due to agricultural practices that go quite far back in time.

Yes, we were quite surprised too, but all key mineralogical and geochemical parameters very clearly and coherently tell the same. The inference is thus considered as robust. Moreover, samples as old as > 500 ka could not have been significantly affected by anthropogenic forcing.

Table 1 indicates that lower fan samples represent a narrow time interval, approximately 300-370 kya (MIS 8, 9). That's pretty old for human agriculture or forest clearing, but perhaps a short-term climatic shift could strongly influence sediment yields. Without a more complete time series suite of samples from the Lower Fan, it seems like picking a single causal mechanism is pretty speculative. My intent here is by no means to demean the nature of this spectacular sample set, but rather simply to point out that there might be numerous alternative factors that determined long term sediment supply to this enormous fan. Perhaps it would be more conservative to say that the Intermediate Basin might have acted as a transient sediment trap at 300-400 kya.

Lower Fan samples are indeed relatively old (both > 500 ka) but Lower Valley samples are not (ca 15 ka and 130-190 ka).

Climatic forcing does represent a theoretical possibility, but our data are insufficient to prove, or even to suggest, such a control. Any statement at this regard would thus remain speculative. Moreover, Fierens et al. (2020) found no correspondence with climatic or eustatic changes, and thus considered gravitational failure from the continental slope as the main trigger of turbidity currents.

Eustatism is certainly another potentially important control, because turbidity current are activated during lowstands. Our data, however, do not show any clear evidence for eustatic control and we tried to avoid statements founded on current beliefs, however plausible they may appear.

Figure 4: I understand the interest in conserving space, but in terms of visualization, I find that the truncation of the QmFLt(?) and QmPK plots (especially the latter display) hinders my ability to

mentally compare these sand suites with other sand and sandstone suites that have long been displayed on complete compositional and provenance ternary plots. I would prefer to see the entire triangles.

We fully understand the problem, and thus added the full triangles to panels A and B of Figure 4 in order to show the area represented in the zoomed fields where samples are plotting.

Figure 7: Lines 904-907 of caption: "Zambezi sand is dominated by late Stenian (~1.05 Ga; Irumide) ages, whereas in river sands of SW Madagascar ages are mostly Neoproterozoic (0.5-1.0 Ga: Pan-African), the main peak getting younger from north to south. In the submarine system, Upper Channel samples display more Pan-African ages than Zambezi River samples, and the Intermediate Basin sample has notably more Orosirian (Eburnean) ages, indicating conspicuous supply from the upper and middle Zambezi catchment in pre-Anthropocene times."
Although this statement is in the caption, it is a sweeping conclusion to make on the basis of a couple of samples from a very complex, admittedly perturbed sediment-routing system. Samples of modern fluvial sand, for example the lower Orinoco, have been shown to vary significantly in local parts of a system of bars (e.g., located hundreds of meters apart; Ibañez-Mejia et al., 2018, Geology). You need to nuance this statement a bit to indicate that the dataset suggests post-dam changes. It does not confidently indicate those changes, because the sample number and density of this dataset are probably not adequate to reject the possibility of local compositional variation in the upper channel. I suspect this kind of variation could also depend on which major tributary system was contributing most water and sediment from a major rainfall event. I suppose that such high-frequency fluvial signals could be damped out as sediment passes through the shallow marine part of the system, but it would be useful to stipulate such a filter as a possibility. The MDS plots do not seem to indicate that Quelimane serves that function, at least on the basis of a single sample.

We have eliminated the statement "*indicating conspicuous supply from the upper and middle Zambezi catchment in pre-Anthropocene times*". The caption was indeed too long. Following the Reviewer's advice we also toned down a bit our statements concerning this issue through the text.

Figure 10: The stars, circles, and colors need to be explained in the caption. I can't see that they carry through from previous symbol schemes.

In both Figure 10 and Figure 11, we have added a further legend to indicate that circles are for river sand, squares for beach sand, and stars for turbidite sand. Color codes are the same as in other figures (e.g., Figure 7) and now we have modified the color of several symbols in Figure 1 and Figure 4 in order to have the same color code in all figures.

Table 1: It would have found it very helpful to have a column in Table 1, or a parenthetical statement next to the various MIS ages, stating how old the sample is (Holocene, middle Pleistocene, etc.). These are not ages that I carry around in my head, and there are many readers who don't routinely deal with the Quaternary who may be similarly challenged. I could go back to lines 154-163 when I encounter these MIS ages again further on in the paper, but it would be easier to simply consult Table 1 for a translation of MIS to Quaternary stage/age.

In Table 1 we have added one new column that provides the age correspondence between Marine Isotope Stages (MIS, spelled out in the table caption) after Railsback et al. (2015). Most studied samples are Middle Pleistocene in age, as also indicated in the first part of section SAMPLING AND ANALYTICAL METHODS.